8-2018

Membrane-based Separation Processes for Treating High Salinity Produced Waters

Kamyar Sardari
University of Arkansas, Fayetteville

Membrane-based Separation Processes for Treating High Salinity Produced Waters

A dissertation submitted in partial fulfillment
of the requirements for the degree of
Doctor of Philosophy in Engineering with a concentration in Chemical Engineering

by

Kamyar Sardari
University of Tehran
Bachelor of Science in Chemical Engineering, 2014

August 2018
University of Arkansas

This dissertation is approved for recommendation to the Graduate Council.

S. Ranil Wickramasinghe, Ph.D.
Dissertation Director

David Ford, Ph.D.
Committee Member

Xianghong Qian, Ph.D.
Committee Member

Lauren Greenlee, Ph.D.
Committee Member

Wen Zhang, Ph.D.
Committee Member

Abstract

Produced waters (PW) generated in the oil and gas industry within the United States often contain extreme levels of total dissolved solids (TDS). These high TDS waste streams need to be treated cost-effectively as the costs associated with the current management techniques can exceed 15 USD per barrel of discharged PW. Thermally and osmotically-driven membrane separation technologies can show promising potential for treating high TDS waste streams, as onsite low-grade waste heat may be used for their operation. In this dissertation, the application of membrane distillation (MD), forward osmosis (FO) and a hybrid FO-MD process for treating synthetic and actual high TDS PW is investigated. The aim is to maximize water recovery and minimize the high TDS sludge volume.

A number of commercially available hydrophobic membranes with varying properties have been extensively characterized and tested in a bench-scale MD system. A bulk membrane structural parameter has been defined and used to identify membranes that display the highest permeate fluxes. Then, the maximum achievable brine concentration for higher flux membranes was determined. When treating actual PW feed streams, which contain not only high TDS, but also dissolved organics, surfactants and low surface tension contaminants, pretreatment of the feed is essential to suppress the onset of membrane fouling. In this study, the feasibility of electrocoagulation (EC) followed by MD is investigated. EC was reported effective in mitigating fouling during MD.

FO is another emerging membrane-based separation technology that could find niche applications in the treatment of oil and gas PW. Here, the feasibility of treating hydraulic fracturing PW using a combined EC-FO process has been investigated. EC is shown to be effective

for removing suspended solids and organic compounds which foul the membrane during FO. By accounting for internal and external concentration polarization as well as fouling, the expected FO flux may be determined. Finally, we have studied hybrid FO-MD system and shown that this process integration can combine the advantages of both processes; low fouling tendency and high quality permeate. The actual treatment used, EC-MD, EC-FO or EC-FO-MD will depend on the quality of the PW.

Acknowledgements

First and foremost, I would like to express my sincere gratitude to my advisor Prof. Ranil Wickramasinghe for the continuous support of my Ph.D. study and research, for his patience, trust and immense knowledge. I appreciate all his contributions of time, ideas, and funding to make my Ph.D. experience productive. I could not have imagined having a better advisor and mentor for my Ph.D. study. I also would like to thank my committee members, Dr. Wen Zhang, Dr. Lauren Greenlee, Dr. Xianghong Qian and Dr. Jamie Hestekin along with all other professors in the Ralph E. Martin Department of Chemical Engineering for their advice and help along the way. In addition, I need to thank all members of my research group for their help.

The membrane characterization studies discussed in this dissertation would not have been possible without the high quality SEM and EDX analysis from the Arkansas Nano-Bio Materials Characterization Facility. I have appreciated the collaboration from Dr. Mourad Benamara, Dr. Liu and Dr. Sengupta for their help with the above-mentioned analysis. In addition, I would like to thank Mr. Kamaz and Mr. Chaio for their help during membrane distillation and forward osmosis experiments. Moreover, I would like to thank Dr. Vu for his help with AFM, contact angle and FTIR measurements.

Raw and treated produced waters have been extensively characterized and discussed in this dissertation. All these efforts could not have been possible without the help form Arkansas Water Resources Center, University of Arkansas staff. In specific, my sincere acknowledgement goes to Mr. Keith Trost and Ms. Jennifer Purtle for conducting the water analysis experiments and preparing the reports. I would also like to thank Mr. George Fordyce for all his technical supports in establishment of the experimental setups.

I gratefully acknowledge the funding sources that made my Ph.D. work possible. I was funded by Southwestern Energy through the National Science Foundation Industry/University Cooperative Research Center for Membrane Science, Engineering and Technology, the National Science Foundation and the University of Arkansas. I also would like to appreciate the industrial mentorship received from Mr. Peter Fyfe, Mrs. Dianne Lincicome, Mr. Derk Dehn, Mr. Uwe Beuscher and Mr. John Askegaard.

Lastly, I would like to thank my family for all their love and encouragement. For my parents who raised me with a love of life and for my brother Mazyar who supported me in all my pursuits, and most of all for my loving, supportive, encouraging, and patient wife Negin whose faithful support during this Ph.D. is so appreciated. Thank you.

Kamyar Sardari
Ralph E. Martin Department of Chemical Engineering
University of Arkansas
May 2018

Dedication

To my father, who sacrificed his life for a better world

To my beloved mother, a strong soul who taught me to believe in hard work

To Mazyar, my brother and my best friend, for his unending support

and to Negin, the love of my life

Table of Content

List of Published Papers

Chapter 2 (Published): M. Malmali, P. Fyfe, D. Lincicome, K. Sardari, S.R. Wickramasinghe, Selecting Membranes for Treating Hydraulic Fracturing Produced Waters by Membrane Distillation, Separation Science and Technology, 52 (2017) 266–275.

Chapter 3 (Accepted): K. Sardari, P. Fyfe, D. Lincicome, S.R. Wickramasinghe, Combined Electrocoagulation and Membrane Distillation for Treating High Salinity Produced Waters, Journal of Membrane Science.

Chapter 4 (Published): K. Sardari, P. Fyfe, D. Lincicome, S.R. Wickramasinghe, Aluminum Electrocoagulation Followed by Forward Osmosis for Treating Hydraulic Fracturing Produced Waters, Desalination, 428 (2018) 172–181.

Chapter 5 (Under preparation): K. Sardari, P. Fyfe, S.R. Wickramasinghe, Integrated Electrocoagulation, Forward Osmosis and Membrane Distillation Processes for Water Recovery from Hydraulic Fracturing Flowback Waters, Desalination.

Chapter 1. Introduction

The significance of oil and natural gas in modern civilization is well known. Nevertheless, like most production activities, oil and gas extraction and production activities generate large volumes of waste streams. Oil and gas field wastewater or produced water (PW) contains a wide range of organic and inorganic components [1]. Discharging PW can pollute surface water as well as underground water and soil. On the other hand, due to the generation of large volumes of PW, many countries are increasingly focusing on efforts to find efficient, environmentally friendly and cost-effective treatment methods to remove pollutants as a way to supplement their limited fresh water resources. Reuse and recycling of PW include underground injection to increase oil and gas production, use for irrigation, livestock or wildlife watering and habitats, and various industrial uses (e.g., dust control, vehicle washing, power plant makeup water, and fire control) as well as ground water recharge for direct potable water reuse [2,3].

The physical and chemical properties of PW vary considerably depending on the geographic location of the field, the geologic formation from where the water is produced, and the type of hydrocarbon product being produced. For those sites where water flooding is conducted, the properties and volumes of the PW may vary dramatically due to the injection of additional water into the formation to increase hydrocarbon production. In general, the major constituents of concern in PW can be categorized as following [3,4]:

- Salt content, often expressed as salinity or total dissolved solids (TDS)
- Oil and grease (O&G), various organic compounds associated with hydrocarbons in the formation
- Inorganic and organic compounds introduced as chemical additives to improve

drilling and production operations

- Naturally occurring radioactive material.

Treatment of PW has the potential to lead to a valuable product rather than a waste. The general objectives for operators for treating PW are as follows [5]:

- De-oiling: removing dispersed oil and grease
- Soluble organics removal
- Suspended solids (SS) removal
- Disinfection
- Desalination: removing TDS
- Softening: removing excess water hardness

Induced and diffused gas flotation technologies are widely used for dispersed oil removal from PW [6–8]. Adsorption and filtration techniques are often used for soluble organic compounds removal [9]. Sedimentation and floatation methods can be used to remove SS from PW streams. Disinfection is normally performed using chemicals (e.g. chlorine gas) and ultra-violet (UV) treatment [10]. Ion-exchange as well as precipitation are most widely used PW softening methods [11].

The rapid rise of shale gas development through horizontal drilling and high volume hydraulic fracturing has expanded the extraction of hydrocarbon resources in the United States (U.S.) [12]. The U.S. Energy Information Administration estimates that about 15.8 trillion cubic feet (Tcf) of dry natural gas was produced directly from shale and tight oil resources in the U.S. in 2016, an increase from 0.3 Tcf in 2000 [13,14]. Hydraulic fracturing process generates large

quantities of PW that needs to be managed efficiently and economically to ensure sustainable development of unconventional extraction industry [15]. The management and disposal of these PWs is one of the greatest challenges associated with unconventional oil and gas development. Currently, hydraulic fracturing produced water (HFPW) is the largest wastewater stream produced in oil and gas industry within the U.S. [12].

Development of cost effective methods to manage these high TDS PWs is of crucial importance. Many separate and combined physical, chemical, biological and thermal methods are proposed for PW treatment. However, among the treatment objectives, removing TDS has historically been the most challenging step. Currently, deep-well injection is the primary means of management for high salinity PWs, such as HFPW. However, in many areas where oil and gas production will be abundant, deep-well injection sites are not available [4]. Current practice for oil and gas production companies is to transport the high salinity PW to deep-well injection sites using commercial trucks. This process could cost up to 10 to 15 USD per barrel of PW [15]. In addition, U.S geological survey (USGS) has recently revealed that fracking is not causing most of the induced earthquakes and the wastewater disposal through deep-well injection is the primary cause of the recent increase in earthquakes in the central U.S. [16]. Therefore, there is an urgent need for novel processes to eliminate or minimize the deep-well injection.

The volume and dissolved solids content of HFPW of a well depends on a number of factors including: the geographical location, geological formation, well depth and time following hydraulic fracturing [17,18]. Kondash *et al.* [19] has estimated the median volume of HFPW to range from 1.7 to 14.3 million L per well over the first 5–10 years of production. The TDS of HFPWs can vary from 650 to 400,000 mg L^{-1} [20].

1.1. Membrane Separation

A membrane is defined as a barrier that facilitates transport of targeted materials and restricts transport of unwanted species. A membrane can be homogenous or heterogeneous, symmetric or asymmetric in structure, can carry a surface charge or be neutral and can be made of organic (e.g. polymeric) and inorganic (e.g. ceramic) materials. Transport through a membrane may take place by convection or diffusion of individual compounds. The driving force for mass transfer across a membrane can be stablished by concentration, pressure or temperature gradient or even by an electric field [21]. Compared to conventional separation techniques, membranes can offer a simple, easy-to-operate, low-maintenance process with minimal use of added chemicals. In addition, membrane processes can be readily scaled up considering their modular design. In the past two decades, membrane-based separation technologies have been increasingly used for a wide range of applications.

Membrane-based separation technologies such as microfiltration (MF), ultrafiltration (UF) and nanofiltration (NF) are routinely used for treatment of various wastewaters [22]. MF and UF are not usually used for TDS removal due to their relatively large pore sizes. RO and NF are frequently used for water recovery from saline wastewaters. RO is used for desalination of seawater to produce drinking water [23]. NF and RO are very effective and applicable desalination process for treatment of low TDS waters (NF: TDS <15,000 mg L^{-1}, RO: TDS <47,000 mg L^{-1}) [24]. However, RO and NF can achieve only moderate water recovery for high TDS concentrations due to very high feed pressure required to overcome the osmotic back-pressure. In addition, membrane fouling and scaling are primary concerns when operating NF and RO systems [25]. The feed water requires rigorous pre-treatment to prevent fouling of the NF/RO membrane

[25,26]. Many new processes involving osmotically and thermally driven membrane technologies are being investigated for desalination of highly impaired wastewaters [23,27].

In our studies, we will investigate the potential of membrane-based separation processes for treatment of high TDS HFPW streams. The overall goal of this work is to develop a cost-effective membrane-based process that leads to a very high TDS concentrate and a clean effluent. We will investigate three promising technologies:

- Membrane Distillation (MD)
- Forward Osmosis (FO)
- Integrated FO-MD

1.2. Membrane Distillation

Treatment of very high TDS streams is possible using distillation technologies. MD is a very promising technology for treating high TDS wastewater streams [27]. MD is a physical separation process whereby the separation takes place by means of a vapor pressure gradient across a microporous hydrophobic membrane. The vapor pressure difference across the membrane is the driving force for vapor transport [28]. A number of methods have been employed to establish the driving force across the MD membrane and each method has led to a specific MD configuration. The permeate side of the MD membrane may consist of a condensing liquid in direct contact with the microporous membrane (DCMD), a sweeping gas stream (SGMD), a cold condensing surface separated by an air gap (AGMD), or a vacuum (VMD). In the most common arrangement of MD, DCMD, the hot saline feed is passed on one side of a hydrophobic microporous membrane. The membrane acts as a thermal insulator as well as a physical barrier between the hot feed and the

cold distillate that flow on opposite side of the membrane. Water and other volatile components vaporize from the hot feed, pass through the membrane pores and condense on the distillate side. Here, we focus on DCMD configuration. Figure 1 illustrates the concept of DCMD for water recovery from PW.

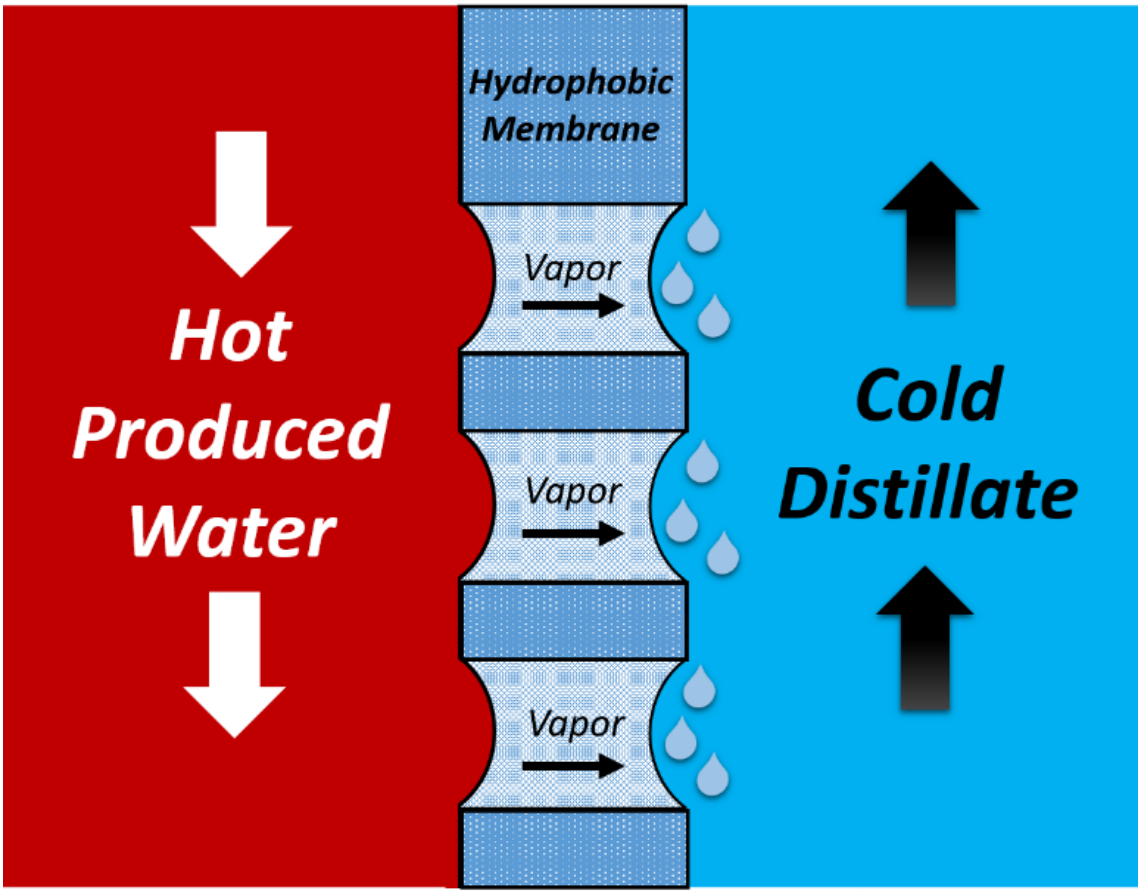

Figure 1. DCMD concept.

The nature of the driving force in MD, in synergy with the water repellent characteristic of the hydrophobic MD membrane, allows for the complete rejection of non-volatile solutes such as cations, anions, organic macromolecules, colloidal species, etc. Unlike RO, the efficiency of vapor

transport and water recovery is not significantly affected by feed salinity. Further, lower temperatures and pressures with respect to those usually used in conventional distillation columns are generally sufficient to establish considerable transmembrane fluxes, with consequent reduction of energy costs and mechanical requirements of the membrane. Typical MD feed water temperatures vary in the range of 35 – 70 ºC, thus permitting the efficient recycle of low-grade or waste heat streams, as well as the use of alternative energy sources (solar, wind, geothermal, etc.). In addition, the possibility of using plastic equipment also reduces or avoids erosion problems [29,30].

1.2.1. Mass Transfer in Membrane Distillation

Mass transport in MD can be described using the dusty gas model in terms of series resistances upon transfer between the bulks of two phases contacting the membrane according to an electrical analogy [31]. Figure 2 presents the possible mass transfer resistances across a hydrophobic membrane in MD. Mass transfer boundary layers could result in a substantial contribution to the overall mass transfer resistance. However, molecular and Knudsen diffusion across the membrane often represents the dominant resistance. The mass transfer resistances within the membrane thickness are associated with molecular, Knudsen and surface diffusion mechanisms as well as viscous transport [32].

A number of models have been developed in the literature in order to describe the MD mass transfer [33]. The differences between these models may be linked to the arrangement of the transport resistances in the analog circuit. In most cases, one or more of the resistances may be eliminated. As an example, in most VMD systems the number of molecule-molecule collisions is negligible compared to the number of molecule-pore wall collisions, as the average pore size of

the membrane is often significantly smaller than the mean free path of water vapor molecules. Thus, the molecular diffusion may be eliminated and VMD may be modeled as a Knudsen diffusion limited process. In addition, resistance to mass transfer on the distillate side can be omitted in VMD. This resistance is also neglected when MD operates with pure water as distillate stream in DCMD mode.

For hydrophobic MD membranes with air-filled pores in the range of 0.1 to 0.5 μm, molecule-pore wall collisions can happen as frequently as molecule-molecule collisions, and the Knudsen resistance along with molecular resistance may be considered as dominating mass transfer resistances, while for smaller pore sizes (e.g. < 0.05 μm), molecule-pore wall collisions mostly occur and Knudsen diffusion will be dominant. As can be seen, a pathway for surface diffusion is shown in Figure 2, but this mechanism is considered negligible in MD as the surface diffusion area is relatively small compared to the pore area [34].

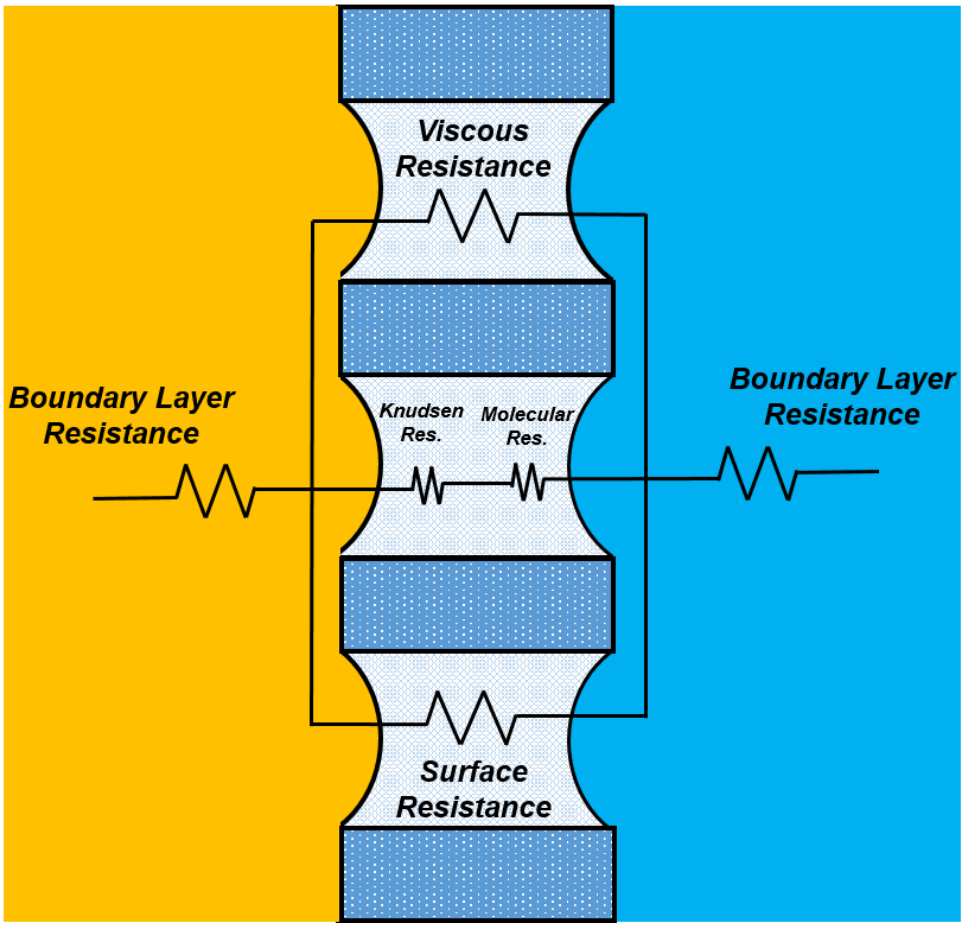

Figure 2. Mass transfer in MD according to circuit electrical analogy.

1.2.2. Heat Transfer in Membrane Distillation

In general, the relations between heat and mass transfer are described in terms of a number of resistances starting from the boundary layers and through the membrane itself [35]. Figure 3 illustrates the heat transfer resistance across a hydrophobic MD membrane using electrical circuit analogy. Analogous to the case of mass transfer, simplifications deriving from the possibility to omit one or more resistances can be made for specific MD configurations.

The heat transport across the MD membrane takes place according to heat conduction

across the membrane material as well as the latent heat flow associated with the mass flux [36]. Heat transfer across the boundary layers is often recognized as the rate-limiting step in MD mass flux since heat must be supplied to the feed surface of the MD membrane in order to vaporize the water. A number of efforts have been considered regarding minimization of the external boundary layer resistances including use of spacers as well as turbulent flow [37]. The magnitude and impact of boundary layer resistances is commonly described using temperature polarization phenomena, whereby the bulk temperature on the feed and distillate side of the membrane differ from the temperature at the membrane surface. Boundary layer heat transfer coefficients are usually estimated using empirical correlations (e.g. Sieder-Tate correlation) [38].

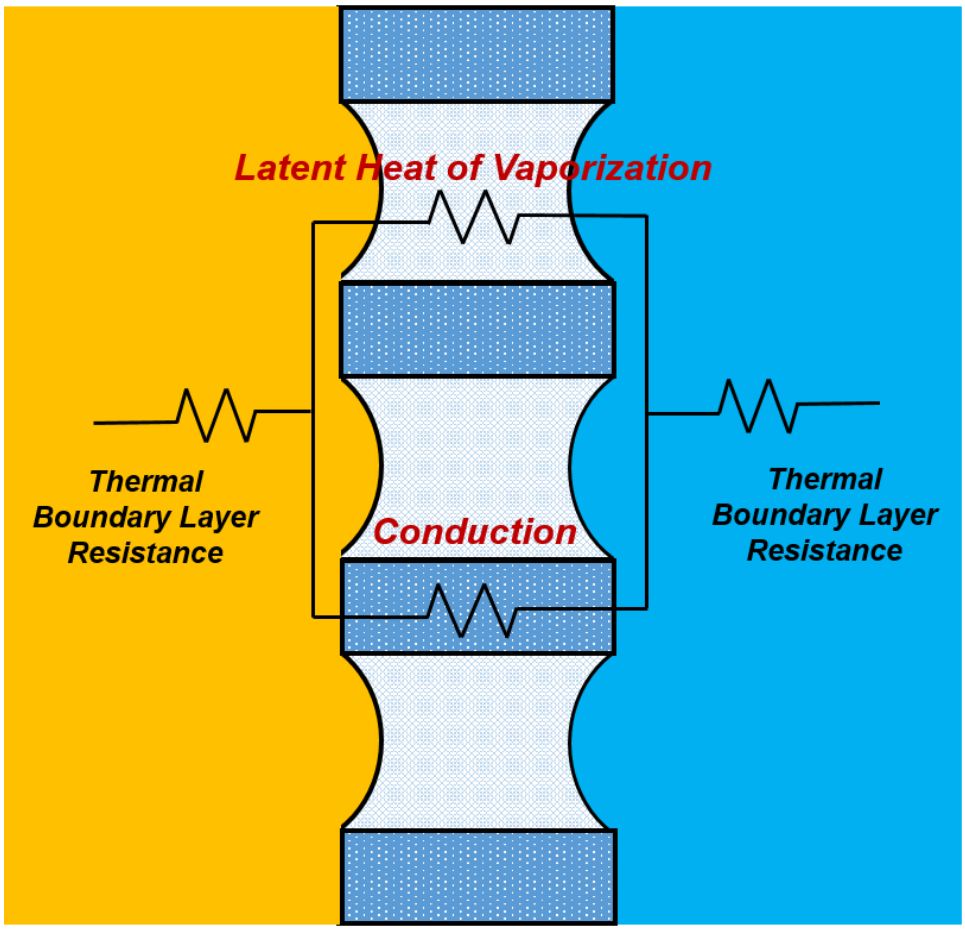

Figure 3. Heat transfer in MD according to circuit electrical analogy.

1.3. Forward Osmosis

FO has also been proposed as a new membrane-based separation technology for treating high salinity PWs [39]. Osmosis is defined as the net movement of water across a semi-permeable membrane driven by a difference in osmotic pressure across the membrane [40]. In FO, a draw solution, having a significantly higher osmotic pressure than the feed, flows on the permeate side of the membrane. Due to the osmotic pressure gradient, water flows from the feed to the draw solution. Using dense non-porous membranes with rejection properties similar to RO membranes, the feed solution is concentrated and the draw solution diluted [40,41]. The advantages of FO include a high rate of water recovery, minimization of brine discharge, low fouling and low energy consumption [42]. However, the viability of FO depends on efficient regeneration of the draw solution. The availability of low-grade waste heat during oil and gas extraction and production activities provides the possibility of using a thermolytic salt such as sodium bicarbonate, as a draw solute, which can be easily regenerated by heating. Figure 4 represents the concept of FO.

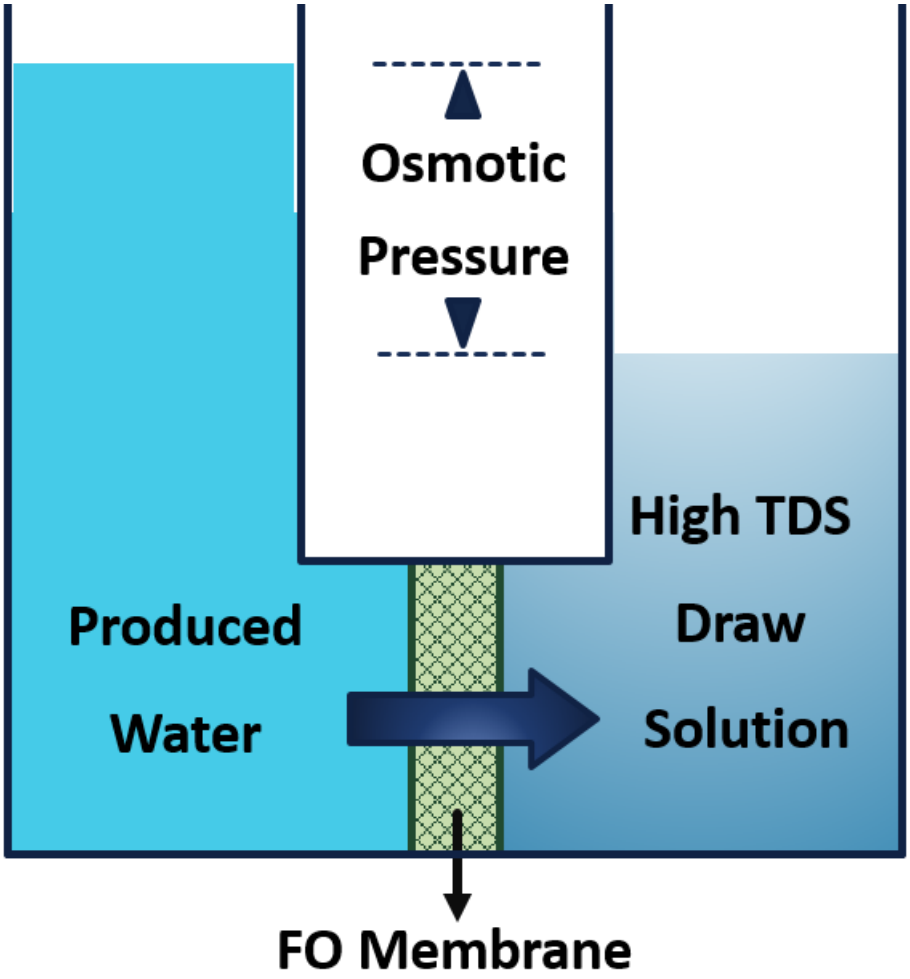

Figure 4. FO concept.

The concept of using FO for seawater desalination was introduced decades ago. However, most efforts in the FO area were ended soon due to the followings: (1) ineffective semi-permeable membranes, which are the heart of desalination systems, (2) lack of effective draw solutes for desalination, and (3) elevated costs associated with draw solution regeneration [43]. FO has been investigated in a wide range of applications in three general areas: water, energy and life sciences. These applications include water desalination, wastewater treatment, power generation and food processing. Here, we focus on the application of FO for treatment of high salinity produced waters.

1.3.1. Mass Transfer in Forward Osmosis

Water transport in osmotic-driven membrane processes takes by diffusion of water molecules through a semi-permeable salt-rejecting membrane. This transport is driven by the osmotic pressure difference across the FO membrane. Figure 5 shows a conceptual illustration of mass transfer across a semi-permeable FO membrane. In this figure, $\Delta\pi$ represents the osmotic pressure difference across the membrane, while C represents the solute concentration at each location. As can be seen in Figure 5, the osmotic pressure difference across the active layer is much lower than the bulk osmotic pressure difference. This deference can result in much lower permeate flux than expected [25,44]. The diminished permeate flux is often related to a number of membrane-associated transport phenomena; Specifically, internal and external concentration polarization [45].

In pressure-driven and osmotic-driven membrane processes, convective permeate flow leads to solute build-up on the active layer of the membrane. This behavior is referred to as concentrative external concentration polarization. At the same time, the draw solution is being diluted at the permeate side of the membrane by the permeating water. This is referred to as dilutive external concentration polarization [40]. FO membranes are often composite or asymmetric membranes consisting of a dense active layer and a porous support. As water permeates across the active layer of the FO membrane, the draw solution within the porous support becomes diluted and creates a different type of polarization referred to as dilutive internal concentration polarization. Both concentrative and dilutive external concentration polarization as well as internal concentration polarization within the membrane support affect the water flux adversely as they reduce the effective osmotic pressure difference across the FO membrane [41].

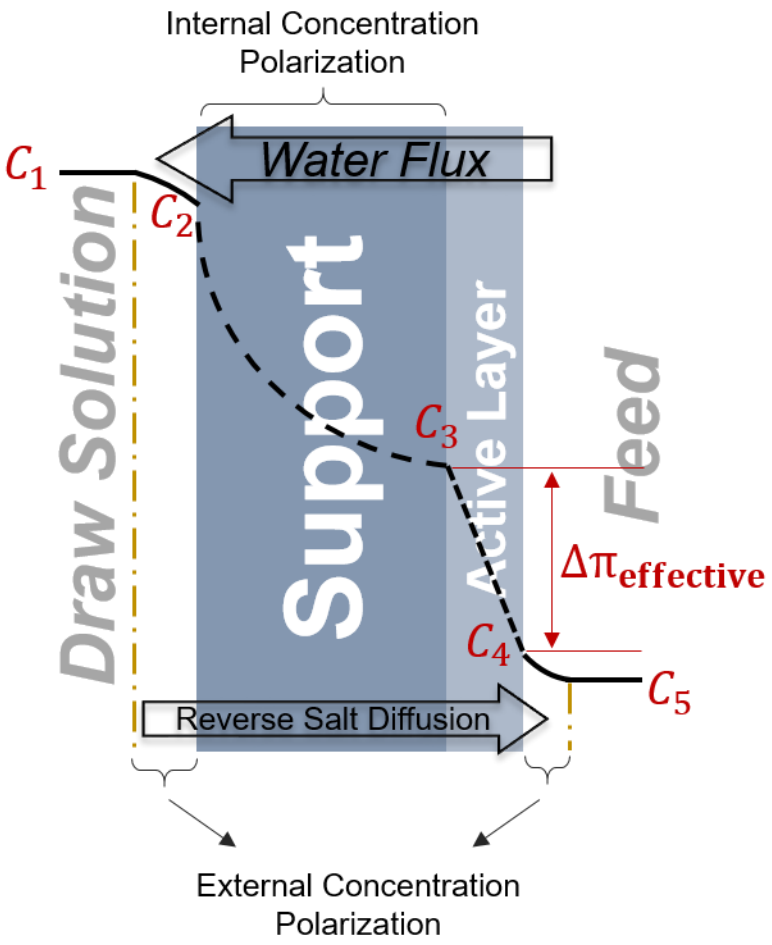

Figure 5. Mass transfer in FO.

1.4. Integrated Forward Osmosis-Membrane Distillation

The integrated FO-MD system is a membrane-based hybrid technology [46]. During the operation of the FO process, the concentration of draw solution decreases due to dilution; thus, the driving force decreases with the operational time. MD has great potential to be integrated with FO as it can offer complete rejection of nonvolatile substances in the feed solution. In addition, the efficiency of the MD process is relatively independent of salt concentration in the feed solution.

In a FO-MD hybrid system, the FO section draws water from the feed solution, while the MD process re-concentrates the diluted draw solution and produces pure water. The integration of FO and MD processes combines the strengths of both processes and can provide high permeate quality (produced by MD) and low fouling tendency. So far, only a limited number of studies on FO-MD have been reported for solution concentration and wastewater treatment [47,48]. The current investigation aims to demonstrate the feasibility and stability of the hybrid FO-MD process in water recovery from high salinity PW streams. Figure 6 shows the concept of integrated FO-MD process.

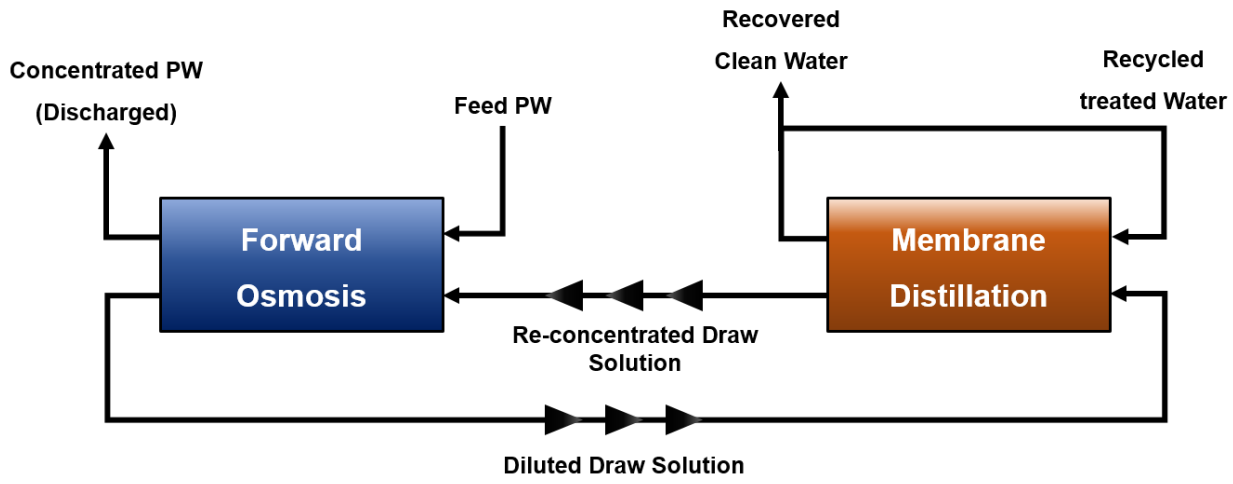

Figure 6. Integrated FO-MD process concept.

1.5. Membrane Fouling and Pretreatment

All membrane processes suffer from fouling. Fouling is one of the main limitations to faster development of membrane-based processes. Membrane fouling is characterized as a reduction of permeate flux as a result of increased flow resistance [49]. Fouling is mainly caused by adsorption of organic material on the membrane surface and/or pore blocking, and by inorganic

scaling due to the precipitation of minerals [50]. The likelihood of each one of these fouling mechanisms depends on a number of factors including the nature of the driving force, membrane characteristics, membrane material, operating conditions, etc. While the immediate effect of fouling is to cause a reduction in permeate flux, the long-term effects may lead to irreversible fouling and the reduction of membrane lifetime [51,52]. Various techniques can be used to reduce membrane fouling including backwashing, air sparing, chemical cleaning and feed pretreatment [53].

Numerous pretreatment processes have been considered prior to membrane filtration [51]. Biological pretreatment is impractical for treating HFPWs due to long retention times and the low biodegradability of most of the contaminants [54]. Coagulation, adsorption, preoxidation and prefiltration are among the most popular pretreatment methods prior to membrane filtration [55]. Chemical pretreatment such as coagulation is frequently used to remove colloidal and organic matter [55]. Here we focus on electrocoagulation (EC) for removal of colloidal and dissolved organic compounds that could foul the MD or FO membrane.

1.5.1. Electrocoagulation

EC is an electrochemical method for treating polluted water whereby sacrificial anodes (here we use aluminum) corrode to release active coagulant precursors into solution [56]. Compared to chemical coagulation e.g. using alum, EC provides a number of advantages including simple equipment, easy operation, less maintenance, colorless and odorless effluent, low sludge production and efficient removal of colloidal particles. Flocs formed by EC are similar to chemical flocs, except that EC flocs tends to be much larger, contain less bound water, are acid-resistant and more stable, and therefore, can be separated faster [57,58]. Further, in EC, there are no moving

parts; thus, requiring less maintenance compared to coagulation where efficient mixing is required. Use of electricity, which can be expensive in many places, and regular replacement of sacrificial electrodes are two major disadvantages of EC technology [57,59,60]. However, Kobya et al. [57] indicate that electrical energy consumption of EC decreases dramatically when the wastewater has higher conductivity due to the presence of dissolved salts. In case of HFPW, the conductivity is high due to high TDS.

In EC, sacrificial electrodes are utilized to release coagulant counter ions into solution using electricity. The following electrode reactions occur at the anode, cathode and consequently, in the solution [61]:

At the anode: $$M_{(s)} \rightarrow M_{(aq)}^{n+} + ne^{-} \quad (1)$$

At the cathode: $$2H_2O + 2e^{-} \rightarrow 2OH^{-} + H_2 \quad (2)$$

where *M* is the electrode metal material (usually *Al* or *Fe*). Analogous to chemical coagulation, the metal and hydroxide ions form various monomeric species such as $M(OH)^{(n-1)+}$, $M(OH)_2^{(n-2)+}$ and also polymeric species such as $M_6(OH)_{15}^{(6n-15)+}$ [62,63]. As the solution 'ages', polynuclear complexes develop and amorphous $M(OH)_{n(s)}$ forms in the solution, as given by the following general scheme, according to complex precipitation kinetics [57]:

In solution: $$M_{(aq)}^{n+} + nOH^{-} \rightarrow M(complex) \rightarrow M(OH)_{n(s)} \quad (3)$$

Metal complexes eventually transform to solid $M(OH)_{n(s)}$ with a large surface area that can adsorb organic compounds, trap suspended particles and form flocs. Finally, $M(OH)_{n(s)}$ flocs (with

adsorbed organics and colloidal particles) will polymerize and deposit according to the following reaction [64]:

$$x\,M(OH)_n \rightarrow M_x(OH)_{xn} \quad (4)$$

While the fundamental chemical basis for chemical coagulation (e.g. alum or ferric chloride coagulation) and EC are similar, EC has gained significant attention from many researchers due to its advantages including: reduced sludge production, lack of moving parts and added chemicals, ease of operation, minimal pH decrease (alkalinity consumption) and low operating costs [65–67]. EC also has the potential for treating oily wastewaters, where the presence of an electric current can contribute to the electro-coalescence of oil droplets [68]. We investigate the impact of PW pretreatment via EC prior to FO and MD for fouling mitigation and water recovery. We design and develop an EC system as a pre-treatment operation.

1.6. Research Objectives

1.6.1. Membrane Distillation Studies

Here, we screen and characterize a number of commercially available microporous hydrophobic membranes to be tested in MD system. Using bulk membrane properties, we calculate a structural parameter that allows prediction of which membranes will display the highest permeate flux. We investigate feed pretreatment and membrane regeneration regarding fouling mitigation in MD and run long-term MD experiments. The following lists the objectives of the MD investigations:

- Objective (1): Estimate performance of MD membranes using membrane properties.

- Objective (2): Determine the practical limit for the maximum TDS in the concentrate stream from MD.
- Objective (3): Investigate application of MD for treating actual high TDS HFPW.
- Objective (3): Investigate cleaning and EC-pretreatment strategies for fouling mitigation.
- Objective (4): Develop cost curves for MD.

1.6.2. Forward Osmosis Studies

In this work, the performance of FO for water recovery from high TDS PW streams is evaluated. We design and stablish a lab-scale FO system and carry out water recovery experiments with synthetic and real HFPW. In addition, we simulate the FO process in MatLab and estimate the performance of the FO system using the developed code. We introduce a new definition for water permeability coefficient to better model the FO water flux when the fouling layer forms on the membrane surface. Moreover, we investigate the use EC pretreatment to mitigate fouling during FO. In general, the following research objectives will be followed:

- Objective (1): Investigate application of FO for treating HFPW.
- Objective (2): Study effects of EC-pretreatment prior to FO.
- Objective (3): Model FO system water flux for treating actual HFPW.

1.6.3. Integrated Forward Osmosis-Membrane Distillation

Here, we evaluate the application of the FO-MD process for treating synthetic and actual HFPWs samples obtained from Marcellus and Fayetteville shale. We aim to demonstrate the feasibility and stability of the integrated FO-MD process in water recovery from these high salinity PW streams. We show that this process integration can be used to systematically enhance and

reconcile various project objectives, such as cost effectiveness, recovery and energy efficiency. Followings lists the FO-MD research objectives:

- Objective (1): Investigate application of FO-MD for treating HFPW.
- Objective (2): Determine practical recovery rates in FO-MD.
- Objective (3): Conduct cyclic experiments with hybrid FO-MD process.

Symbols

AGMD	Air gap membrane distillation
DCMD	Direct contact membrane distillation
EC	Electrocoagulation
FO	Forward osmosis
HFPW	Hydraulic fracturing produced water
Membrane distillation	MD
MF	Microfiltration
NF	Nanofiltration
O&G	Oil and grease
PW	Produced water
RO	Reverse osmosis
SS	Suspended solids
SGMD	Sweep gas membrane distillation
TDS	Total dissolved solids
UF	Ultrafiltration
UV	Ultraviolent
USGS	United states geological survey
VMD	Vacuum membrane distillation

References

[1] A. Fakhru'l-Razi, A. Pendashteh, L.C. Abdullah, D.R.A. Biak, S.S. Madaeni, Z.Z. Abidin, Review of technologies for oil and gas produced water treatment, J. Hazard. Mater. 170 (2009) 530–551. doi:10.1016/j.jhazmat.2009.05.044.

[2] G.T. Tellez, N. Nirmalakhandan, J.L. Gardea-Torresdey, Performance evaluation of an activated sludge system for removing petroleum hydrocarbons from oilfield produced water, Adv. Environ. Res. 6 (2002) 455–470. doi:10.1016/S1093-0191(01)00073-9.

[3] C. Clark, J. Veil, Produced Water Volumes and Management Practices in the United States, Argonne Natl. Lab. Rep. (2009) 64. doi:10.2172/1007397.

[4] K.B. Gregory, R.D. Vidic, D.A. Dzombak, Water management challenges associated with the production of shale gas by hydraulic fracturing, Elements. 7 (2011) 181–186. doi:10.2113/gselements.7.3.181.

[5] J. Arthur, B. Langhus, C. Patel, Technical Summary of Oil & Gas Produced Water Treatment Technologies, Tulsa, Oklahoma, USA, ALL …. (2005) 1–53. http://w.all-llc.com/publicdownloads/ALLConsulting-WaterTreatmentOptionsReport.pdf.

[6] M. Eftekhardadkhah, K.N. Kløcker, H.H. Trapnes, B. Gaweł, G. Øye, Composition and Dynamic Adsorption of Crude Oil Components Dissolved in Synthetic Produced Water at Different pH Values, Ind. Eng. Chem. Res. 55 (2016) 3084–3090. doi:10.1021/acs.iecr.5b04459.

[7] J. Rubio, M.L. Souza, R.W. Smith, Overview of flotation as a wastewater treatment technique, Miner. Eng. 15 (2002) 139–155. doi:10.1016/S0892-6875(01)00216-3.

[8] M. Padaki, R. Surya Murali, M.S. Abdullah, N. Misdan, A. Moslehyani, M.A. Kassim, N. Hilal, A.F. Ismail, Membrane technology enhancement in oil-water separation. A review, Desalination. 357 (2015) 197–207. doi:10.1016/j.desal.2014.11.023.

[9] M. Owlad, M.K. Aroua, W.A.W. Daud, S. Baroutian, Removal of hexavalent chromium-contaminated water and wastewater: A review, Water. Air. Soil Pollut. 200 (2009) 59–77. doi:10.1007/s11270-008-9893-7.

[10] V.K. Gupta, I. Ali, T.A. Saleh, A. Nayak, S. Agarwal, Chemical treatment technologies for waste-water recycling—an overview, RSC Adv. 2 (2012) 6380. doi:10.1039/c2ra20340e.

[11] N. Esmaeilirad, K. Carlson, P. Omur Ozbek, Influence of softening sequencing on electrocoagulation treatment of produced water, J. Hazard. Mater. 283 (2015) 721–729. doi:10.1016/j.jhazmat.2014.10.046.

[12] A. Vengosh, R.B. Jackson, N. Warner, T.H. Darrah, A. Kondash, A critical review of the risks to water resources from unconventional shale gas development and hydraulic fracturing in the United States, Environ. Sci. Technol. 48 (2014) 8334–8348. doi:10.1021/es405118y.

[13] U.S.E.I. Administration, Technically Recoverable Shale Oil and Shale Gas Resources : An Assessment of 137 Shale Formations in 41 Countries Outside the United States, U.S. Energy Inf. Adm. 2013 (2013) 76 pp. doi:www.eia.gov/analysis/studies/worldshalegas/.

[14] U.S. Energy Information Administration (EIA), (n.d.). https://www.eia.gov/tools/faqs/faq.php?id=907&t=8 (accessed January 17, 2018).

[15] O.R. Lokare, S. Tavakkoli, S. Wadekar, V. Khanna, R.D. Vidic, Fouling in direct contact membrane distillation of produced water from unconventional gas extraction, J. Memb. Sci. 524 (2017) 493–501. doi:10.1016/j.memsci.2016.11.072.

[16] Induced Earthquakes, (n.d.). https://earthquake.usgs.gov/research/induced/myths.php (accessed August 30, 2017).

[17] H. Thomas, Sampling and Analysis of Water Streams Associated with the Development of Marcellus Shale Gas, Final Rep. Marcellus Shale Coalit. (2009) 249 pp.

[18] A. Fakhru'l-Razi, A. Pendashteh, L.C. Abdullah, D.R.A. Biak, S.S. Madaeni, Z.Z. Abidin, Review of technologies for oil and gas produced water treatment, J. Hazard. Mater. 170 (2009) 530–551. doi:10.1016/j.jhazmat.2009.05.044.

[19] A.J. Kondash, E. Albright, A. Vengosh, Quantity of flowback and produced waters from unconventional oil and gas exploration, Sci. Total Environ. 574 (2017) 314–321. doi:10.1016/j.scitotenv.2016.09.069.

[20] R.L. McGinnis, N.T. Hancock, M.S. Nowosielski-Slepowron, G.D. McGurgan, Pilot demonstration of the NH3/CO2 forward osmosis desalination process on high salinity brines, Desalination. 312 (2013) 67–74. doi:10.1016/j.desal.2012.11.032.

[21] M. Takht Ravanchi, T. Kaghazchi, A. Kargari, Application of membrane separation processes in petrochemical industry: a review, Desalination. 235 (2009) 199–244. doi:10.1016/j.desal.2007.10.042.

[22] S. Munirasu, M.A. Haija, F. Banat, Use of membrane technology for oil field and refinery produced water treatment—A review, Process Saf. Environ. Prot. 100 (2016) 183–202. doi:10.1016/j.psep.2016.01.010.

[23] T.Y. Cath, Osmotically and thermally driven membrane processes for enhancement of water recovery in desalination processes, Desalin. Water Treat. 15 (2010) 279–286. doi:10.5004/dwt.2010.1760.

[24] J. Drewes, T. Cath, P. Xu, J. Graydon, An Integrated Framework for Treatment and Management of Produced Water, Tech. Assess. Prod. Water Treat. Technol. (2009) 8–128. http://www.rpsea.org/media/files/user/cath1.pdf.

[25] B.D. Coday, P. Xu, E.G. Beaudry, J. Herron, K. Lampi, N.T. Hancock, T.Y. Cath, The sweet spot of forward osmosis: Treatment of produced water, drilling wastewater, and other complex and difficult liquid streams, Desalination. 333 (2014) 23–35. doi:10.1016/j.desal.2013.11.014.

[26] C. Fritzmann, J. Löwenberg, T. Wintgens, T. Melin, State-of-the-art of reverse osmosis desalination, Desalination. 216 (2007) 1–76. doi:10.1016/j.desal.2006.12.009.

[27] F. Edwie, T.S. Chung, Development of hollow fiber membranes for water and salt recovery from highly concentrated brine via direct contact membrane distillation and crystallization, J. Memb. Sci. 421–422 (2012) 111–123. doi:10.1016/j.memsci.2012.07.001.

[28] D. Singh, K.K. Sirkar, Desalination of brine and produced water by direct contact

membrane distillation at high temperatures and pressures, J. Memb. Sci. 389 (2012) 380–388. doi:10.1016/j.memsci.2011.11.003.

[29] C. Charcosset, R. Kieffer, D. Mangin, F. Puel, Coupling between Membrane Processes and Crystallization Operations, Ind. Eng. Chem. Res. 49 (2010) 5489–5495. doi:10.1021/ie901824x.

[30] E. Drioli, M. Romano, Progress and New Perspectives on Integrated Membrane Operations for Sustainable Industrial Growth, Ind. Eng. Chem. Res. 40 (2001) 1277–1300. doi:10.1021/IE0006209.

[31] E. Curcio, E. Drioli, Membrane Distillation and Related Operations—A Review, Sep. Purif. Rev. 34 (2005) 35–86. doi:10.1081/SPM-200054951.

[32] A. Alkhudhiri, N. Darwish, N. Hilal, Membrane distillation: A comprehensive review, Desalination. 287 (2012) 2–18. doi:10.1016/j.desal.2011.08.027.

[33] H. Susanto, Towards practical implementations of membrane distillation, Chem. Eng. Process. Process Intensif. 50 (2011) 139–150. doi:10.1016/j.cep.2010.12.008.

[34] R.B. Saffarini, B. Mansoor, R. Thomas, H.A. Arafat, Effect of temperature-dependent microstructure evolution on pore wetting in PTFE membranes under membrane distillation conditions, J. Memb. Sci. 429 (2013) 282–294. doi:10.1016/j.memsci.2012.11.049.

[35] L.M. Camacho, L. Dumée, J. Zhang, J. de Li, M. Duke, J. Gomez, S. Gray, Advances in membrane distillation for water desalination and purification applications, Water (Switzerland). 5 (2013) 94–196. doi:10.3390/w5010094.

[36] K.W. Lawson, D.R. Lloyd, Membrane distillation, J. Memb. Sci. 124 (1997) 1–25. doi:10.1016/S0376-7388(96)00236-0.

[37] M.S. El-Bourawi, Z. Ding, R. Ma, M. Khayet, A framework for better understanding membrane distillation separation process, J. Memb. Sci. 285 (2006) 4–29. doi:10.1016/j.memsci.2006.08.002.

[38] G. Rao, S.R. Hiibel, A.E. Childress, Simplified flux prediction in direct-contact membrane distillation using a membrane structural parameter, Desalination. 351 (2014) 151–162. doi:10.1016/j.desal.2014.07.006.

[39] K.L. Hickenbottom, N.T. Hancock, N.R. Hutchings, E.W. Appleton, E.G. Beaudry, P. Xu, T.Y. Cath, Forward osmosis treatment of drilling mud and fracturing wastewater from oil and gas operations, Desalination. 312 (2013) 60–66. doi:10.1016/j.desal.2012.05.037.

[40] T. CATH, A. CHILDRESS, M. ELIMELECH, Forward osmosis: Principles, applications, and recent developments, J. Memb. Sci. 281 (2006) 70–87. doi:10.1016/j.memsci.2006.05.048.

[41] J.R. McCutcheon, R.L. McGinnis, M. Elimelech, A novel ammonia-carbon dioxide forward (direct) osmosis desalination process, Desalination. 174 (2005) 1–11. doi:10.1016/j.desal.2004.11.002.

[42] Q. Ge, M. Ling, T.S. Chung, Draw solutions for forward osmosis processes: Developments, challenges, and prospects for the future, J. Memb. Sci. 442 (2013) 225–237. doi:10.1016/j.memsci.2013.03.046.

[43] T.-S. Chung, S. Zhang, K.Y. Wang, J. Su, M.M. Ling, Forward osmosis processes: Yesterday, today and tomorrow, Desalination. 287 (2012) 78–81. doi:10.1016/j.desal.2010.12.019.

[44] J.R. McCutcheon, M. Elimelech, Influence of concentrative and dilutive internal concentration polarization on flux behavior in forward osmosis, J. Memb. Sci. 284 (2006) 237–247. doi:10.1016/j.memsci.2006.07.049.

[45] A. Seppälä, M.J. Lampinen, On the non-linearity of osmotic flow, Exp. Therm. Fluid Sci. 28 (2004) 283–296. doi:10.1016/j.expthermflusci.2003.10.001.

[46] Q. Liu, C. Liu, L. Zhao, W. Ma, H. Liu, J. Ma, Integrated forward osmosis-membrane distillation process for human urine treatment, Water Res. 91 (2016) 45–54. doi:10.1016/j.watres.2015.12.045.

[47] T.Y. Cath, D. Adams, A.E. Childress, Membrane contactor processes for wastewater reclamation in space: II. Combined direct osmosis, osmotic distillation, and membrane distillation for treatment of metabolic wastewater, J. Memb. Sci. 257 (2005) 111–119. doi:10.1016/j.memsci.2004.07.039.

[48] K.Y. Wang, M.M. Teoh, A. Nugroho, T.S. Chung, Integrated forward osmosis-membrane distillation (FO-MD) hybrid system for the concentration of protein solutions, Chem. Eng. Sci. 66 (2011) 2421–2430. doi:10.1016/j.ces.2011.03.001.

[49] A.L. Lim, R. Bai, Membrane fouling and cleaning in microfiltration of activated sludge wastewater, J. Memb. Sci. 216 (2003) 279–290. doi:10.1016/S0376-7388(03)00083-8.

[50] B. Van Der Bruggen, C. Vandecasteele, T. Van Gestel, W. Doyen, R. Leysen, A review of pressure-driven membrane processes in wastewater treatment and drinking water production, Environ. Prog. 22 (2003) 46–56. doi:10.1002/ep.670220116.

[51] W. Guo, H.H. Ngo, J. Li, A mini-review on membrane fouling, Bioresour. Technol. 122 (2012) 27–34. doi:10.1016/j.biortech.2012.04.089.

[52] D.M. Warsinger, J. Swaminathan, E. Guillen-Burrieza, H.A. Arafat, J.H. Lienhard V, Scaling and fouling in membrane distillation for desalination applications: A review, Desalination. 356 (2015) 294–313. doi:10.1016/j.desal.2014.06.031.

[53] K. Kimura, Y. Hane, Y. Watanabe, G. Amy, N. Ohkuma, Irreversible membrane fouling during ultrafiltration of surface water, Water Res. 38 (2004) 3431–3441. doi:10.1016/j.watres.2004.05.007.

[54] E. Metcalf, H. Eddy, Wastewater engineering: treatment and reuse, 2003. doi:10.1016/0309-1708(80)90067-6.

[55] H. Huang, K. Schwab, J.G. Jacangelo, Pretreatment for Low Pressure Membranes in Water Treatment: A Review, Environ. Sci. Technol. 43 (2009) 3011–3019. doi:10.1021/es802473r.

[56] P.K. Holt, G.W. Barton, C.A. Mitchell, The future for electrocoagulation as a localized water treatment technology., Chemosphere. 59 (2005) 355–367. doi:10.1016/j.chemosphere.2004.10.023.

[57] M. Kobya, O.T. Can, M. Bayramoglu, Treatment of textile wastewaters by electrocoagulation using iron and aluminum electrodes, J. Hazard. Mater. 100 (2003) 163–

178. doi:10.1016/S0304-3894(03)00102-X.

[58] E. Butler, Y.-T. Hung, R.Y.-L. Yeh, M. Suleiman Al Ahmad, Electrocoagulation in Wastewater Treatment, Water. 3 (2011) 495–525. doi:10.3390/w3020495.

[59] M.Y. Mollah, R. Schennach, J.R. Parga, D.L. Cocke, Electrocoagulation (EC)--science and applications., J. Hazard. Mater. 84 (2001) 29–41. doi:10.1016/S0304-3894(01)00176-5.

[60] O. Sahu, B. Mazumdar, P.K. Chaudhari, Treatment of wastewater by electrocoagulation: A review, Environ. Sci. Pollut. Res. 21 (2014) 2397–2413. doi:10.1007/s11356-013-2208-6.

[61] T. Picard, G. Cathalifaud-Feuillade, M. Mazet, C. Vandensteendam, Cathodic dissolution in the electrocoagulation process using aluminium electrodes., J. Environ. Monit. 2 (2000) 77–80. doi:10.1039/a908248d.

[62] K. Sardari, P. Fyfe, D. Lincicome, S.R. Wickramasinghe, Aluminum electrocoagulation followed by forward osmosis for treating hydraulic fracturing produced waters, Desalination. 428 (2018) 172–181. doi:10.1016/j.desal.2017.11.030.

[63] Electrocoagulation treatment of raw landfill leachate using iron-based electrodes: Effects of process parameters and optimization, J. Environ. Manage. 204 (2017) 75–81. doi:10.1016/J.JENVMAN.2017.08.028.

[64] M. Rebhun, M. Lurie, Control of organic matter by coagulation and floc separation, in: Water Sci. Technol., 1993: pp. 1–20.

[65] Electrocoagulation for the treatment of textile industry effluent – A review, J. Environ. Manage. 128 (2013) 949–963. doi:10.1016/J.JENVMAN.2013.06.043.

[66] B. Zhu, D.A. Clifford, S. Chellam, Comparison of electrocoagulation and chemical coagulation pretreatment for enhanced virus removal using microfiltration membranes, Water Res. 39 (2005) 3098–3108. doi:10.1016/j.watres.2005.05.020.

[67] Electrocoagulation treatment of raw landfill leachate using iron-based electrodes: Effects of process parameters and optimization, J. Environ. Manage. 204 (2017) 75–81. doi:10.1016/J.JENVMAN.2017.08.028.

[68] A comprehensive review of electrocoagulation for water treatment: Potentials and challenges, J. Environ. Manage. 186 (2017) 24–41. doi:10.1016/J.JENVMAN.2016.10.032.

Chapter 2. Selecting Membranes for Treating Hydraulic Fracturing Produced Waters by Membrane Distillation

Abstract

Membrane distillation is an emerging technology for treating highly impaired wastewaters. Here a number of commercial membranes have been tested. Bulk membrane and surface properties have been determined. Permeate flux has been determined using model 20,000 ppm NaCl feed streams. A bulk membrane structural parameter has been defined. The structural parameter is used to identify membranes that display the highest permeate fluxes. These membranes were tested with 100,000 ppm NaCl solutions. The maximum feed concentration was determined. For model low-fouling feed streams, membrane surface properties such as hydrophobicity and roughness have less effect on permeate flux than bulk membrane properties.

2.1. Introduction

Water is a tremendously valuable natural resource. Thus harnessing new water resources is of tremendous societal importance [1]. Produced water, water that is co-produced during oil and gas extraction, is a major source of oily water [2] Production of oil and gas from non-traditional sources such as tar sands, oil shale and coal bed methane has expanded greatly in recent years. Development of new horizontal drilling and hydraulic fracturing techniques has led to significant new energy resources [3]. Hydraulic fracturing produced waters are subset of produced waters which often have very high salinity. The concentration of total dissolved solids (TDS) can be as high as 360,000 mg L^{-1}, more than an order of magnitude higher than sea water [4]. Treatment of

these highly impaired wastewaters is a major challenge due to the presence of high TDS and organic contaminants [5].

Pressure driven membrane processes such as reverse osmosis are impractical for treating very high salinity wastewaters due to the high osmotic back pressure that must be overcome. Desalination technologies that are being investigated include: mechanical vapour compression[6], electrodialysis [7], ion-concentration-polarization desalination [8], forward osmosis [5], humidification-dehumidification [9] and membrane distillation [10,11]. Many emerging technologies such as electrodialysis, forward osmosis and membrane distillation make use of membranes. Here we focus on membrane distillation.

Treatment of very high TDS feed streams is possible using distillation technologies. Membrane distillation is a very promising technology for treating high TDS produced water [12]. The hot produced water flows on one side of a hydrophobic microporous membrane. The membrane acts as a thermal insulator as well as a physical barrier between the hot feed and the cold distillate that flow on opposite sides of the membrane. Water vaporizes from the hot feed passes through the membrane pores and condenses on the distillate side [13]. The vapor pressure difference across the membrane is the driving force for vapor transport [14]. Unlike reverse osmosis, the efficiency of vapor transport is not significantly affected by the feed TDS. Further low-grade heat, often a by-product of oil and gas production, can be used to heat the feed stream. Unlike conventional distillation it is not necessary to boil the entire feed. As long as a vapour pressure gradient exists between the feed and permeate sides, water vapour will pass from the feed to the permeate through the gas filled membrane pores.

Several investigators have considered the use of membrane distillation to treat highly concentrated feed streams [15-17]. Because dissolved salts are nonvolatile very high TDS feed streams could be concentrated (in theory) to the solubility limit. In practice, like all membrane based separation processes, fouling of the membrane by precipitation of dissolved salts as well as adsorption of organic species present in the wastewater will compromise membrane performance. Numerous membrane distillation configurations have been described [18-24]. Here we focus on direct contact membrane distillation where the microporous membrane is in direct contact with both feed and permeate streams.

One of the major impediments for commercialization of membrane distillation is the lack of optimized membranes. Maximizing permeate flux and minimizing fouling are essential when selecting a membrane. In general, membranes should display high hydrophobicity, high porosity, a uniform pore size with a narrow distribution, low tortuosity and thickness in order to maximize permeate flux and minimize fouling [25]. Rao et al. [26] indicate that ideal membrane properties will depend on the particular application. Here we focus on concentration of high TDS feed streams where fouling by dissolved organics as well precipitation of dissolved salts on the membrane surface are concerns. The presence of surfactants can lead to a reduced surface tension of the feed. These effects can lead to wetting of the membrane pores followed by direct passage of the feed through the membrane pores compromising performance [5, 19, 27]. Similar to pressure driven filtration processes, membrane performance depends on the interplay between feed properties, membrane properties and operating conditions [28]. Consequently, selection of an appropriate membrane for a membrane distillation process is complicated.

If the same feed and operating conditions are used to screen a variety of membranes, performance should depend only on the membrane properties. Previous investigators have attempted to develop a bulk membrane structural parameter that can be used to predict membrane performance [18, 29, 30]. Rao et al. [26] have investigated the feasibility of developing a membrane structural parameter in order to predict the permeate flux during direct contact membrane distillation. The structural parameter they proposed depends only on bulk membrane properties. Thus, membrane surface properties such as hydrophobicity and roughness are assumed to be less significant. However when treating high TDS feed streams, as is the case here, suppression of precipitation by salts and fouling by dissolved organics is likely to be dependent on membrane surface properties

Here we have screened a number of commercially available microporous hydrophobic membranes. We have characterized membrane surface as well as bulk properties. Using bulk membrane properties we calculate a structural parameter that predicts which membranes will display the highest permeate flux. Permeate fluxes were determined for all membranes using a model feed stream containing a 20,000 ppm (0.34 M) NaCl. We have compared the observed permeate fluxes with values obtained for the structural parameter. Importantly, we have experimentally validated the applicability of the structural parameter over a large range of membrane properties. Next membranes that displayed the highest permeate fluxes were challenged with feed streams containing 100,000 ppm (1.7 M) NaCl. The feed stream was concentrated until the permeate flux rose quickly with a concurrent rapid increase in conductivity of the permeate above 50 $\mu S\ cm^{-1}$ indicating the passage of the feed through the membrane pores. Our results suggest a semi-quantitative method based on membrane bulk and surface properties, for selecting appropriate membranes for treating high TDS produced water streams.

2.2. Material and Methods

2.2.1. Bulk Membrane Properties

Table 1 lists the 13 commercially available membranes that were sourced from 3M (Maplewood, MN), EMD Millipore (Billerica MA), Pall Corporation (Port Washington, NY), and WL Gore Associates (Newark, DE). As can be seen a range of membrane materials, ethylene chlorotrifluoroethylene (ECTFE), polypropylene, polyvinylidene fluoride (PVDF), polytetrafluoroethylene (PTFE) as well as superhydrophobic PVDF have been tested.

Table 1. Membranes tested in this study

Membrane	Material	Density (g cm^{-3})	Comment
PP-A	Polypropylene	0.9 [31]	Non-supported. Provided by 3M
PP-B			
PP-C			
ECTFE	ECTFE	1.68 [32]	
PTFE-A	PTFE	2.17 [33]	Contains polystyrene support, provided by Pall Corporation
PTFE-B	PTFE	2.17 [33]	Non-supported, provided by W. L. Gore Associates
PTFE-C			
PVDF-A	PVDF	1.78 [34]	Non-supported, provided by EMD Millipore
PVDF-B			
SH-PVDF-A	Superhydrophobic PVDF		
SH-PVDF-B			
SH-PVDF-C			
SH-PVDF-D			

2.2.1.1. Porosity

The porosity of the barrier layer was determined using the method described by Nejati et al. [34]. Briefly, for the supported PTFE membrane (Table 1) the support was initially removed. An approximately 50 cm^2 sample of each membrane was submerged in a 50 mL beaker filled with isopropanol. The beaker was sonicated for 2 hours. The membrane surface was dried to remove the excess isopropanol. The membrane was placed on a balance and the change in weight was recorded as a function of time. The point at which rate of evaporation changed was assumed to be the point where all the isopropanol on the membrane surface had evaporated and evaporation of isopropanol from the membrane pores commenced. It was assumed that once the mass of the membrane did not change over a 30 min period, all the isopropanol in the membrane pores had evaporated. The porosity, was then determined from the following equation,

$$\varepsilon = \frac{V_{pore}}{V_{total}} = \frac{\frac{m_{ipa}}{\rho_{ipa}}}{V_{pore}+V_{membrane}} = \frac{\frac{m_{ipa}}{\rho_{ipa}}}{\frac{m_{ipa}}{\rho_{ipa}}+\frac{m_{membrane}}{\rho_{membrane}}} \quad (1)$$

where V_{total}, V_{pore}, are the total membrane and membrane pore volume, ρ_{ipa}, $\rho_{membrane}$, are the densities of isopropanol and the membrane material, m_{ipa}, $m_{membrane}$ are the weight of isopropanol in the membrane pores and the weight of the membrane respectively. The density of isopropanol is 0.786 g cm^{-3} [34] while the densities of the various membrane polymers is given in Table 1. The mass of the membrane and the mass of isopropanol in the membrane pores was determined by subtraction of the membrane mass from the mass of the membrane with isopropanol filled pores.

2.2.1.2. Thickness

Scanning Electron Microscopy (SEM) using a Nova Nanolab 200 Duo-Beam Workstation (FEI, Hillsboro, Oregon) was used to obtain cross sectional images of the membranes. Membranes were fractured using liquid nitrogen. These images were used to determine the membrane thickness.

2.2.1.3. Tortuosity

Membrane tortuosity was determined by gas permeability measurements using the method described by Hwang et al. [35]. Briefly, the nitrogen flux across a 47 mm membrane disc was determined at a range of feed pressures (1-140 kPa). A needle valve was placed on both sides of the filter holder (Pall Corporation) which contained the membrane disc in order to set the mean transmembrane pressure across the membrane at 1 kPa for the range of feed pressures tested. Assuming flow through various membranes is due to contributions from Knudsen diffusion and convective Poiseuille flow, the total nitrogen flux is given by the equation:

$$N = \left(\frac{8}{3} \frac{\varepsilon r_m}{\tau \delta} \sqrt{\frac{1}{2\pi RMT}} + \frac{\varepsilon r_m^2}{\tau \delta} \frac{1}{8\eta} \frac{P_m}{RT} \right) \Delta P \qquad (2)$$

in which N is the nitrogen flux (mol m^{-2} s^{-1}), ε, r_m, τ and δ are the membrane porosity, average pore size, tortuosity, and thickness respectively, R is the gas constant, M and η are the molecular weight and viscosity of nitrogen at the operating temperature T, and P_m and ΔP are the average pressure within the membrane pores and the transmembrane pressure respectively. Since the transmembrane pressure is held constant Equation (2) may be written as

$$N = A + B \times P_m \qquad (3)$$

where A and B are constants given by

$$A = \frac{8}{3}\frac{\varepsilon r_m}{\tau\delta}\Delta P\sqrt{\frac{1}{2\pi RMT}} \quad (4)$$

$$B = \frac{\varepsilon r_m^2}{\tau\delta}\frac{1}{8\eta}\frac{\Delta P}{RT} \quad (5)$$

Plotting nitrogen flux versus the average pressure within the pores should result in a straight line. If the thickness and porosity are known, then the average membrane pore size and tortuosity can be calculated.

2.2.1.4. Liquid Entry Pressure (LEP)

Liquid entry pressure was determined as described by Smolder and Franken[36]. Briefly the LEP of the 13 membranes tested here was measured using a Sterlitech HP4750 (Kent, WA) stainless steel cell at 20 ˚C. The cell was filled with deionized water and pressurized to 13.8 kPa. The feed side pressure was gradually increased at 13.8 kPa min^{-1}. The LEP is the pressure at which a continuous flow of DI water through the membrane is first observed. Since water will begin to flow through the largest pores first, the Laplace Equation may be used to determine the maximum pore size:

$$d_{max} = \frac{4\gamma\cos\theta}{\Delta P} \quad (6)$$

where d_{max} is the maximum pore diameter, γ is the surface tension of water (72.75 dyne cm^{-1} at 20 °C [37]) and θ is the contact angle. Since the permeate side is at atmospheric pressure, the transmembrane pressure ΔP, is the LEP.

2.2.2. Membrane Surface Properties

2.2.2.1. Contact Angle

Static contact angles were measured using a sessile drop contact angle goniometer (Model 100, Rame-Hart Instrument Company, Netcong, NJ). A deionized water droplet (5 μL) at a rate of 1 μL/s was formed on the tip of a microsyringe (Hamilton, Reno, NV). The microsyringe was moved down vertically towards the sample until it made the contact with the sample. Then, the syringe was moved up and detached from the droplet. Using the circle fitting method, the angle made between the left and right hand side of the water droplet and the membrane surface was measured every 0.1 seconds. For each membrane, data were collected for 5 seconds at five locations and averaged.

2.2.2.2. Atomic Force Microscopy (AFM)

Surface roughness was characterized by AFM using a Dimension Icon (Bruker Corporation, MA) in ScanAsyst mode, was used to probe the roughness. Bruker's ScanAsyst-AIR probes (0.4 N/m, 2 nm radius) were used. The scan rate was set for 1 Hz with a resolution of 256 samples per line. After scanning, the image was first processed with a third order flatten with Bruker's nanoscope analysis program (v 1.5 R3). Roughness was then calculated by the nanoscope analysis program.

2.2.3. Direct Contact Membrane Distillation

All 13 membranes listed in Table 1 were tested using artificial feeds stream consisting of 20,000 ppm NaCl in DI water, conductivity < 10 μS cm^{-1} and resistance > 18.5 MΩ obtained from

a Labconco (Kansas City, MO) water purification system. Figure 1(a) gives the experimental set up while Figure 2(b) shows the custom-built DCMD module. The module was made of 0.054 m thick PTFE slab. Two channels with length and width of 0.1 and 0.05 m and depth of 2 mm were carved in each side of the cell. PTFE shims and spacers (ET 8700, Industrial Netting, Minneapolis, MN) were used to ensure the brine and distillate streams mixed in the module and membrane does not deform when exposed to high flow rates. Two silicone O-rings where located on the edge of the channels, and the cell was sandwiched between two plates in a membrane holder, as shown in Figure 1(b). The active membrane surface area was 40 cm^2.

The feed and permeate streams were circulated in countercurrent mode on opposite sides of the membrane by means of two peristaltic pumps (Masterflex I/P, Cole Parmer, Vernon Hills, IL). Three feed flow rates; 0.25, 0.5 and 0.9 L min^{-1} were investigated. The temperature of the feed and permeate streams was kept at 60 and 20℃, respectively. A custom-made level controlled tank with capacity of 1.5 liters was employed as the feed tank. The level controller in this tank was connected to a third peristaltic pump (Masterflex L/S Digital Standard Drive, Cole Parmer). As permeate was collected in the permeate reservoir, the NaCl concentration in the feed tank increased. In order to ensure a constant NaCl concentration in the feed, the third pump added DI water to the feed tank. The permeate flux was calculated based on the rate of DI water addition to the feed tank. The conductivity of the permeate was recorded using a conductivity meter (VWR, Radnor, PA). Each test continued for approximately 12 hours and average water fluxes are reported.

The membranes that displayed the highest fluxes for 20,000 ppm NaCl feed streams, were challenged with artificial 100,000 ppm NaCl stream. The membranes were tested in concentration

mode where the make-up water added by the third pump also consisted of 100,000 ppm NaCl in DI water. Each experiment was run until the conductivity of the permeate increased rapidly above 50 □S cm^{-1} with a concurrent rapid increase in permeate flux.

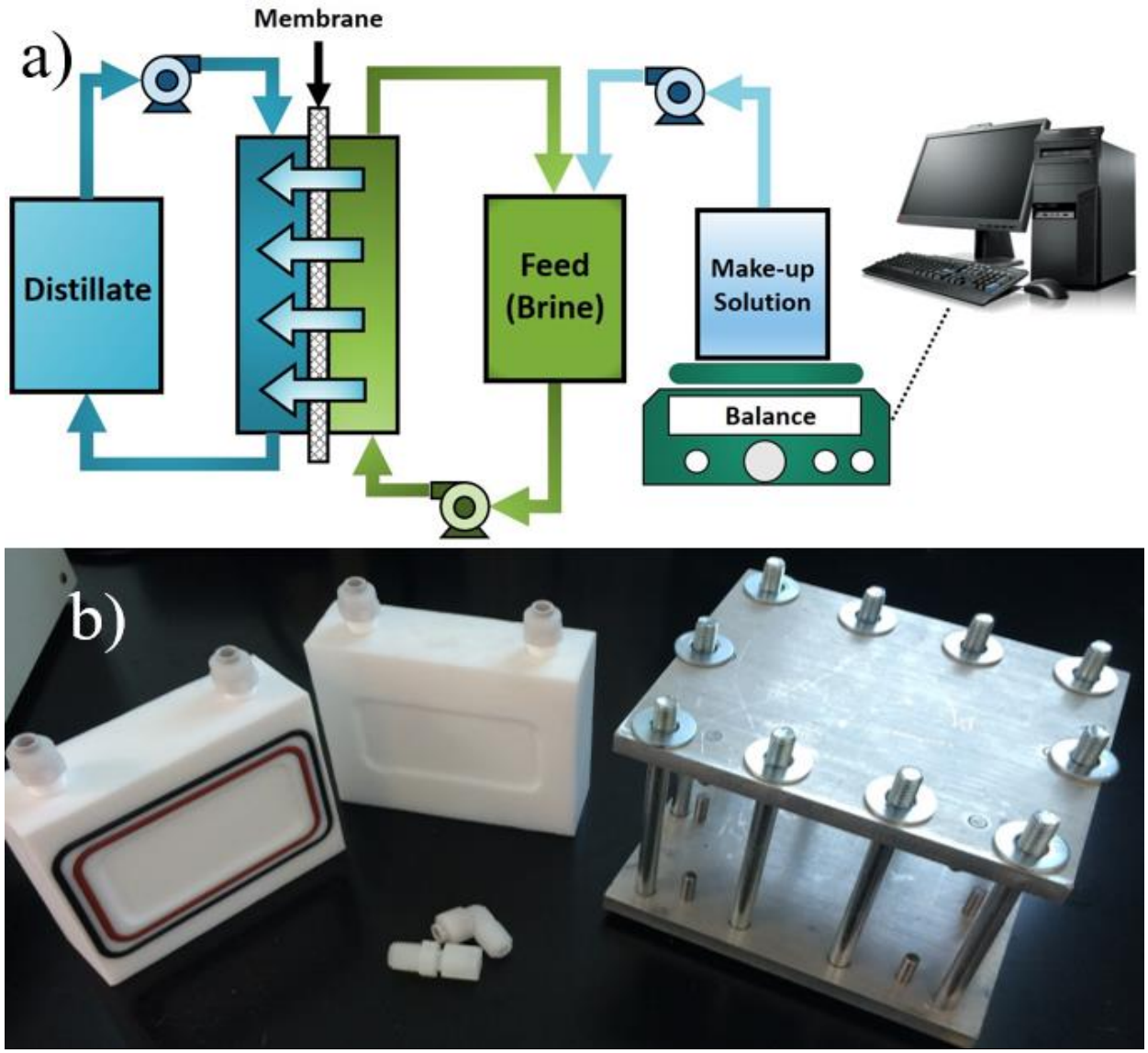

Figure 1. (a) Schematic diagram of DCMD Apparatus; (b) DCMD cell; the cell is sandwiched between the stainless steel membrane holder.

2.3. Results and Discussions

Tables 2 and 3 summarize the results from the various membrane characterization studies that have been conducted. The membranes are listed in groups that correspond to the membrane polymer. Within each group membranes are listed in order of increasing porosity. All the membranes are highly porous with porosity values ranging from 0.69 to 0.81 (see table 2, column 2). In the porosity calculations it was assumed that the density of super-hydrophobic PVDF is the same as PVDF. Since super-hydrophobicity involves modifying the membrane surface it is likely that these modifications have little influence on the bulk membrane polymer density.

The second column in Table 2 gives the measured membrane thicknesses from cross-sectional SEM analysis (see supporting documents for SEM images). As can be seen the thickness of the membrane varies considerably from 13 to 145 μm. The thickness reported for the supported PTFE membrane (PTFE-A) is the thickness of the PTFE barrier layer only and not the polystyrene support structure. While the thickness of the PVDF membranes are similar, the thickness of the polypropylene and PTFE membranes show considerable variability.

Table 2. Bulk membrane properties.

Membrane	Porosity (ε)	Thickness (δ) (μm)	d_{mean} Gas Permeation (μm)	d_{max} LEP (μm)	Structural factor $\varepsilon/\tau\delta$	Tortuosity (τ)	LEP (kPa)
PP-A	0.70	73	0.11	2.18	3370	2.84	540
PP - B	0.76	135	0.16	6.13	4330	1.45	260
PP - C	0.79	110	0.35	5.02	5970	1.29	280
ECTFE	0.71	82	0.18	3.49	7400	3.29	330
PTFE-A	0.77	36	0.20	3.33	13300	1.61	540

Table 2. Bulk membrane properties (Cont.)

Membrane	Porosity (ε)	Thickness (δ) (μm)	d_{mean} Gas Permeation (μm)	d_{max} LEP (μm)	Structural factor $\varepsilon/\tau\delta$	Tortuosity (τ)	LEP (kPa)
PTFE-B	0.78	13	0.10	4.22	16300	3.67	365
PTFE-C	0.81	73	0.25	5.84	7150	1.55	290
PVDF-A	0.69	97	0.24	5.51	2880	2.47	225
PVDF-B	0.71	119	0.63	12.89	2700	2.21	100
SH-PVDF-A	0.69	91	0.14	2.61	2500	3.02	580
SH-PVDF-B	0.69	110	0.22	4.39	3120	2.01	400
SH-PVDF-C	0.7	105	0.64	6.50	2520	2.64	240
SH-PVDF-D	0.72	112	1.30	12.62	2760	2.31	120

Table 3. Membrane surface properties.

Membrane	Contact Angle (°)	R_{max} (nm)
PP-A	127	274
PP-B	135	404
PP-C	142	546
ECTFE	130	711
PTFE-A	154	296
PTFE-B	140	182
PTFE-C	147	357
PVDF-A	128	578
PVDF-B	130	605
SH-PVDF-A	139	774
SH-PVDF-B	151	524
SH-PVDF-C	140	504
SH-PVDF-D	139	187

Mean membrane pore sizes, determined by gas permeation measurements as well as the maximum pore diameter measured by LEP measurements are given in columns 4 and 5 in Table 2. As can be seen, the maximum pore size is significantly greater than the average pore size indicating the existence of a pore size distribution. The PVDF and superhydrophobic PVDF membranes (all membranes supplied by EMD Millipore) display an increasing average and maximum pore size with increasing porosity. However, the same is not true for the polypropylene and PTFE membranes which also display considerable variability in thickness. The observed differences are probably due to different manufacturing procedures used for the various polypropylene and PTFE membranes [38].

Columns 6 and 7 give the value of the bulk membrane structural parameter $\varepsilon/\tau\delta$ and the tortuosity. The parameter $\varepsilon/\tau\delta$ is often used as a structural parameter to describe bulk membrane properties. As can be seen, there is significant variability in the structural parameter. From Table 2 the largest values of the membrane structural parameter are as follows: PTFE-B, 16,340; PTFE-A 13,300; ECTFE, 7,400; PTFE-C, 7,150 and PP-C, 5970. The very large values of the membrane structural parameters for PTFE-B and PTFE-A are due to their very low thickness. All the membranes display tortuosity factors between 1.29 and 3.67. The variability is greatest for the polypropylene and PTFE membranes again suggesting different manufacturing procedures for the various polypropylene and PTFE membranes.

Rao et al. [26] have summarized the many bulk membrane structural parameters that have been proposed for prediction of membrane fluxes. Many of these bulk membrane structural parameters have been proposed by developing empirical correlations of membrane flux with bulk membrane properties such as thickness, tortuosity, porosity and average pore size. However, three

commonly used bulk membrane structural parameters can be related to different mass transport mechanism through the membrane.

If convective flow dominates, the Hagen Poiseuille equation for laminar flow is often assumed. The bulk membrane structural parameter that results from this equation is $\frac{r^2\epsilon}{\tau\delta}$ where r is the average pore radius. If Brownian or Knudsen diffusion dominate the bulk membrane structural parameters that arise are $\frac{\epsilon}{\tau\delta}$ and $\frac{r\epsilon}{\tau\delta}$ respectively. In the case of water vapor transport through microporous membranes, Brownian diffusion is expected to dominate [39]. Thus we have chosen to use the bulk membrane structural parameter $\frac{\epsilon}{\tau\delta}$ given in the 6th column of Table 1. As can be seen the value of this parameter varies greatly from 2,500 to over 16,000. The greater the porosity and the lower the thickness and tortuosity of the membrane, the greater the value of this structural parameter, and the greater the expected permeate flux, as a result. It can be noted that the pore size of the membrane does not appear in the structural parameter as it is assumed that Brownian diffusion dominates. Rao et al. [26] show that the structural parameter $\frac{\epsilon}{\tau\delta}$ gives one of the best correlations to experimental flux data. However the correlation coefficient is only 0.71. This highlights the fact that use of a bulk membrane structural parameter has a number of implicit assumptions e.g. membrane surface properties are less important, the membrane pore size distribution is such that transport is dominated by Brownian diffusion etc.

Tortuosity values show variations from about 1.29 to 3.67 (see table 2, column 7). Cussler [40] indicates that typical tortuosity values range for 2 to 6. Our results are in general agreement with this observation. Tortuosity values for the PVDF and superhydrophobic PVDF membranes are similar while they vary considerably for the polypropylene and PTFE membranes. This is not unexpected given the observed variation in thickness of these membranes.

The final column in Table 2 gives the LEP. As expected, from Equation (2) lower liquid entry pressures correspond to larger maximum pore sizes. While the membrane pore size does not appear in the bulk structural parameter, it will affect the onset of leakage of water through the pores as a result of fouling due to adsorption organics and dissolved salts.

Table 3 gives data on membrane surface properties. Membrane contact angles (column 2) vary from 127 to 154 indicating all the membranes are hydrophobic. The superhydrophobic membranes display contact angles similar to the PTFE membranes. Column 3 presents membrane roughness from analysis of the AFM images. As can be seen a significant variation in roughness exists. Changes in roughness for membranes made from the same polymer are most likely due to different manufacturing conditions.

The permeate flux during membrane distillation using an artificial feed stream consisting of 20,000 ppm NaCl in DI water is given in Figures 2 to 4. Figure 2 gives the variation of permeate flux with feed flow rate for the polypropylene and PVDF membranes, Figure 3 gives analogous results for the ECTFE and PTFE membrane while Figure 4 gives analogous results for the PVDF membranes. Comparing Table 2 with Figures 2-4 indicates that in general the permeate flux increases with increasing values of the membrane structural parameter. The lowest fluxes are observed for the PVDF and superhydrophobic PVDF membranes. In general the bulk membrane structural parameter is lowest for these membranes. Higher fluxes are observed for the PTFE and ECTFE membranes which also display a larger value of the structural parameter. The polypropylene membranes are less consistent. The structural parameter is larger than for the PVDF and superhydrophobic PVDF membranes but less than the PTFE and ECTFE membranes. However with the exception of PP-B, the observed fluxes are similar to the PTFE and ECTFE

membranes. PP-B however displays a much lower flux than PP-A and PP-C. Nevertheless the membranes with the largest value of the structural parameter: PTFE-B; PTFE-A; ECTFE, PTFE-C, PP-C, also displayed the highest permeate fluxes. Our results indicate that the structural parameter provides a semi-quantitative method for screening expected permeate fluxes.

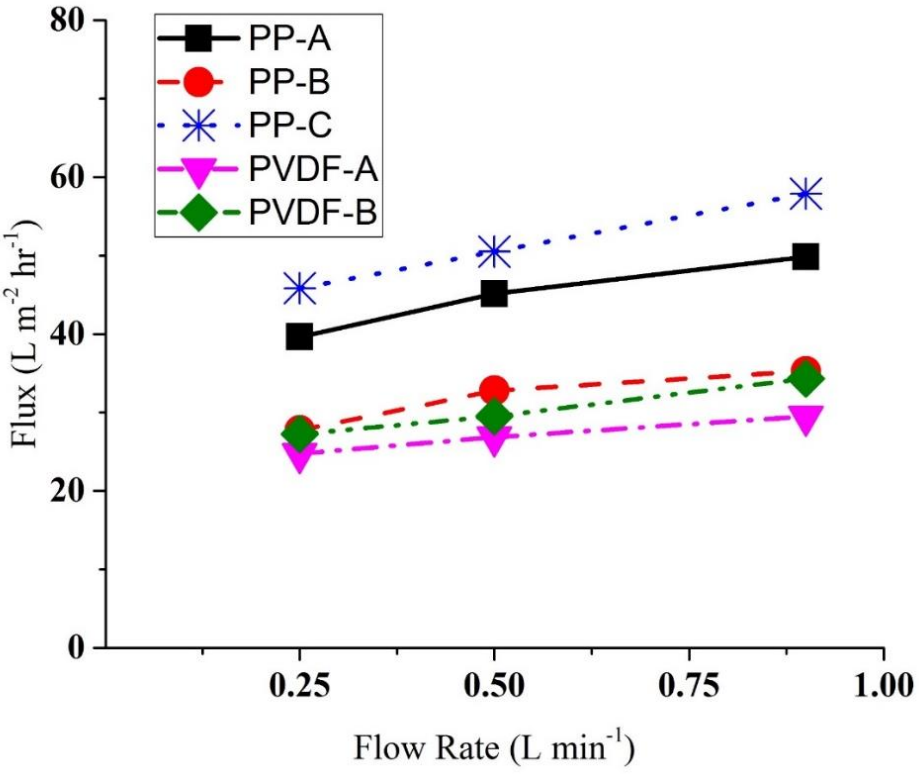

Figure 2. Variation of permeate flux with feed flow rate for polypropylene and PVDF membranes. The feed stream consisted of 20,000 ppm NaCl in DI water.

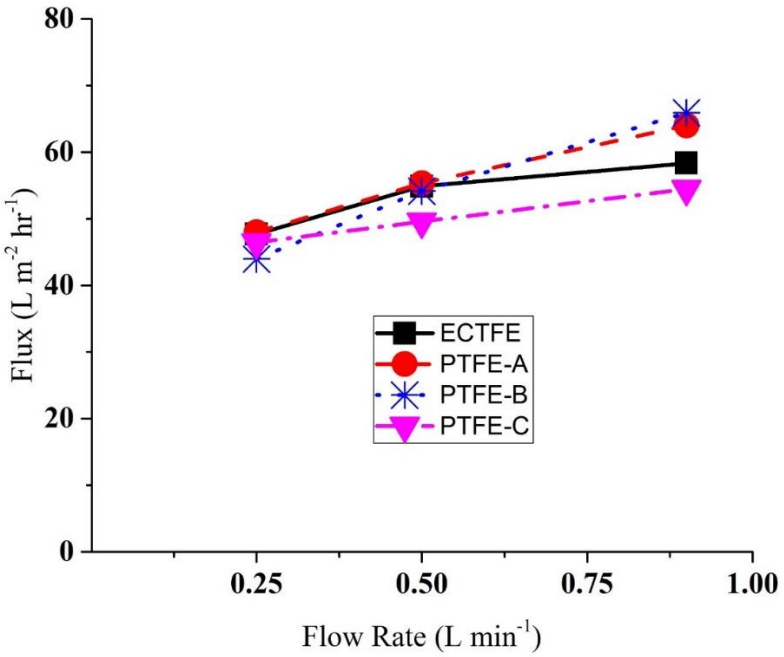

Figure 3. Variation of permeate flux with feed flow rate for ECTFE and PTFE and PVDF membranes. The feed stream consisted of 20,000 ppm NaCl in DI water.

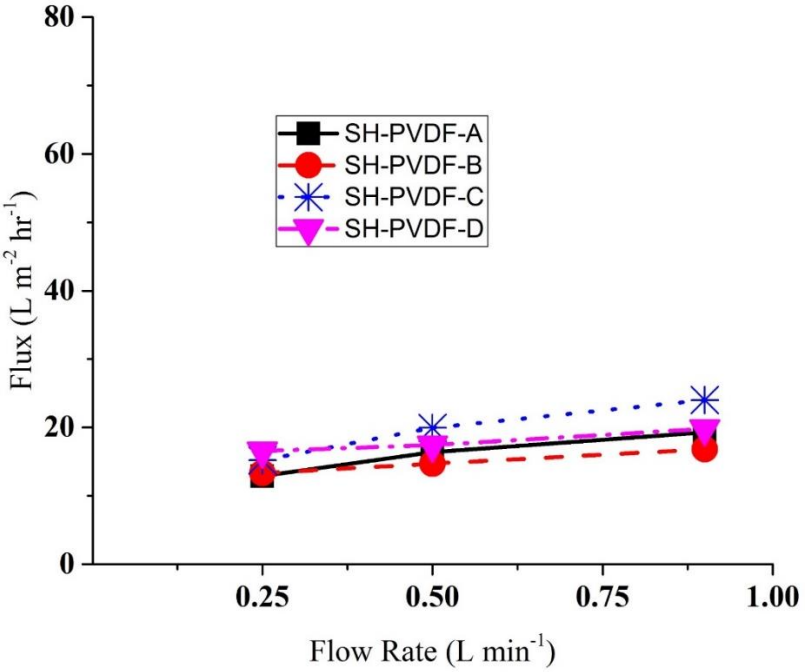

Figure 4. Variation of permeate flux with feed flow rate for superhydrophobic PVDF membranes. The feed stream consisted of 20,000 ppm NaCl in DI water.

Figures 2-4 indicate the permeate flux increases with increasing feed flow rate. The width of the feed channel is 0.05 m. The density and viscosity for 20,000 ppm NaCl solution are 1.0108 kg L^{-1} and 9.1828 x 10^{-4} Pas respectively [41]. Thus the feed Reynolds numbers are 100, 200 and 370 for feed flow rates of 0.25, 0.5 and 0.9 L min^{-1} respectively. It is expected therefore that the flow is laminar. Given the low salt concentration in the feed, significant concentration polarization boundary layer effects are not expected on the feed side. However temperature polarization due to the development of a thermal boundary layer is frequently observed in many membrane distillation configurations [18, 27]. Increasing the feed velocity will lead to an increase in the feed side heat transfer coefficient which in turn will lead to higher rates of water evaporation and hence higher observed permeate fluxes.

The membranes that displayed the highest permeate fluxes: PTFE-B; PTFE-A; ECTFE, PP-C, PTFE-C, were challenged with 100,000 ppm NaCl solutions. Figure 5 shows the variation of permeate flux with time for theses five membranes. The membranes were tested until breakthrough. Breakthrough was assumed to occur when both the conductivity and permeate flux increase rapidly. Figure 6 indicates the breakthrough point for the ECTFE membrane. As can be seen at breakthrough the permeate conductivity rises rapidly. Table 4 gives the feed concentration at which breakthrough occurred for the 5 membranes tested with 100,000 ppm NaCl solution.

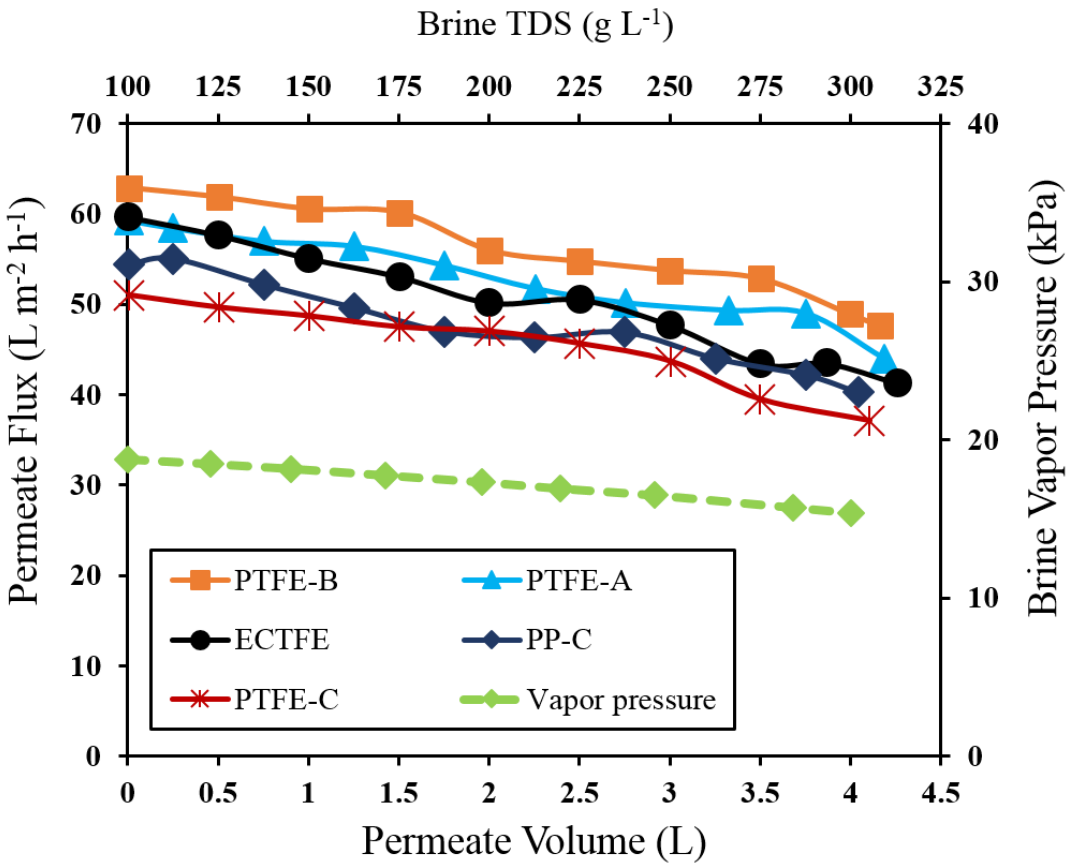

Figure 5. Variation of permeate flux with permeate volume. The initial feed concentration was 100,000 ppm NaCl. Experiments were run till breakthrough.

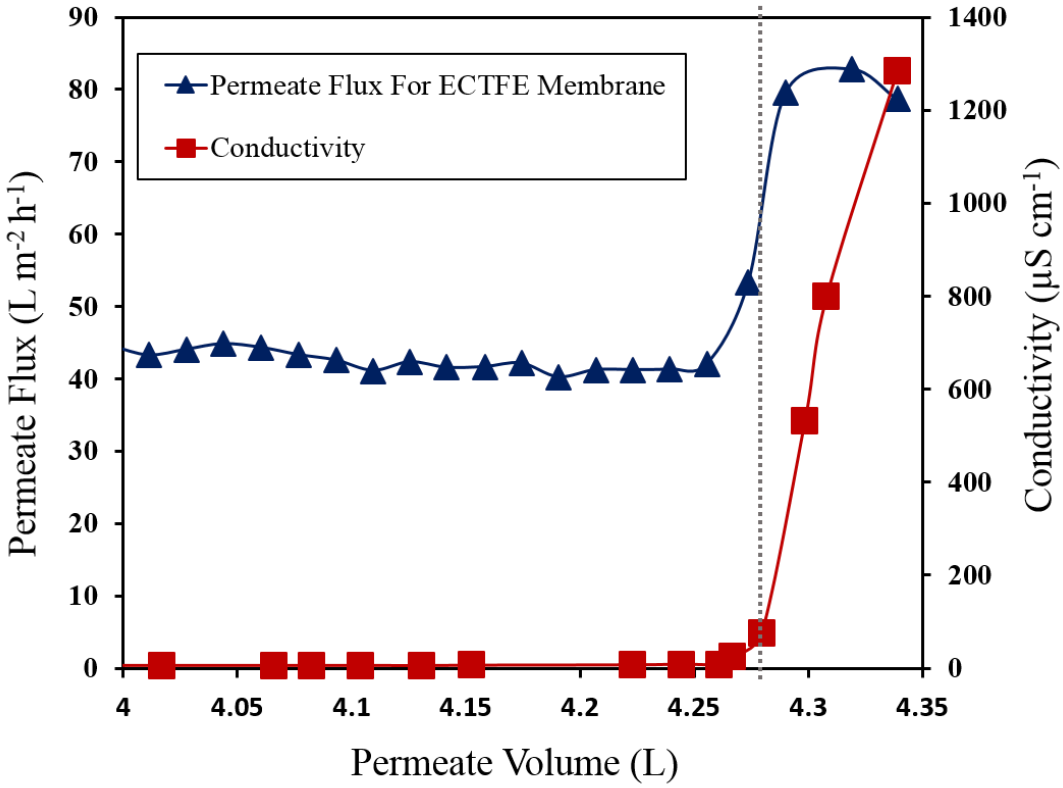

Figure 6. Variation of permeate flux and conductivity with permeate volume. Breakthrough occurs when a rapid increase in permeate flux and conductivity is observed.

Table 4. Feed concentration at breakthrough

Membrane	Feed concentration at breakthrough (g L^{-1})
PP-C	302
PTFE-A	309
PTFE-B	308
PTFE-C	305
ECTFE	313

As can be seen in Figure 5, the permeate flux decreases with increasing NaCl concentration in the feed. As a model feed solution consisting of NaCl in DI water is used here, little membrane fouling is expected. Figure 5 also shows the decrease in water vapor pressure with NaCl concentration. While the thermal and concentration polarization boundary layers will be affected by the increasing NaCl concentration in the feed, Figure 5 suggests that the decrease in water vapor pressure with increasing NaCl concentration will contribute to the observed decree in permeate flux.

The results obtained here indicate that breakthrough occurs at approximately the same NaCl concentration for all 5 membranes. Table 3 indicates that all 5 membranes display similar water contact angles but the surface roughness varies from 289 to 711 nm. These results suggest that for the model feed streams tested here membrane surface properties are likely to be of secondary importance. Using a lower flux membrane could lead to breakthrough of the feed at a higher concentration. However real hydraulic fracturing produced waters have the potential for greater fouling. Besides very high TDS, small volatile organic compound and dissolved gases could pass through the membrane pores degrading the permeate quality. Further the presence of alcohols and surfactants can cause wetting of the membrane due to a lowering of the liquid surface tension [18, 19, 23]. Consequently in applications using real hydraulic fracturing produced waters, it is likely that the permeate flux will decrease more rapidly than observed in Figure 5 and breakthrough of the feed will occur at a lower TDS.

The results presented here provide a quick method to determine membranes that are likely to give the highest permeate fluxes based on the bulk membrane structural parameter. These membranes could be used to concentrate the feed rapidly. The actual TDS at which breakthrough

occurs will depend on the feed components (dissolved organics etc.) as well as the membrane surface properties such as hydrophobicity and roughness. A lower flux (smaller pore size) membrane could be used to concentrate the feed beyond the breakthrough point for higher flux membranes. Our results suggest that a multistage process using membranes of different permeabilities could be used to maximize the concertation of the reject brine solution enabling maximum water recovery.

2.4. Conclusion

The results obtained here indicate the utility of defining an appropriate bulk membrane structural parameter. If appropriately chosen, the structural parameter will provide insights into expected membrane performance when tested with low fouling model feed streams. Under these conditions bulk membrane properties such as pore size, pore size distribution, tortuosity and thickness will have a greater effect on membranes performance compared to surface properties such as hydrophobicity and roughness. Treatment of hydraulic fracturing produced waters often involves maximizing water recovery in order to minimize the volume of concentrated brine that has to be transported to a centralized treatment or disposal facility. Membrane distillation could be used to concentrate the wastewater to close to the solubility limit of the dissolved salts in the water. However it is likely that an optimized process will be a multistep process. As the TDS of the feed increases lower flux membranes with smaller pore sizes will be required in order to prevent breakthrough the of the feed solution. For real feed streams containing surfactant and other dissolved organic compounds either pre-treatment or optimized membrane surface properties will be required in order minimize a flux decrease due to membrane fouling as well as early breakthrough of the feed due do adsorption of surfactant molecule onto the membrane surface.

Acknowledgements

Funding for this work was provided by Southwestern Energy through the National Science Foundation Industry/University Cooperative Research Center for Membrane Science, Engineering and Technology, the National Science Foundation (IIP 1361809) and the University of Arkansas.

References

[1] Gleick, P.H., Wolff, G. H., Cooley, H. (2000) The World's water 2006-2007, The Biennial Report on Freshwater Resources; Island Press: Washington, DC.

[2] Igunnu, E.T.; Chen, G.Z. (2012) Produced water treatment technologies. Int. J. Low-Carbon Tech., 9 (4): 157-177

[3] United States Energy Information Administration. World shale gas resources: an initial assessment of 14 regions outside the United States; United States Department of Energy: Washington, DC, April 2001, 1-365.

[4] Yang, R.; Goktekin, E.; K. Gleason, K. (2015) Zwitterionic Antifouling Coatings for the Purification of High-Salinity Shale Gas Produced Water. Langmuir, 31(43): 11895-11903.

[5] Shaffer, D.L.; Arias Chavez, L.H.; Ben-Sasson, M.; Romero-Vargas Castrillon, S.; Yip, N.Y.; Elimelech M. (2013) Desalination and reuse of high-salinity shale gas produced water: Drivers, technologies, and future directions. Environ. Sci. Technol, 47 (17): 9569−9583.

[6] Koren, A.; Nadav, N. (1994) Mechanical vapour compression to treat oil field produced water. Desalination, 98 (1-3): 41-48.

[7] Hao, H.; Huang, X.; Gao, C.; Gao, X. (2015) Application of an integrated system of coagulation and electrodialysis for treatment of wastewater produced by fracturing. Desalin. Water Treat., 55 (8): 2034-2043.

[8] Kim, S.J.; Ko, S.H.; Kang, K.H.; Han, J. (2010) Direct seawater desalination by ion concentration polarization. Nat. Nanotechnol., 5 (4): 297-301.

[9] Prakash Narayan, G.; St. John, M.G.; Zubair, S.M.; Lienhard, J.H. (2013) Thermal design of the humidification dehumidification desalination system: An experimental investigation. Int. J Heat Mass Tran., 58 (1-2): 740-748.

[10] Sirkar, K. K. (1992) Other new membrane processes in Membrane Handbook, eds: Ho, W. S. W., Sirkar, K. K. van Nostrand Reinhold, NY, New York.

[11] Martinetti, C.R.; Childress, A.E.; Cath, T.Y. (2009) High recovery of concentrated RO brines using forward osmosis and membrane distillation. J. Membr. Sci., 331 (1-2): 31-39.

[12] Edwie, F.; Chung, T.S. (2012) Development of hollow fiber membranes for water and salt recovery from highly concentrated brine via direct contact membrane distillation and crystallization. J. Membr. Sci., 421-422: 111-123.

[13] Singh, D.; Sirkar, K.K. (2012) Desalination of brine and produced water by direct contact membrane distillation at high temperatures and pressures. J. Membr. Sci., 389: 380-388.

[14] Guan, G.; Wang, R.; Wicaksana, F.; Yang, X.; Fane, A.G. (2012) Analysis of Membrane Distillation Crystallization System for High Salinity Brine Treatment with Zero Discharge Using Aspen Flowsheet Simulation. Ind. Eng. Chem. Res., 51 (41): 13405-13413.

[15] Charcosset, C.; Kieffer, R.; Mangin, D.; Puel, F. (2010) Coupling between membrane processes and crystallization operations. Ind. Eng. Chem. Res., 49 (12): 5489-5495.

[16] Curcio, E.; Criscuoli, A.; Drioli, E. (2001) Membrane Crystallizers. Ind. Eng. Chem. Res., 40 (12): 2679-2684.

[17] Chan, M.T.; Fane, A.G.; Matheickal, J.T.; Sheikholeslami, R. (2005) Membrane distillation crystallization of concentrated salts - Flux and crystal formation. J. Membr. Sci., 257 (1-2): 144-155.

[18] El-Bourawi, M.S.; Ding, Z.; Ma, R.; Khayet, M. (2006) A framework for better understanding membrane distillation separation process. J. Membr. Sci. 285 (1–2): 4–29.

[19] Lawson, K.W.; Lloyd, D.R. (1997) J. Membr. Sci. 124 (1): 1–25.

[20] Zhao, K.; Heinzl, W.; Wenzel, M.; Büttner, S.; Bollen, F.; Lange, G.; Heinzl, S.; Sarda, N. (2013) Experimental study of the memsys vacuum-multi-effect-membrane-distillation (V-MEMD) module. Desalination, 323: 150-160.

[21] Francis, L.; Ghaffour, N.; Alsaadi, A.A.; Amy, G.L. (2013) Material gap membrane distillation: A new design for water vapor flux enhancement. J. Membr. Sci., 448: 240-247.

[22] Dotremont, C.; Kregersman, B.; Sih, R.; Lai, K.C.; Koh, K.; Seah, H. (2010) Seawater desalination with memstill technology - a sustainable solution for the industry. WaterPract.Technol. 5 (2): 1-7.

[23] Souhaimi, M.K.; Matsuura, T. (2011) Membrane distillation: principles and applications; Elsevier, Amsterdam, Netherlands.

[24] Essalhi, M.; Khayet, M. (2014) Application of a porous composite hydrophobic/hydrophilic membrane in desalination by air gap and liquid gap membrane distillation: A comparative study. Sep. Purif. Technol., 133: 176-186.

[25] Tijing, L.D.; Woo, Y.C.; Choi, J.S.; Lee, S.; Kim, S.H.; Shon, H.K. (2015) Fouling and its control in membrane distillation-A review. J Membr. Sc., 475: 215-244.

[26] Rao, G.; Hiibel, S.R.; Childress, A.E. (2014) Simplified flux prediction in direct-contact membrane distillation using a membrane structural parameter. Desalination, 351: 151-162.

[27] Curcio, E.; Drioli, E. (2005) Membrane Distillation and Related Operations—A Review. Sep. Purif. Technol., 34: 35-86.

[28] Loh, S.; Beuscher, U.; Poddar, T.K.; Porter, A.G.; Wingard, J.M.; Husson, S.M.; Wickramasinghe, S.R. (2009) Interplay among membrane properties, protein properties and operating conditions on protein fouling during normal-flow microfiltration. J. Membr. Sci., 332 (1-2): 93-103.

[29] Saffarini, R.B.; Mansoor, B.; Thomas, R.; Arafat, H.A. (2013) Effect of temperature-dependent microstructure evolution on pore wetting in PTFE membranes under membrane distillation conditions. J. Membr. Sci., 429: 282-294.

[30] Kim, H.; Choi, J.S.; Lee, S.H. (2011) Effect of Membrane Material Properties on Efficiency of Membrane Distillation. Mater. Sci. Forum., 695: 85-88.

[31] Mishra, R.; Tripathy, S.P.; Sinha, D.; Dwivedi, K.K.; Ghosh, S.; Khathing, D.T.; Muller, M.; Fink, D.; Chung, W.H. (2000) Optical and electrical properties of some electron and proton irradiated polymers. Nucl. Instr. Meth. Phys. Res., 168 (1): 59-64.

[32] Pan, J.; Xiao, C.; Huang, Q.; Liu, H.; Hu, J. (2015) ECTFE porous membranes with conveniently controlled microstructures for vacuum membrane distillation. J. Mater. Chem. A, 3 (46): 23549-23559.

[33] Cui, Z.; Drioli, E.; Lee, Y.M. (2014) Recent progress in fluoropolymers for membranes. Prog. Polym. Sci., 39: 164-198.

[34] Nejati, S.; Boo, C.; Osuji, C.O.; Elimelech, M. (2015) Engineering flat sheet microporous PVDF films for membrane distillation. J. Membr. Sc., 492: 355-363.

[35] Hwang, H.J.; He, K.; Gray, S.; Zhang, J.; Moon, I.S. (2011) Direct contact membrane distillation (DCMD): Experimental study on the commercial PTFE membrane and modeling. J. Membr. Sc., 371 (1-2): 90-98.

[36] Smolders, K.; Franken, A.C.M. (1989) Terminology for Membrane Distillation. Desalination, 72 (3): 249-262.

[37] Vargaftik, N.B.; Volkov, B.N.; Voljak, L.D. (1983) International Tables of the Surface Tension of Water. J. Phys. Chem. Ref. Data, 12 (3): 817-820.

[38] Grzenia, D.L.; Carlson, J.O.; Czermak, P.; Han, B.; Specht, R.K.; Wickramasinghe, S.R. (2006) Purification of densonucleosis virus by tangential flow ultrafiltration. Biotechnol. Prog., 22 (5): 1346-1353.

[39] Kenfield, C.F.; Qin, R.; Semmens, M.J.; Cussler, E.L. (1988) Cyanide recovery across hollow fiber gas membranes. Environ. Sci. Technol., 22 (10): 1151-1155.

[40] Cussler, E. (1997) Diffusion, 2nd Ed.; Cambridge Univ Pr, Cambridge, UK.

[41] Hai-Lang, Z.; and Han, S.J. (1996) Viscosity and Density of Water + Sodium Chloride + Potassium Chloride Solutions at 298.15 K. J. Chem. Eng. Data, 41 (3): 516-520.

Chapter 3. Combined Electrocoagulation and Membrane Distillation for Treating High Salinity Produced Waters

Abstract

Membrane distillation has been investigated for treating high TDS hydraulic fracturing produced water (HFPW). When treating real HFPW feed streams which contain not only high TDS, but also dissolved organics, surfactants and low surface tension contaminants pretreatment of the feed is essential to suppress the onset of membrane fouling. The objective of this study was to investigate the feasibility of electrocoagulation (EC) followed by direct contact membrane distillation (DCMD). EC was shown to be effective in reducing suspended solids and the organic content of raw HFPW samples.

Raw and EC pretreated HFPW samples were treated with DCMD system under variety of operational conditions. Higher contaminate removal during EC resulted in lower membrane fouling and consequently, lower flux decline during DCMD. The membrane permeability was modeled by summing the membrane and feed side fouling layer resistances. Long-term EC-DCMD experiments were conducted, concentrating the feed water, containing 135 g L^{-1} TDS, up to 265 g L^{-1}. Stable water flux with minimal fouling are reported over 434 h experimental run.

3.1. Introduction

Unconventional natural gas resources offer an opportunity to access a relatively clean fossil fuel that could potentially lead to energy independence for some countries. Unconventional shale gas and tight sand production account for more than 60 percent of the total natural gas production in the US. Horizontal drilling and hydraulic fracturing make the extraction of tightly bound natural

gas from shale formations economically feasible [1,2]. Following hydraulic fracturing, varying percentages (8–70%) of the injected water will return back to the surface during the lifetime of the well, containing very high concentrations of total dissolved solids (TDS) [3]. The volume and TDS content of hydraulic fracturing produced water (HFPW) of a well depends on a number of factors including: the geographical location, geological formation, well depth and time following hydraulic fracturing [4,5]. Kondash *et al.* [6] has estimated the median volume of HFPW to range from 1.7 to 14.3 million L per well over the first 5–10 years of production. TDS concentration of HFPW ranges from 650 to 400,000 mg L^{-1} [4,7].

Over the last decade, the most common disposal practice in the U.S. has involved injection of HFPW into brine disposal wells [8–10]. However, in many areas where oil and gas production is abundant, brine disposal sites are not available and the HFPW has to be transported to the disposal facilities [11]. This transportation can be very costly (up to $4.00 per bbl) [12]. In addition several environmental concerns have emerged surrounding HFPW discharge, notably induction of micro-scale earthquakes and the potential to contaminate the groundwater [6,13]. Thus, treatment of HFPW streams is critical for developing economically viable hydraulic fracturing operations [14].

Primary consideration when treating high salinity produced waters is TDS reduction to a quality suitable for discharge or for external reuse [10]. Reverse osmosis (RO) is the most practiced desalination technique in recent years and accounts for over 60% of the world's capacity for water desalination [15]. However, RO is inefficient for treating produced waters containing elevated TDS concentrations due to very high hydraulic pressure requirements [16]. Mechanical vapor compression [17], membrane distillation (MD) [18] and forward osmosis (FO) [19] are three

examples of desalination technologies for high TDS brines that are appropriate for the produced water streams in shale gas plays where conditions promote external reuse [10]. In this study, we focus on MD.

MD is a thermally driven separation process, in which only vapor molecules are able to pass through a porous hydrophobic membrane. This separation process is driven by a vapor pressure gradient across a porous hydrophobic membrane [20]. Direct contact membrane distillation (DCMD) is the most commonly used configuration of MD [21]. In DCMD, hot feed water and cold distilled water flow on opposite sides of a hydrophobic membrane. The membrane acts as a thermal insulator as well as a physical barrier between the hot feed and the cold distillate. Water vaporizes from the hot feed, passes through the membrane pores and condenses on the distillate side [22,23]. In this study, we investigate the application of DCMD for treating high TDS HFPW.

MD can provide variety of advantages when treating high salinity produced waters, including: near complete rejection of dissolved and suspended species, lower operating pressures than pressure-driven separation processes (such as RO), lower operating temperatures compared to thermal distillation and the possibility of using waste-heat as the energy source for the process [18,24]. Since it is mostly the water vapor that crosses the membrane, dissolved solids remain in the concentrated retentate and high quality permeate is recovered.

Like all membrane technologies, fouling is a major obstacle when operating MD for treating brines [25–30]. Fouling results in a decrease of the membrane permeability due to deposition of suspended or dissolved substances on the membrane surface and/or within its pores. Several studies have indicated the negative effect of membrane fouling on MD [28]. Moreover,

the role of particulate matter in real feed streams on membrane fouling is often neglected. The MD feed stream is usually filtered (e.g. 0.25 and 0.45 μm filters) prior to introduction to the MD module [16]. In addition to fouling, MD also suffers from membrane wetting. The MD membranes have to remain hydrophobic through the process, thus allowing only vapor and not liquid water to pass through. Wetting refers to the process whereby the membrane starts allowing liquid water to flow into the membrane pores and leads to deterioration of permeate quality [31–33]. Preventing pore wetting is particularly challenging in desalinating HFPW or other feed waters with high levels of surfactants or low surface tension contaminants [34]. In addition scaling due to precipitation of salts is a concern that can lead to membrane wetting [35].

Pretreatment of real feed streams will be essential when developing practical MD processes. Here we focus on pretreatment to suppress fouling by dissolved organic species, surfactants and other low surface tension foulants. Pretreatment of the feed is standard practice in most desalination systems, and pretreatment needs vary significantly by technology and feed water quality [21,36]. Common pretreatment methods include oxidation, filtration, antiscalants, flocculation, and chlorination [27,31,37]. In this study, we investigate electrocoagulation (EC) as the pretreatment prior to MD. EC has been successfully practiced prior to microfiltration [38,39], RO [40] and forward osmosis [14]. EC is an electrochemical method whereby sacrificial anodes (often Al or Fe) corrode to release active precursors into the solution. The released metal ions are further transformed into hydroxides that neutralize charges or act as sweep flocs with large surface areas and hence, they promote aggregation or precipitatation as a sludge, adsorbing the dissolved organic compounds and trapping suspended particles [41]. While the basic chemistry is similar, EC can provide a number of advantages compared to chemical coagulation including reduction of the direct handling of corrosive chemicals, lower amount of sludge production, being readily

employable in portable wastewater treatment systems and less maintenance due to requiring no moving parts [14,42–46]. Another advantage of EC over other conventional methods is the potential for treating oily wastewater, where the presence of electric current can contribute to the electrocoalescence of oil droplets [47].

In this study, we investigate the impacts of EC pretreatment prior to DCMD for treating high TDS HFPW using a commercial membrane. We conduct DCMD experiments with synthetic, non-pretreated and pretreated HFPW under different operational conditions and investigate the water recovery from DCMD for different water qualities. In addition, we conduct long-term EC-DCMD experiments with pretreated HFPW samples and study the impact of pretreatment on longer experimental runs.

3.2. Theory

3.2.1. Mass Transfer in MD

Water Flux across a hydrophobic MD membrane can be expressed as:

$$J = A\,\Delta P \tag{1}$$

where J is water flux, A is membrane permeanility coefficient and ΔP is water partial pressure difference across the membrane [24]. For a membranes with pore sizes around 0.2 µm, the reduced Knudsen-molecular diffusion transition form of the dusty gas model has been used to predict the water flux through teh membrane [48,49]. This expression is as following:

$$A = -\frac{M_w}{\delta R T_{avg}}\left(\frac{D_m\, D_k}{D_m + p_a D_k}\right) \tag{2}$$

where M_w is molecular weight of water, δ is membrane thickness, R is universal gas constant, T_{avg} is average temperature across the membrane and p_a is partial pressure of air. D_m is molecular diffusion coefficient and is defined as follows:

$$D_m = 4.46 * 10^{-6} \left(\frac{\varepsilon}{\tau}\right) T_{avg}^{2.334} \quad (3)$$

where $\mathcal{E}$ and τ are membrane porosity and tortuosity, respectively. In Eq. (2), D_k is Knudsen diffusion coefficient and is defined as follows:

$$D_k = \frac{2\varepsilon r}{3\tau} \left(\frac{8RT_{avg}}{\Pi M_w}\right)^{0.5} \quad (4)$$

where r represents the nominal pore radius of membrane.

Resistance in series modeling can address changes in membrane permeability due to fouling [50]. The overall MD permeability coefficient (A) depends on both membrane permeability (A_m) as well as fouling layer permeability coefficient (A_f), as follows:

$$\frac{1}{A} = \frac{1}{A_m} + \frac{1}{A_f} \quad (5)$$

In equation (5) it is assumed that there is no mass transfer resistance on the permeate side as the permeate is solute free water. We will use Eq. (5) to model our experimental results, assuming fouling does not affect the feed side concentration polarization boundary layer as well as feed and distillate side temperature boundary layer.

3.2.2. MD Flux Prediction

A mathematical code was developed in Matlab 2016a in order to predict MD water flux. Physio-chemical properties of water and different concentrations of sodium chloride in water as well as all other required parameters such as membrane module geometries, membrane physical properties and operational conditions were introduced into the code. Then, a flat sheet membrane was subdivided into n differential elements. Transmembrane ΔP at each element was estimated using the method described by Yun *et al.* [48] and consequently, the water flux at each element was estimated using Eq. (1). The modeling algorithm is given in appendix A.

3.2.3. EC

The following reactions occur in the EC reactor when applying an electric current:

At the anode: $$M_{(s)} \rightarrow M_{(aq)}^{n+} + ne^{-} \quad (6)$$

At the cathode: $$2H_2O + 2e^{-} \rightarrow 2OH^{-} + H_2 \quad (7)$$

where *M* is the electrode metal material (often Al or Fe) [51]. According to complex precipitation kinetics, the released metal and hydroxide ions react to from various metal complexes such as $M(OH)^{(n-1)+}$, $M(OH)_2^{(n-2)+}$ and $M_6(OH)_{15}^{(6n-15)+}$ that can neutralize negatively charged species and eventually, transform to amorphous $M(OH)_{n(s)}$ particles, as given by the following general scheme [14,52]:

In solution: $$x\, M_{(aq)}^{n+} + y\, OH^{-} \rightarrow M_x(OH)_y^{(xn-y)} \rightarrow x\, M(OH)_{n(s)} \quad (8)$$

$M(OH)_{n(s)}$ particles, with their large surface area, can adsorb organic compounds, trap suspended particles and finally, polymerize and deposit as sweep floc (with the adsorbed organics and colloidal particles) according to the following reaction, [53]:

$$x\,M(OH)_n \rightarrow M_x(OH)_{xn} \quad (9)$$

3.3. Materials and Methods

3.3.1. HFPW: Source and Characterization

HFPW samples were collected from Marcellus shale gas production facilities in Pennsylvania and provided by Southwestern Energy (Houston, TX). The water samples were disinfected on-site using a Balckwater unit (MOIX, Albuquerque, NM) and received in 20 L containers. Raw and pretreated water samples were characterized for the levels of TDS, total suspended solids (TSS), total organic carbon (TOC), dissolved organic carbon (DOC) and turbidity as well as inorganic composition at Arkansas Water Resources Center, University of Arkansas (Fayetteville, AR). TDS and TSS were measured using EPA standard methods 160.1 and 160.2 [54], respectively. TOC was measured using a Skalar Formacs TOC analyzer (Breda, Netherlands), DOC was measured using EPA method 415.1 [54] and turbidity was measured using a Turb 550 (WTW, Weilheim, Germany) turbidity-meter. Cations and anions present were measured using Spectro Genesis ICP OES (Kleve, Germany) and Dionex DX-120 ion chromatograph (Sunnyvale, CA), respectively. The percent difference between the sum of anions and cations in equivalent weight per liter (electroneutrality) was calculated to assure the accuracy of measurements.

3.3.2. Pretreatment

EC was investigated as the primary pretreatment method. Fig. 1 represents a schematic diagram of the EC setup. Five electrodes with an active surface area of 180 cm^2 (6061 aluminum alloy) and 5 mm spacing were placed vertically in a home-made polycarbonate reactor (600 ml). The first and last electrodes were connected to a DC power source (Hewlett Packard, Palp Alto, CA) and acted as the cathode and anode. All EC experiments were carried out in batch mode. In each experiment, 550 ml HFPW sample was collected in the EC unit. The current was maintained at 1 to 5 A (equivalent to 5.5 to 27.8 mA cm^{-2} current density) and the corresponding voltage was recorded. After 30 a second reaction time, electrocoagulated samples was transferred to a separatory funnel for sludge sedimentation. After a 6 h sedimentation time, the clear portion of the sample was recovered and the deposited sludge as well as floating skimmings were wasted.

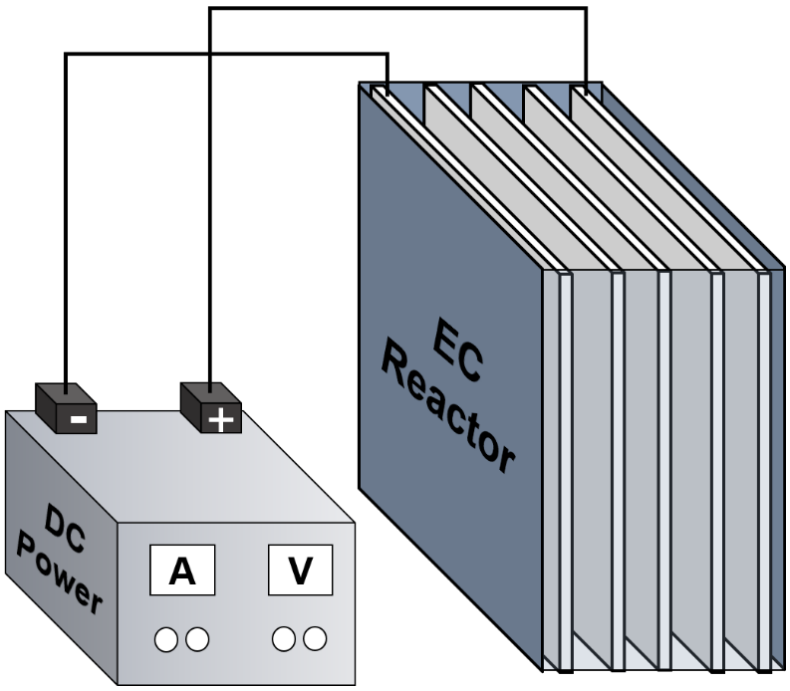

Fig. 1. EC setup. EC unit consisted of a polycarbonate reactor, five aluminum electrodes and a DC power source.

3.3.3. MD Membrane

Ethylene chlorotrifluoroethylene (ECTFE) copolymer flat sheet membrane samples were provided by 3M (Maplewood, MN). Table 1 represents the characteristics of these ECTFE membranes, including mean pore size, porosity, thickness, contact angle, maximum roughness and liquid entry pressure (LEP). All membrane properties were measured and discussed in our previous work [55].

Table 1. Characteristics of ECTFE membrane.

Membrane	Mean Pore size (μm)	Porosity	Thickness (μm)	Contact Angle	Max Roughness (nm)	LEP (kPa)
ECTFE	0.18	0.71	82±4	130±1	711	330

3.3.4. DCMD Test System

Fig. 2 is a schematic diagram of the DCMD apparatus. A home-made PTFE tangential flow cell with 40 cm^2 effective surface area and 2 mm channel depth was employed for DCMD experiments. In order to provide mechanical support for the membrane, PTFE spacers (ET 8700) were acquired from Industrial Netting (Minneapolis, MN) to fill the channels on both sides of membrane cell. As can be seen in Fig. 1, feed and distillate streams recirculated countercurrent on opposite surfaces of the membrane by means of two peristaltic pumps (Masterflex I/P, Cole Parmer, Vernon Hills, IL) at equal flow rates of 0.3 to 0.9 L min^{-1} (equal to flow velocity of 5.5 to 16.7 cm^{-1} sec). A range of feed temperatures, from 50 to 70 ℃ were tested. Temperature of distillate stream was kept at 20℃ for all experiments. The conductivity of distillate was recorded

using a conductivity meter (VWR, Radnor, PA) and kept under 20 µS cm^{-1} during all membrane distillation experiments to make sure that experiment runs without membrane damage or wetting. Membrane damage/wetting was recognized when the conductivity of permeate stream increased rapidly above 20 µS cm^{-1} with a concurrent rapid increase in water flux.

A custom-made level controlled tank with capacity of 2 L was employed as the feed tank. The level controller in this tank was connected to a dosing and a discharge pump (Masterflex L/S Digital Standard Drive, Cole Parmer). The dosing pump was used to inject fresh feed as make-up water into the feed tank. The discharge pump was employed to enable the process to run in continuous mode. The outlet line from the feed tank was open in all continuous experiments and was closed in all batch experiments. Both dosing and discharge pumps were activated by the level controller installed in the feed tank. The flow rate of dosing and discharge pumps were proportionally adjusted to maintain a constant TDS in the feed tank in continuous experiments. While permeate was collected in the distillate reservoir, the make-up water and high TDS brine tanks were placed on computer-connected analytical balances (Mettler Toledo, Columbus, OH). Water flux calculation in L m^{-2} h^{-1} was performed using Eq. (10):

$$J = \frac{\Delta m}{SA\ x\ t\ x\ \rho} \tag{10}$$

where J is transmembrane water flux, Δm is the recorded net weight difference between make-up water and high TDS brine tanks, SA is membrane surface area, t is time interval of weight record and ρ is the feed water density.

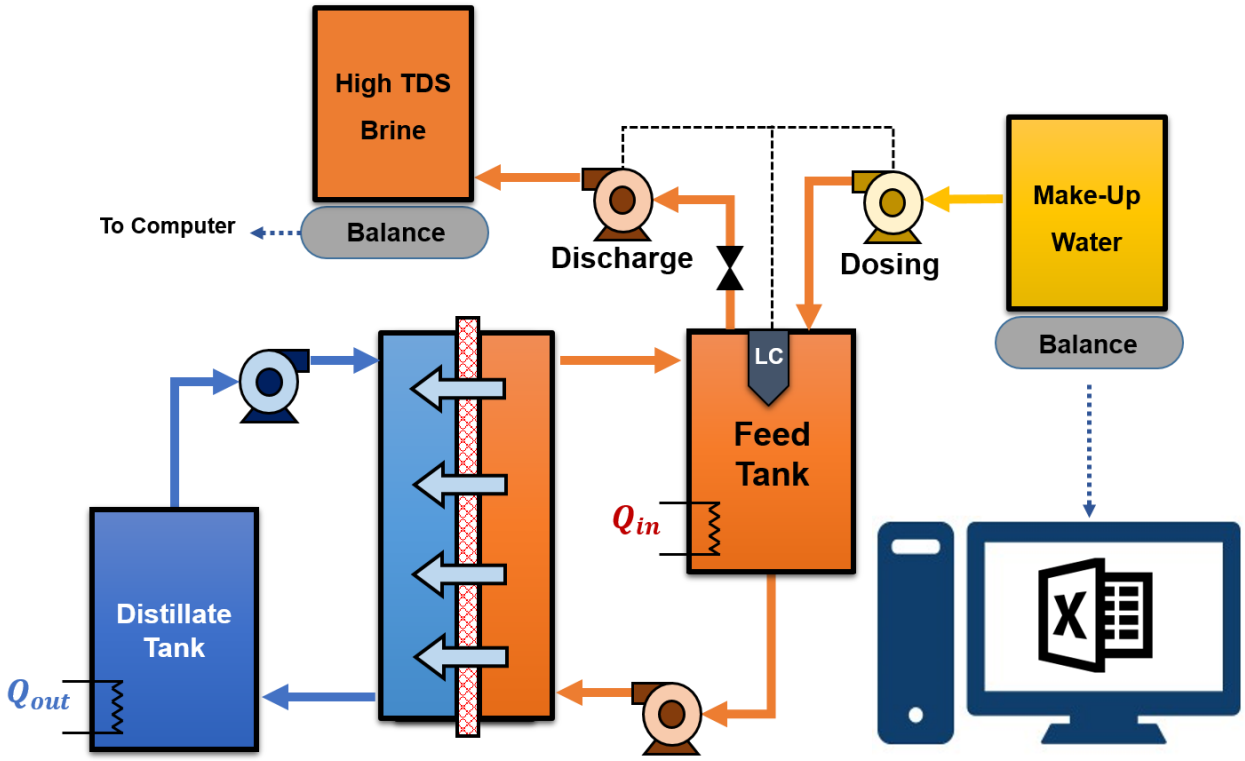

Fig. 2. Schematic diagram of the established DCMD setup.

3.3.5. DCMD Experiments

Table 2 gives the various DCMD experiments carried out in this study. Experiments were performed using different feed streams. A set of experiments were carried out with synthetic HFPW to provide a baseline/control for the DCMD system. Synthetic HFPW was prepared using sodium chloride in de-ionized (DI) water, containing the same TDS as the raw HFPW. DCMD experiments were also performed employing raw HFPW obtained from oil and gas extraction facilities. For synthetic and actual HFPW, different feed temperatures as well as a range of flow velocities were tested. In addition, DCMD experiments were performed with EC pretreated HFPW samples. In these experiments, experiments were continued until feed water was concentrated up

to 300 g L^{-1} TDS. Finally, a long-term experiment was conducted over 434 h to evaluate the performance of ECTFE membrane in longer experimental runs.

Table 2. Summary of DCMD experiments in this study.

Experiment	Feed	Feed Temp.	Flow Velocity	Operating Mode	Feed Tank Discharge line	Duration
		ºC	cm s^{-1}	Batch | continuous	Open | Close	
Baseline Control	Synthetic HFPW	50 - 70	5.5 – 16.7	Batch	Close	Until ~2.45 L permeate was collected (feed concentrated to 300 g L^{-1} TDS
Actual	Raw HFPW	50 - 70	5.5 – 16.7	Batch	Close	
Pretreatment	Pretreated HFPW	50 - 70	16.7	Batch	Close	
Long-Term	Pretreated HFPW	60	9.3 - 16.7	Continuous	Open	Up to 434 h

3.3.6. Membrane Characterization Tests

3.3.6.1. Scanning Electron Microscopy (SEM) and Energy-dispersive X-ray Spectroscopy (EDX)

SEM using a Nova Nanolab 200 Duo-Beam Workstation (FEI, Hillsboro, Oregon) was used to observe changes in the ECTFE membrane surface after DCMD experiments. The same equipment was used to perform EDX spectroscopy on fouled membrane surfaces to obtain chemical information on the foulants.

3.3.6.2. Contact Angle

The static contact angle was measured using a contact angle goniometer (Model 100, Rame-Hart Instrument Company, Netcong, NJ). A DI water droplet (5 μL) at a rate of 2 μL/s was formed on the tip of a micro-syringe (Hamilton, Reno, NV). The micro-syringe was moved down vertically towards the sample until it made the contact with the sample. Then, the syringe was moved up and detached from the droplet. Using the circle fitting method, the angle made between the left and right-hand side of the water droplet and the membrane surface was measured at five locations and averaged.

3.3.6.3. LEP

LEP was determined as described by Smolder and Franken [56]. Briefly, the LEP of virgin and tested ECTFE membranes was measured using a Sterlitech HP4750 (Kent, WA) stainless steel cell at 20 ˚C. The cell was filled with DI water and gradually pressurized at the rate of 13.8 kPa min^{-1}. The LEP is the pressure at which a continuous flow of DI water through the membrane is first observed.

3.4. Results and Discussion

3.4.1. HFPW Characterization Results

Table 3 shows the characteristics of raw and pretreated HFPW samples. All samples were characterized in terms of inorganic composition as well as the following parameters: TDS, TSS, TOC, DOC, pH and Turbidity. Close to four times higher than seawater TDS (135 g L^{-1}) is observed. Sodium and calcium were observed as the main cations, while chloride was the main

anionic component of the HFPW. The HFPW sample contained 97.9 and 41.8 mg L^{-1} TOC and DOC, respectively. It contained relatively high levels of suspended solid and turbidity, compared to municipal wastewaters.

Table 3. Characterization results of raw and pretreated HFPW samples.

	Unit	Raw HFPW	EC 1 A	EC 2 A	EC 3 A
TDS	g L^{-1}	135	134	133	133
TOC	mg L^{-1}	97.9	57.4	46.3	37.8
DOC	mg L^{-1}	41.8	35.7	31.1	29.6
TSS	mg L^{-1}	494.1	107.1	43.3	37.3
Turbidity	Ntu	23.4	4.3	1.1	0.8
pH		6.4	6.5	6.4	6.7
chloride	mg L^{-1}	86,379	84,324	85,122	83,415
Nitrate	mg L^{-1}	0.7	0.3	0.7	0.5
sulfate	mg L^{-1}	1.9	1.4	1.4	1.1
Aluminum	mg L^{-1}	1.5	2.7	3.2	4.6
Boron	mg L^{-1}	25.6	20.7	22.4	21.8
Calcium	mg L^{-1}	12,352	12,194	12,501	11,893
Magnesium	mg L^{-1}	35.07	33.64	33.9	34.5
Potassium	mg L^{-1}	740.4	728.7	719.8	731.5
Sodium	mg L^{-1}	38,720	38,671	38,421	38,122
Electroneutrality Percent Difference	%	< 3	< 2	< 2	< 2

3.4.2. EC Pretreatment

Here, aluminum electrodes were used as EC electrodes. Following EC reactions, Al^{3+} and OH^- ions were released into the solution and formed a variety of aluminum hydroxide complexes (see section 2.3). Positively charged complexes such as $Al(OH)_2^+$ contributed to charge neutralization of negatively charged organic species and suspended solids. As the solution aged, aluminum hydroxide complexes transformed to $Al(OH)_{3(s)}$, producing white-grey flocs [57]. These flocs adsorbed organic molecules, trapped suspended particles and were separated from solution following a 6 h sedimentation time.

Different parameters including voltage, current, reaction time, pH and electrode material can affect EC performance. A range of electric currents, from 1 to 5 A were investigated. The EC reaction time was kept constant at 30 sec for all runs. The impact of EC pretreatment on removal of different parameters is calculated as removal efficiency using Eq. (11):

$$Removal\ Efficiency\ (\%) = \frac{C_f - C_p}{C_f}\ X\ 100 \qquad (11)$$

where C_f and C_p are feed and EC pretreated water concentrations, respectively. Results are presented in Fig. 3. As can be seen, all removal efficiencies increased as the applied current increased. When current rose from the zero to 2 A, all contaminants were rapidly removed. However, the removal efficiency reaches an approximately constant value once the current reached 3 A. For 3 A current, turbidity, TSS and TOC were removed by 96, 91 and 61%, respectively. The removal of DOC was 29%. Only limited removal of TDS is observed.

The voltage was recorded at 15 sec intervals in all EC experiment. Due to the generation of ionic species, the voltage was decreased to ensure a constant current during each EC run.

Energy consumption for EC process (E) was estimated in kWh per m^3 feed using the following equation:

$$E = \frac{V\ x\ I\ x\ t}{Vr} \quad (12)$$

where V is average voltage, I is applied current, t is reaction time and Vr is reactor volume. Energy consumption is shown in the secondary vertical axis of Fig. 3. Higher removal was achieved for higher currents which resulted in higher energy consumption. The estimated energy consumption for 3 A current was 1.41 kWh m^{-3}.

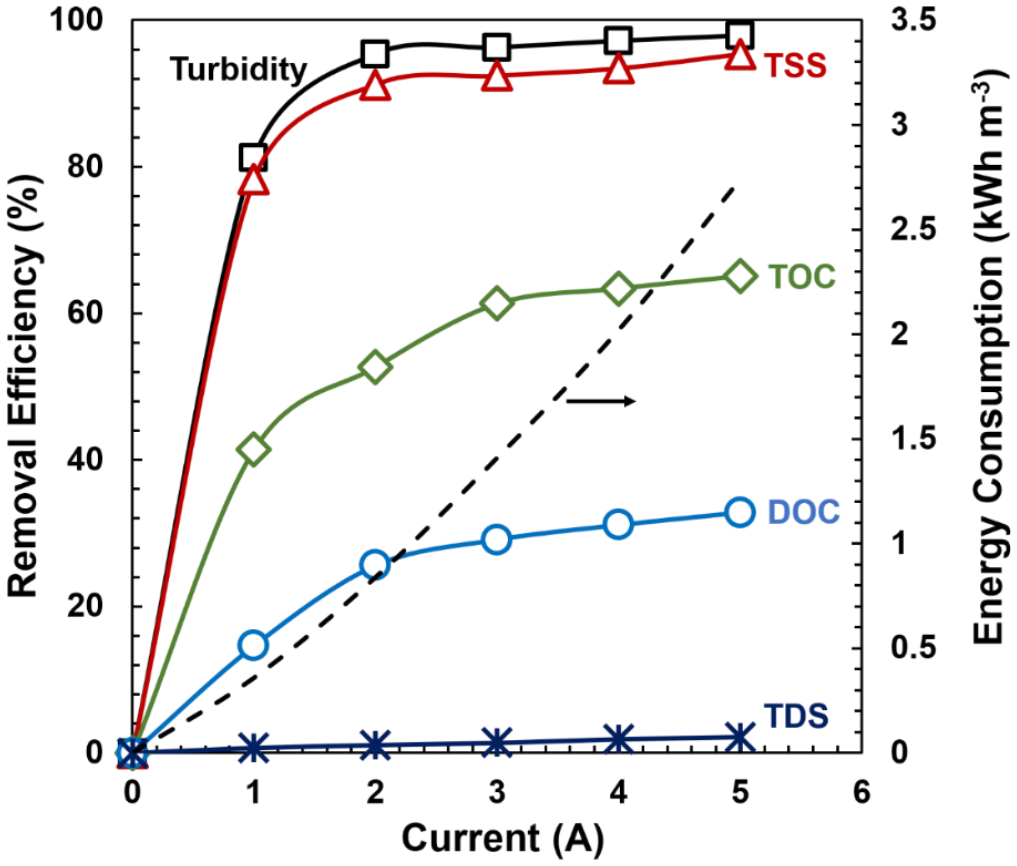

Fig. 3. Removal efficiency of turbidity, TSS, TOC, DOC and TDS as a function of current applied during EC. Energy consumption of the EC process is shown on the secondary vertical axis.

3.4.3. DCMD Results

3.4.3.1. Baseline Experiments with Synthetic Feed

The first set of DCMD experiments were conducted using a synthetic HFPW stream as feed, consisting of 135 g L^{-1} sodium chloride in DI water. TDS level was the same as the actual HDPW sample received form Southwestern Energy. A range of feed temperatures and flow velocities were tested. All experiments were carried out in batch mode, concentrating the feed water up to 300 g L^{-1} TDS (55% water recovery) with continuous addition of saline make-up water to the feed tank. Figs. 4.a and 4.b demonstrate the water flux of the ECTFE membrane for a range of feed temperatures as well as a range of flow velocities as a function of feed TDS. The recovered permeate volume, corresponding to the feed TDS at each point, is presented uisng the secondary horizontal axis. Water fluxes in the range of 18 to 70 L m^{-2} h^{-1} were observed when increasing the feed temperature from 50 to 70 °C. Water vapor transport trough the membrane is driven by the vapor pressure difference across the membrane. Vapor pressure is a function of temperature and increases rapidly by increasing temperature [58]. Thus, higher water fluxes were observed for higher feed temperatures. A slight flux decline is observed with increasing feed TDS. This is not unexpected given the dependence of vapor pressure on feed salinity [23].

Water fluxes in the range of 24 to 47 L m^{-2} h^{-1} were observed for 5.5 to 16.7 cm s^{-1} flow velocities. As can be seen in Fig. 4.b, the water flux increased with increasing flow velocity of distillate and feed streams. An increase in flow velocity increases the heat transfer coefficient for the thermal boundary layer on the feed and distillate sides of the membrane [59]. As the heat transfer coefficient on both sides of the membrane increases, the temperature at the membrane surface increases on the feed side but decreases in the permeate side (approaches the temperature

in the bulk solution). Thus, higher water flux is observed due to a higher water vapor pressure difference across the membrane [21].

As can be seen in Figs. 4.a and 4.b, predicted water fluxes are in good agreement with the experimental results. The results obtained here are in agreement with results reported by Han et al. [60], indicating stable water flux in DCMD system and minimal fouling when the feed stream contains only sodium chloride.

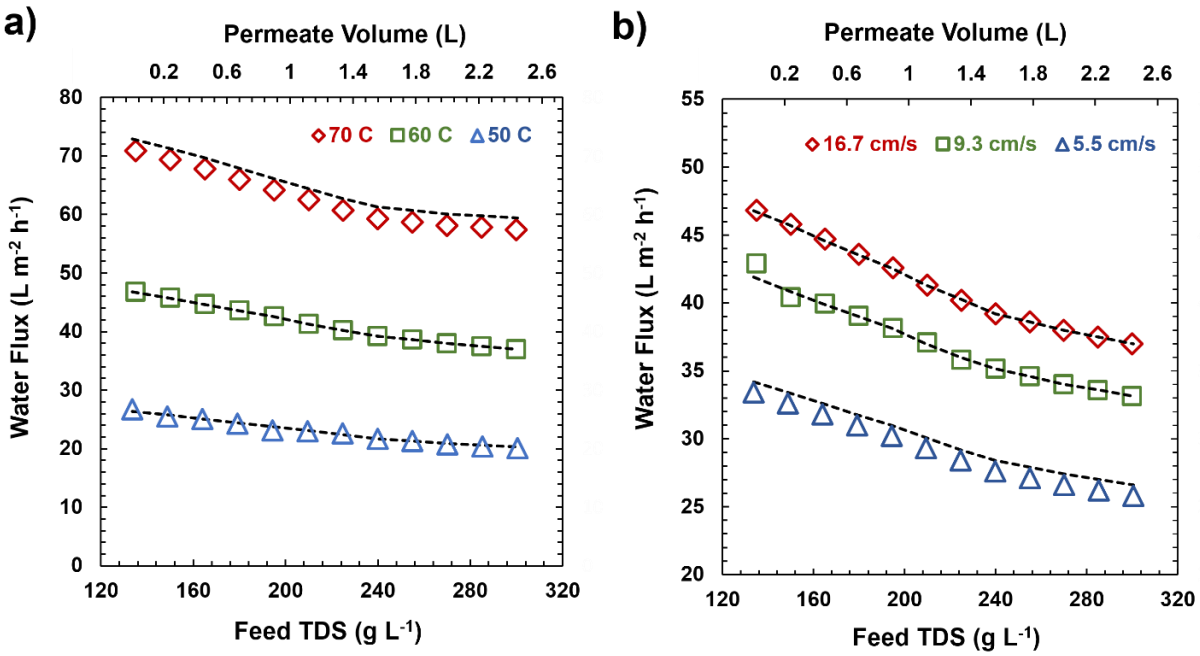

Fig. 4. Experimental and predicted water flux as a function of feed TDS and permeate volume for synthetic HFPW at a) different feed temperatures with flow velocity fixed at 16.7 cm s^{-1} and b) different flow velocities at 60 °C feed temperature. Synthetic water, containing 135 g L^{-1} sodium chloride in DI water, was used as feed and make-up water. Experiments were carried out with feed outlet line closed. Distillate stream was kept at 20 °C for all case studies.

Digital and SEM images taken of the surface of the ECTFE membranes after treating synthetic HFPW are shown in Fig. 5.a and Fig. 5.b, respectively. As can be seen, minimal fouling is observed. SEM images from different locations on the membrane surface did not show significant signs of fouling. For the membrane shown in Fig. 5 a and b, DCMD experiments were conducted at 60 °C feed temperature, 20 °C distillate temperature and 9.3 cm s^{-1} flow velocity. McGaughey *et al.* [61] report a similar observation for a synthetic saline feed using polytetrafluoroethylene (PTFE) membranes. The membrane surface was further analyzed using EDX spectroscopy after treating synthetic HFPW. The EDX spectrum is given in Fig. 5.c. Carbon, fluorine and chlorine peaks are due to the base ECTFE polymer (hydrogen cannot be detected using EDX spectroscopy) [62]. Gold and palladium peaks are also observed due to membrane preparation prior to SEM imaging. A sodium peak was not detected, supporting the idea that solid scales were not formed on the membrane surface during operation.

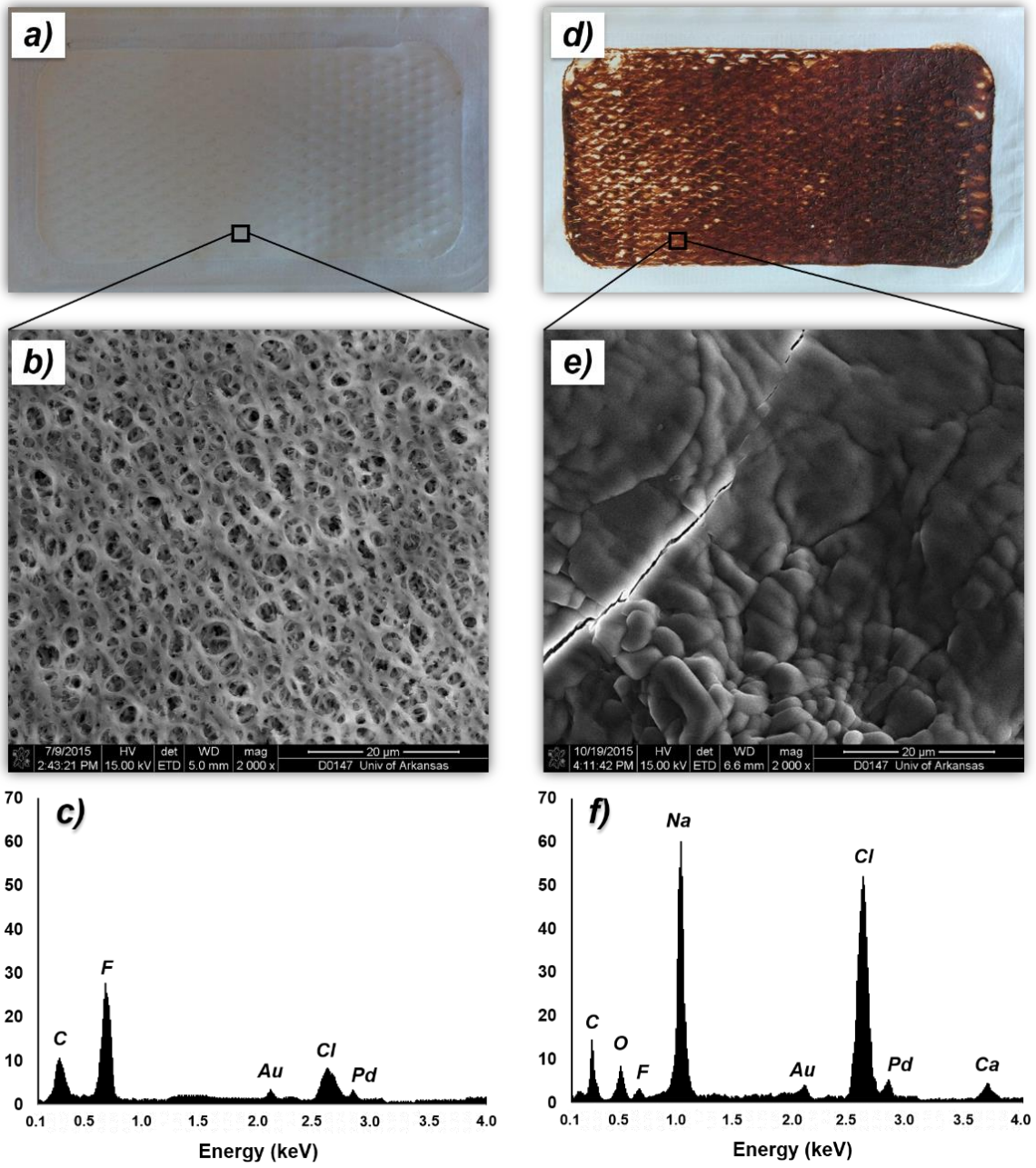

Fig. 5. Digital and SEM images of surface of the ECTFE membranes after DCMD with **a & b)** synthetic HFPW **d & e)** raw actual HFPW. EDX spectra for membranes after DCMD with c) synthetic HFPW and d) raw HFPW. Both synthetic and actual feed streams contained 135 g L^{-1} TDS. Major fouling occurred when treating raw HFPW.

3.4.3.2. DCMD Experiments with Raw HFPW

A second set of DCMD experiments was carried out using raw HFPW, containing 135 g L^{-1} TDS, 97.9 mg L^{-1} TOC and 107.1 mg L^{-1} TSS. Analysis of raw HFPW is shown in Table 3 (see section 4.1). Virgin ECTFE membranes were used in all DCMD runs. Figure 6.a and b show the variation of water flux with feed TDS and permeate volume at different feed temperatures and flow velocities, respectively. The predicted water fluxes are also shown by dashed lines. As can be seen, comparing Figure 4 and 6. the decrease in water flux is significant and cannot be predicted based on the results for synthetic HFPW.

When using actual HFPW membrane fouling leads to a significant decline in water flux. This is not unexpected given the high level of TSS (494.1 mg L^{-1}) and TOC (97.9 mg L^{-1}) in the feed water. Lokare *et al.* [16] report much lower flux decline rates for PTFE and polypropylene (PP) membranes when treating HFPW containing 80 g L^{-1} TDS. However, the feed water was pretreated prior to DCMD experiments in their work, using a microfiltration membrane. Thus, solids and particulates greater than 0.22 μm were removed from the HFPW samples and the resulting pretreated water contained minimal levels of TOC.

Digital and SEM images from the surface of ECTFE membrane after treating raw HFPW are shown in Figs. 5.c and 5.d, respectively. A brownish cake layer was observed on the membrane surface confirming significant membrane fouling. The SEM image indicates blockage of the membrane pores. The membrane surface was further investigated by Energy-dispersive X-ray (EDX) spectroscopy. EDX spectrum is shown in Fig. 5.f. A number of elements were detected on the surface. The fluorine peak was reduced compared to Fig. 5.c due to the formation of a fouled layer on the membrane surface. However the carbon peak as well as a new oxygen peak

are detected, indicating deposition of organic compounds [63]. A significantly stronger chlorine peak as well as a new sodium peak are observed for the membrane used to treat real HFPW. This indicates the formation of sodium chloride scale on the membrane surface. The presence of a calcium peak suggests that calcium based scale also forms. Similar to the EDX spectrum for the membrane challenged with synthetic HFPW, gold and palladium were detected on the surface.

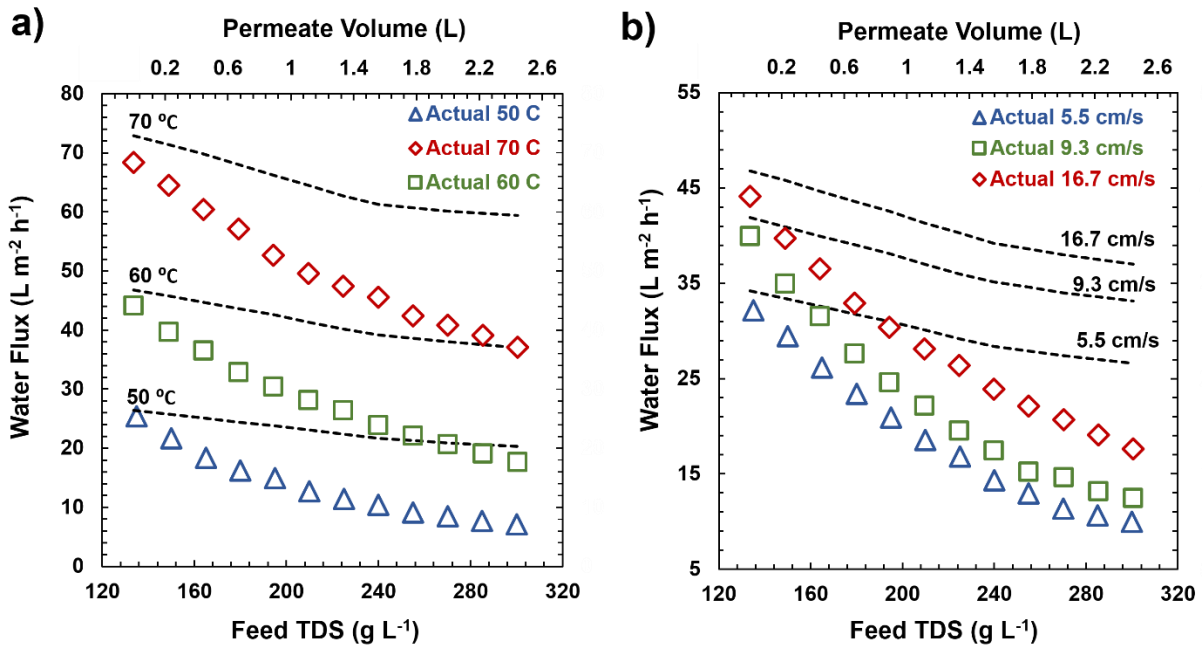

Fig. 6. Variation of experimental water fluxes with feed TDS and permeate volume for real HFPW at a) different feed temperatures with constant flow velocity of 16.7 cm s^{-1} and b) different flow velocities at 60 °C feed temperature. Experiments were run with feed outlet line closed. Distillate stream was kept at 20 °C. Dashed lines represent the predicted water fluxes based on synthetic HFPW.

3.4.3.3. DCMD with EC Pretreated HFPW

Pretreatment of the real HFPW is essential in order to suppress rapid membrane fouling when develop a practical MD process. Further, the pretreatment process must be economically viable and practical to implement in the field. Here we have investigated EC. EC pretreated

samples using 1, 2 and 3 A were introduced to the DCMD system. All experiments were continued until 2.45 L permeate were collected and feed was concentrated to 300 g L^{-1} TDS. Figure 7 give the variation of water flux for different pretreated water samples. Dashed line shows the water flux for synthetic HFPW. In addition, the result for HFPW without EC pretreatment is included. As can be seen as the current used for EC pretreatment is increased, a lower decrease in water flux is observed during DCMD. Using currents higher than 3 A did not lead to a significant improvement in water flux in agreement with the results shown in Figure 3.

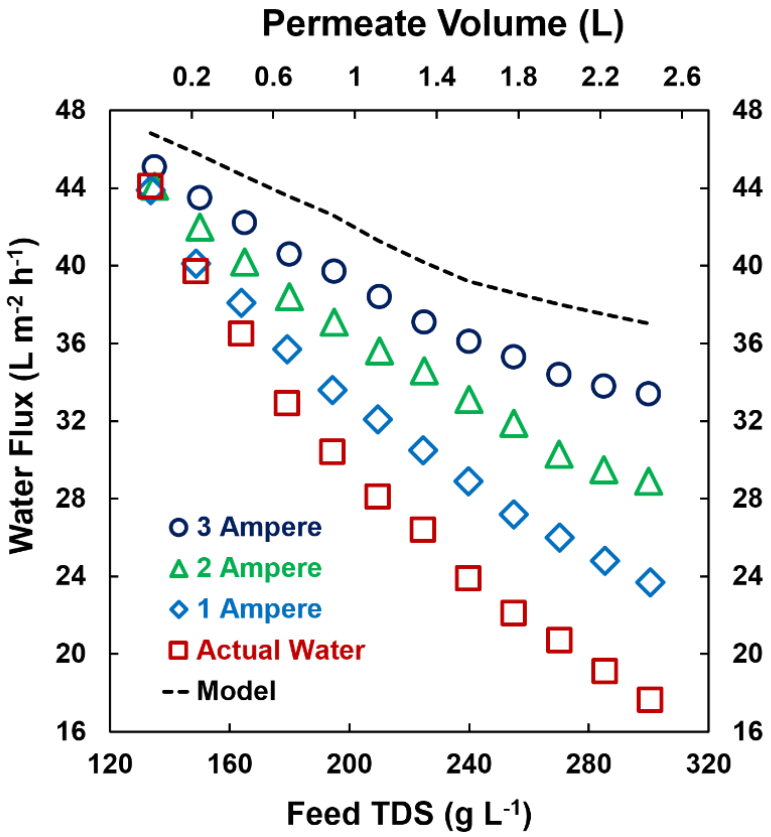

Fig. 7. Variation of water flux for pretreated and non-pretreated HFPW as functions of feed salinity and permeate volume. The feed temperature was maintained at 60 °C. Flow velocity of both feed and distillate streams were maintained at 16.7 cm s^{-1}. Predicted water flux is shown is dashed line.

Fig. 8 give SEM images of the surface of the ECTFE membranes after experiments with pretreated feeds. As can be seen by comparing Figure 8.a,b and c, the degree of fouling decreasd as the current used during EC increases. Comparing Figures 5 and 8, fouling is greatly suppressed by EC pretreatment. These results are in agreement with the results shown in Figure 3 for the removal efficiency of TOC, TSS and turbidity.

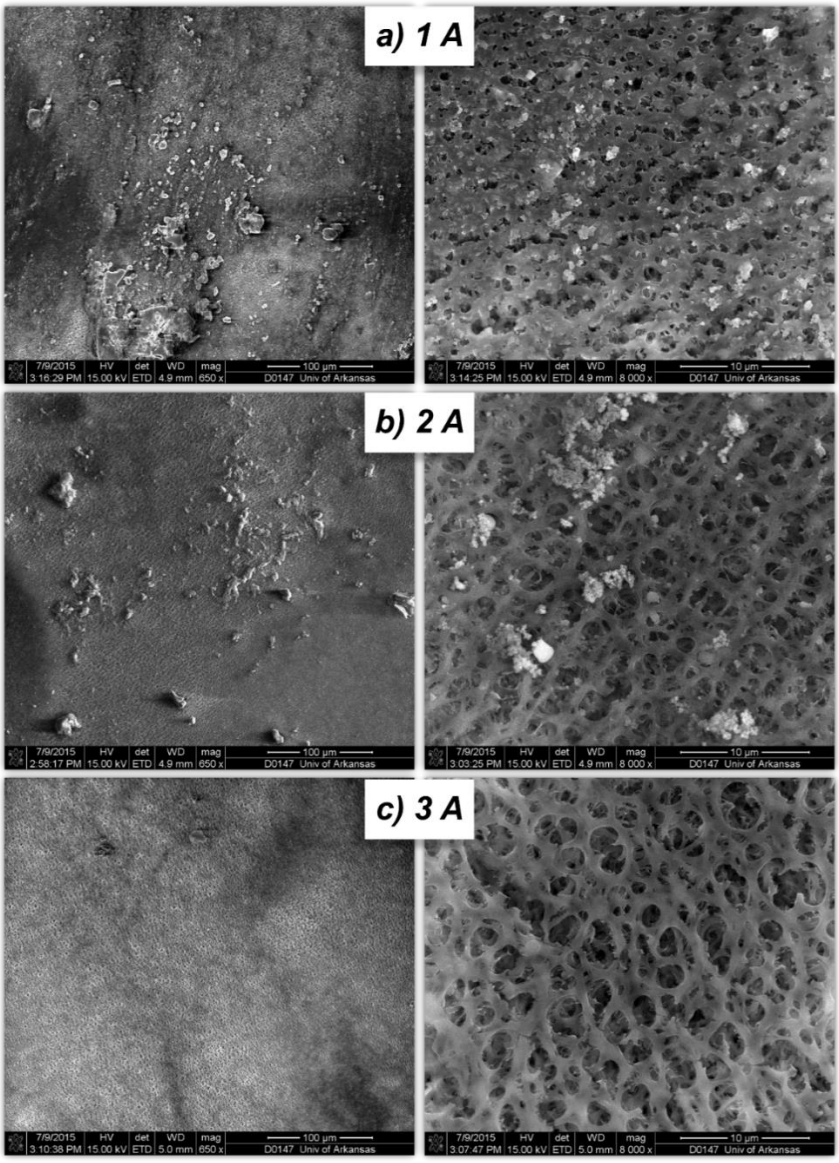

Fig. 8. SEM images of surface of ECTFE membrane after DCMD experiment with EC pretreated HFPW samples. a) 1 A current, b) 2 A current and c) 3 A current.

Preventing membrane wetting is of significant importance when operating MD systems. Fouling induced wetting, resulting in product water contamination, is a significant concern for real MD applications [31,64]. Membrane hydrophobicity and LEP are often related to membrane wetting [21]. Sessile drop contact angle was measured for virgin and used ECTFE membranes. The results are shown in Fig. 9. A contact angle of 130° was measured for virgin ECTFE membrane. After DCMD with synthetic HFPW, the contact angle was slightly decreased to 122°. Although no significant fouling was detected in DCMD experiment with synthetic HFPW to cause the contact angle to decrease, exposure to temperatures around 60 °C can change the membrane hydrophobicity [61]. In the case of pretreated HFPW, the membrane contact angle decreased as the TOC content of feed increased. Contact angle of 76, 105 and 111° were measured for EC pretreated HFPW with 1, 2 and 3 A current, respectively. While for the case of raw HFPW, water droplet could not be formed on membrane surface due to severe fouling and was immediately adsorbed.

The average LEP of membranes is also reported in Fig. 9. The LEP follows the same trend as the contact angle. The LEP decreases as the membrane fouling increases. Reduction of LEP implies a greater likelihood of membrane wetting [60]. The occurrence of membrane wetting depends not only on the LEP but also internal pore hydrophobicity [35]. LEP of 94, 216 and 249 kPa were measured for EC pretreated HFPW with 1, 2 and 3 A current, respectively.

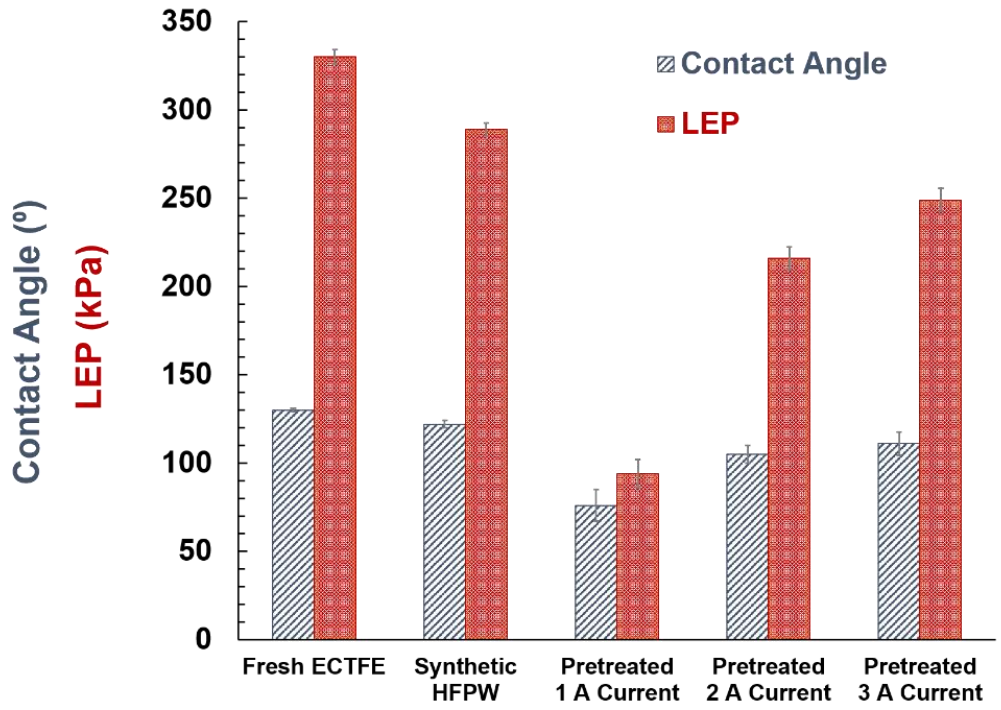

Fig. 9. Contact angle and LEP of fresh and tested ECTFE membranes. Both contact angle and LEP decrease with an increase in organic content of DCMD feed water.

3.4.4. Modified Flux Prediction

Reduction of water flux due to membrane fouling can be related to changes in the overall MD permeability coefficient according to Eq. (5). Here, we have modeled the decrease in flux in terms of a change in the water permeability coefficient (A). Fig. 10.a gives the calculated water permeability coefficient of the fouling layer (A_f) for raw and pretreated HFPW as a function of permeate volume. As can be seen, the permeability of fouling layer decreases as the permeate volume increases. As expected, an increase in EC current resulted in higher fouling layer permeability coefficients. Using Eq. (5) along with our flux prediction tool, water flux of EC pretreated HFPW (3 A current) was estimated for different operating conditions. Fig. 10.b

illustrates the variation of experimental and predicted water flux versus recovered permeate volume. Feed and distillate temperatures were maintained at 60 and 20 °C, respectively. Flow velocities were kept constant at 16.7 cm s^{-1}. The flux was modeled using the fouling layer permeability coefficient calculated in Fig. 10.a. A_f for the pretreated HFPW with 3 A current is used. The fouling layer permeability coefficient could be used as a correction factor when the vapor pressure data of the real feed streams, containing various organic and inorganic species, is not available.

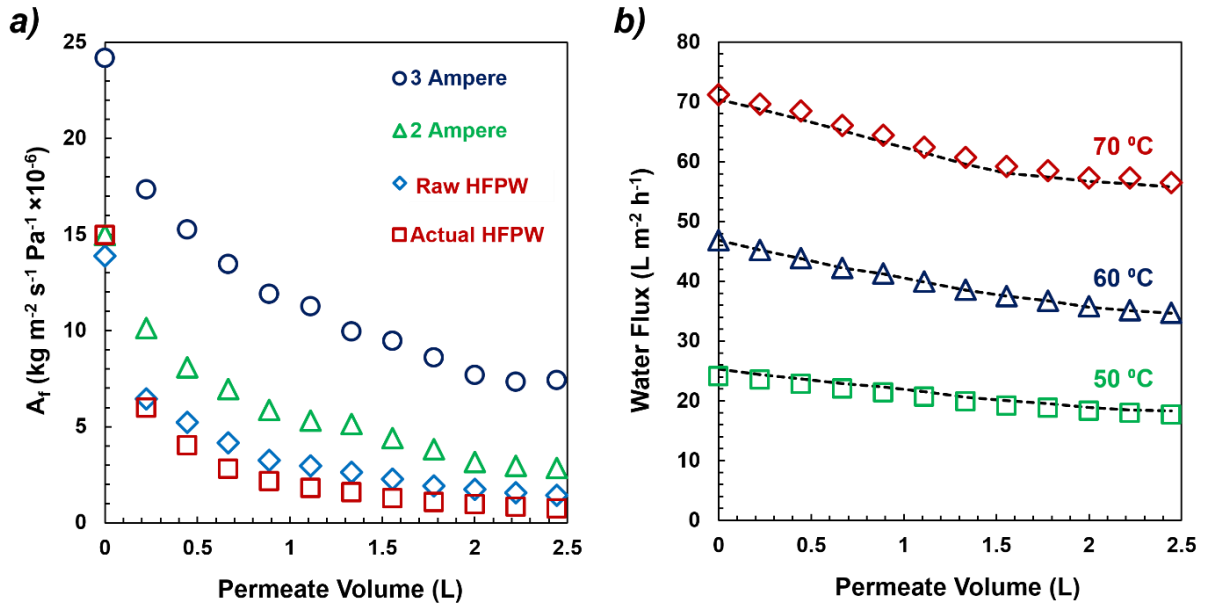

Fig. 10. a) Fouling layer permeability coefficient (*Af*) as a function of permeate volume. b) experimental and predicted (using A_f) water flux.

3.4.5. Long-term EC - DCMD Experiment

A long-term DCMD experiment was conducted to evaluate the performance of ECTFE membrane for water recovery from EC pretreated HFPW. The experiment was carried out using

pretreated HFPW with 3 A current as feed stream. Characteristics of this pretreated sample can be found in Table 3. Feed and distillate temperatures were maintained at 60 and 20 °C, respectively. Flow velocity of both feed and distillate streams were kept constant at 9.3 cm s^{-1}. Experiment was first run in batch mode with the feed discharge outlet line closed. Feed water was concentrated to 265 g L^{-1} (~50% recovery). This step was performed in 13:40 h. Then, the outlet line was opened and TDS of feed was maintained constant at 265 g L^{-1} using proportional dosing and discharge flow rates. Experiment ran for ~420 h in continuous mode. Clean permeate was recovered in distillate tank, fresh pretreated feed was continuously added to feed tank and concentrated brine was withdrawn from the feed tank and collected in the high TDS brine tank (see Fig. 2). Conductivity of distillate was monitored throughout the experiment and maintained below 50 µS cm^{-1} to ensure no wetting.

Fig. 11.a gives the variation of water flux and distillate conductivity as a function of run time. Water flux decline was observed in the batch mode (first ≈14 h), as the feed was concentrated the feed up to 265 g L^{-1} TDS. This flux decline was mainly due to the decrease in transmembrane vapor pressure difference caused by increasing in feed salinity. As can be seen, almost a steady water flux was observed for 420 h when the feed TDS was kept constant at 265 g L^{-1}. time. Lokare et al. [16] report a similar trend over 70 h experimental time for HFPW pretreated with 0.22 µm microfiltration membrane and reducing the TOC content of the feed water to ~6 mg L^{-1} (here 37.8 mg L^{-1}).

The TDS of the brine tank was measured during continuous operation to ensure it remained constant at 265 g L^{-1}. The TDS of the brine tank is lasso given in Figure 11 using the secondary vertical axis. Figs. 11.b and 11.c show SEM images of two locations on the membrane surface

after the long-term experiment. As can be seen, minor fouling and scaling were observed. At the end of experiment, recovered permeate was characterized in terms of TOC and TSS content. 2.94 mg L^{-1} TOC was measured in the permeate, while the TSS was below detection limit. In MD not only water vapor, but also volatile organic compounds, can vaporize and pass through the membrane pores giving rise to the measured. Transport of organics across the membrane is linked to contaminant volatility and hydrophobicity [65].

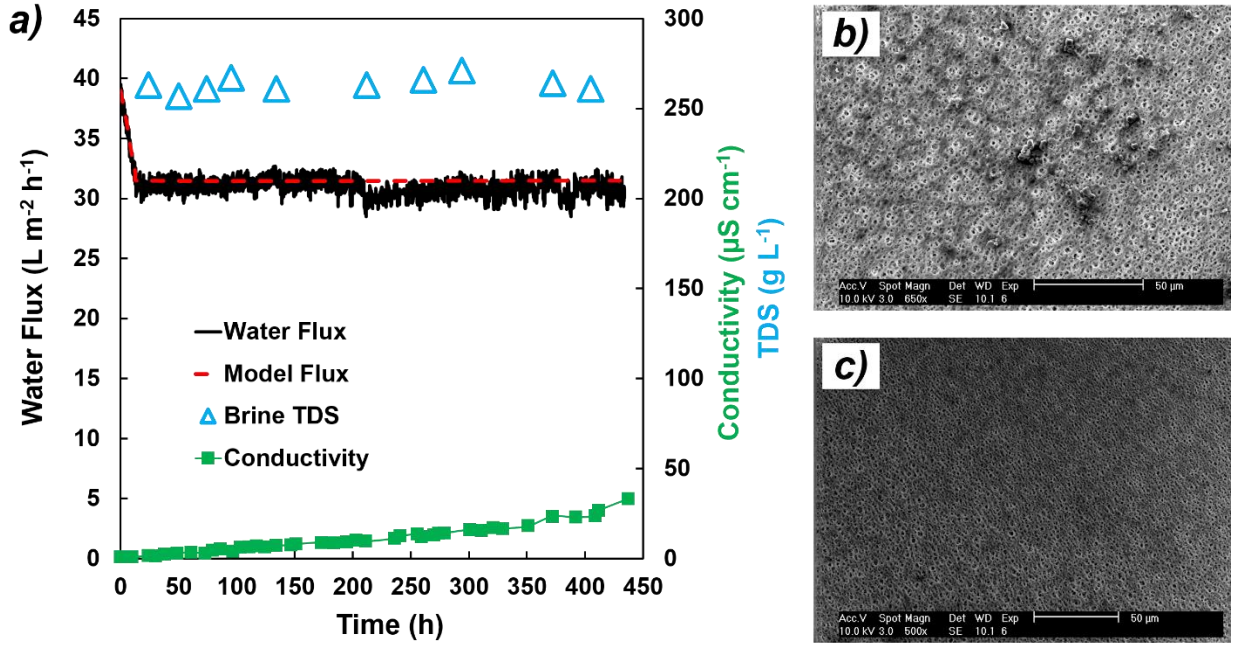

Fig. 11. Water flux and distillate conductivity as functions of time for the long- term DCMD experiment. Pretreated HFPW with 3 A was used feed. Feed and distillate temperatures were kept at 60 and 20 °C, respectively. Flow velocity of both feed and distillate streams were at 9.3 cm s^{-1}.

3.5. Concluding Remarks

Membrane separation processes can be utilized in treatment of HFPWs to maximize water recovery and minimize the volume of concentrated brine that has to be disposed to the

environment. Here, we obtained water recoveries up to 57 percent from an actual HFPW sample containing 135 g L^{-1} dissolved solids. For real feed streams, containing surfactants and other organic compounds, either pretreatment or optimized membrane surface properties will be required in order minimize a flux decrease due to membrane fouling. The results obtained in this work indicate the importance of pretreatment prior to DCMD when treating high salinity PWs. If appropriately designed, pretreatment could successfully mitigate fouling and wetting during real DCMD operations. We show that EC process could effectively remove most contaminations, except for TDS, from actual HFPW. Maintaining a 3 A current in EC reactor for 30 sec, turbidity, TSS and TOC were removed by 96, 91 and 61%, respectively. Higher removal of contaminates such as TSS and TOC resulted in lower membrane fouling as well as lower water flux decline in DCMD. Using resistant in series modeling for membrane permeability, considering a fouling layer permeability coefficient, water flux of DCMD system for pretreated HFPW (3 A current) was accurately estimated. EC pretreated water was concentrated up to 265 g L^{-1} in a continuous DCMD process for over 434 h reporting stable water flux. However, we show that even small levels of organic content could result in membrane fouling in longer experimental runs.

Acknowledgements

Funding for this work was provided by Southwestern Energy through the National Science Foundation Industry/University Cooperative Research Center for Membrane Science, Engineering and Technology, the National Science Foundation (IIP 1361809) and the University of Arkansas.

Appendix A.

Heat transfer rate across the membrane is expressed as follows:

$$Q_m = K\Delta T + J\lambda \quad \text{(A.1)}$$

The first term in Eq. (A.1) represents the conduction heat transfer across the membrane where K and ΔT are conduction heat transfer coefficient and temperature difference across the membrane, respectively. Conduction heat transfer coefficient is defined as follows:

$$K = \frac{(1-\varepsilon)k_m + \varepsilon k_a}{\delta} \quad \text{(A.2)}$$

where k_m is solid membrane thermal conductivity and k_a is thermal conductivity of air. Eq. (A.2) accounts for both solid structure as well as porous nature of the membrane. Second term in Eq. (A.1) represents the heat transfer by water evaporation on feed side and consequent condensation in the distillate stream, where λ is latent heat of vaporization.

In order to calculate the heat transfer across the membrane, bulk temperatures of feed and distillate streams cannot be used due to thermal polarization. Fig. A.1 (a) illustrates the thermal boundary layer on either side of the membrane. As can be seen, feed temperature at surface of the membrane is lower than bulk feed temperature and the distillate temperatures at the surface of membrane is higher than the bulk distillate temperature. The rate of convective heat transfer across the boundary layers on either of the membrane is given as follwos:

$$Q_F = h_F(T_{F,b} - T_{F,m}) \quad \text{(A.3)}$$

$$Q_D = h_D(T_{D,b} - T_{D,m}) \quad \text{(A.4)}$$

where h_F and h_D are convective heat transfer coefficients for the feed dn distillate side thermal boundary layers. As shown in Fig. A.1 (a), F, D and m subscripts imply feed, distillate and

membrane surface, respectively. The heat transfer coefficients within the boundary layers may be estimated from convective heat transfer correlations in rectangular ducts [66]:

$$h = \frac{Nu\ C_p}{d_h} \tag{A.5}$$

where *Nu*, *Cp* and d_h are Nusselt number, specific heat capacity and channel hydraulic diameter, respectively. For spacer-filled channels, the Nusselt number and hydraulic diameter can be calculated as follows [67]:

$$Nu = 0.664\ k_{dc} Re^{0.5} Pr^{0.33} \left(\frac{2d_h}{l_m}\right)^{0.5} \tag{A.6}$$

$$d_h = \frac{2\varepsilon_{sp}}{\frac{2}{\delta_{sp}} + (1-\varepsilon_{sp})\left(\frac{2}{d_f}\right)} \tag{A.7}$$

where *Re* and *Pr* are Reynolds and Prandtl number and l_m, ε_{sp}, δ_{sp} and d_f are spacer filament length, spacer voidage, spacer thickness and spacer filament diameter, respectively. Spacer voidage is calculated as Eq. (A.8):

$$\varepsilon_{sp} = 1 - \frac{\Pi\ d_f^2}{2 l_m \delta_{sp} \sin(\theta)} \tag{A.8}$$

In this equation, θ is the spacer inside angle. In equation (A.6), K_{dc} is a characteristic representative of spacer and is defined as follows:

$$k_{dc} = 1.654\ \varepsilon_{sp}^{0.75} \left(\frac{d_f}{\delta_{sp}}\right)^{0.039} \left(\sin\left(\frac{\theta}{2}\right)\right)^{0.086} \tag{A.9}$$

The feed concentration at the membrane surface can be calculated using following equation [49]:

$$C_m = C_b\, e^{\frac{J}{k_c \rho_F}} \tag{A.10}$$

where C_b is feed bulk concentration, k_c is convective mass transfer coefficient for the feed side concentration boundary layer and ρ_F is feed density. Analogous to convective heat transfer, mass transfer can be calculated as following:

$$k_c = \frac{Sh\, D_F}{d_h} \tag{A.11}$$

where *Sh* is Sherwood number and D_F is solute diffusion coefficient. Given the large amount of NaCl in the HFPW, the diffusion coefficient of NaCl is used. Analogous to definition of Nu number, *Sh* is defined as follows (*Sc* is Schmidt number):

$$Sh = 0.664\, k_{dc} Re^{0.5} Sc^{0.33} \left(\frac{2d_h}{l_m}\right)^{0.5} \tag{A.12}$$

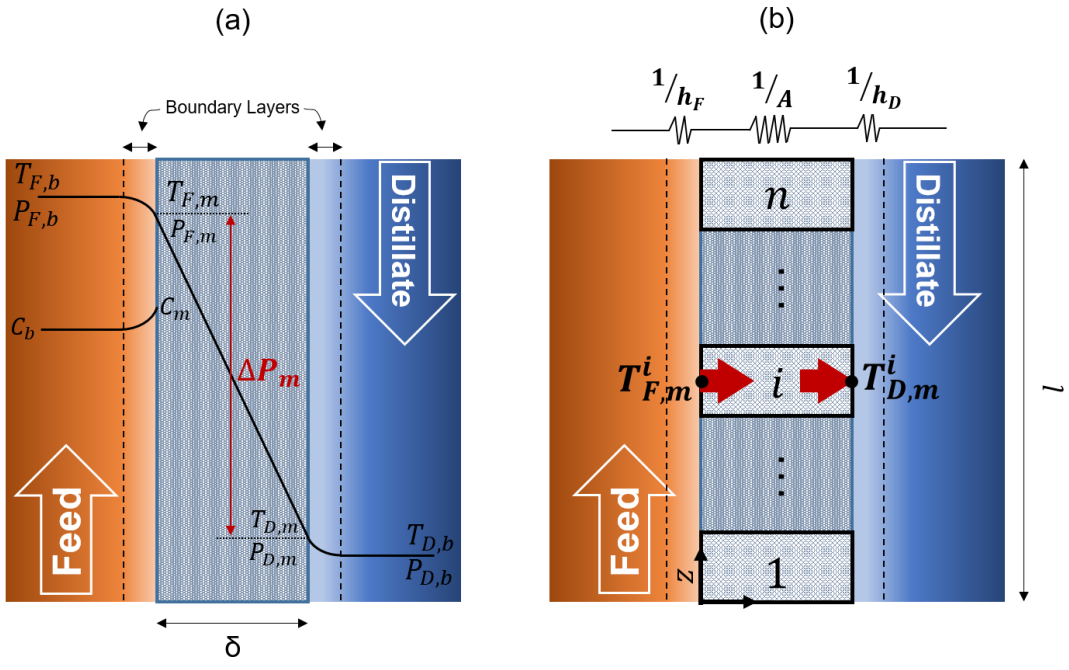

Fig. 1.A. Schematic diagram of **a)** temperature and concentration profiles across the membrane. *b)* differential elements used for modeling.

Modeling Procedure

A mathematical code was developed in MatLab 2016a. Properties of water and different concentrations of sodium chloride in water as well as all other required parameters such as membrane module geometries, membrane physical properties and operational conditions were introduced into the code. Next a flat sheet membrane was subdivided into n differential elements. See Fig. A.1 (b). Mass and heat transfer equations were solved simultaneously for each element separately using following boundary conditions (Note: C_b^{in}, $T_{F,b}^{in}$ and $T_{D,b}^{in}$ are known):

$$at \quad z = 0 \quad , \quad T_{F,b} = T_{F,b}^{in} \tag{A.13}$$

$$at \quad z = l \quad , \quad T_{D,b} = T_{D,b}^{in} \tag{A.14}$$

$$at \quad z = 0 \quad , \quad C_b = C_b^{in} \tag{A.15}$$

Fig. A.2 gives the modeling strategy. The distillate outlet temperature (at z=0) was assumed as the initial guess equal to feed inlet temperature as following:

$$at \quad z = 0 \quad , \quad T_{D,b}^{out} = T_{F,b}^{in}$$

For each ith element, the feed temperature and concentration at the membrane surface as well as the distillate temperature at membrane surface were assumed equal to the bulk concentration and temperatures. For the ith element, the water flux (J) was calculated using the reduced Knudsen-molecular diffusion model, convective heat transfer coefficients on feed and distillate sides (h_f and h_D) were calculated using Eq. (A.5) and consequently, feed and distillate temperatures at membrane surface ($T_{F,m}$ and $T_{D,m}$) were calculated using overall heat balance as follows:

$$Q_F = Q_m = Q_D \tag{A.16}$$

$$T_{F,m} = \frac{h_F T_{F,b} + \left(\frac{k_m}{\delta}\right)\left(\frac{h_F T_{F,b}}{h_D} + T_{D,b}\right) - J\lambda}{\frac{k_m}{\delta} + h_F + \left(\frac{k_m h_F}{\delta h_D}\right)} \tag{A.17}$$

$$T_{D,m} = \frac{h_D T_{D,b} + \left(\frac{k_m}{\delta}\right)\left(\frac{h_D T_{D,b}}{h_F} + T_{F,b}\right) + J\lambda}{\frac{k_m}{\delta} + h_D + \left(\frac{k_m h_D}{\delta h_F}\right)} \tag{A.18}$$

$T_{F,m}$ and $T_{D,m}$ were initially assumed and then calculated using equations (A.17) and (A.18). The difference between the calculated values and assumed guesses was calculated as the error. If the error was more than one percent, new values were substituted as new guesses and the procedure repeated. Then the calculation was marched forward up to nth element. In the case of a difference between boundary condition Eq. (A.14) and calculated T_D^{in}, the initially guessed T_D^{out} was decreased by 0.001 °C. This method was continued until the difference between calculated T_D^{in} and boundary condition (A.14) was less than one percent of calculated T_D^{in}.

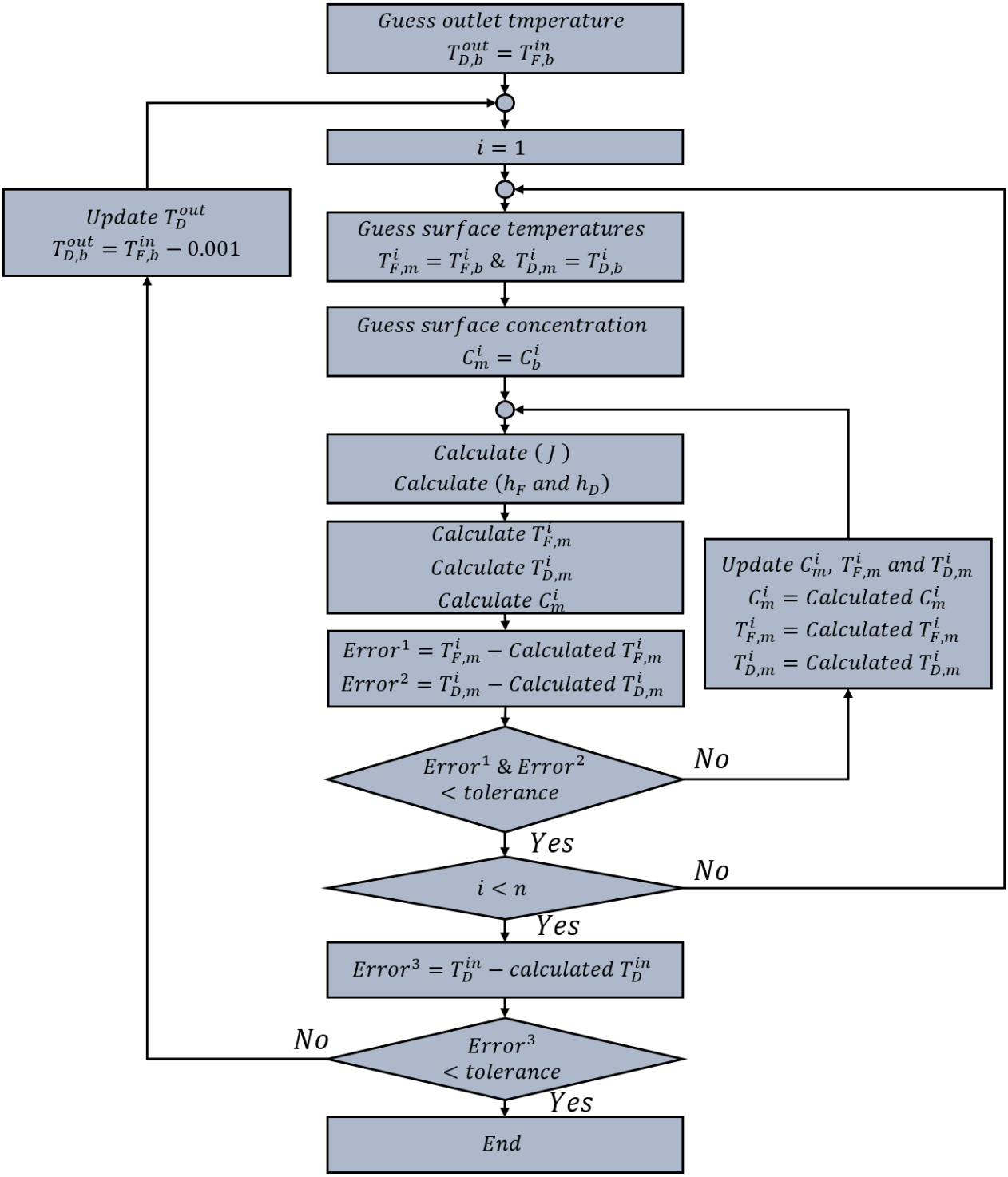

Fig. A.2. Algorithm of the MD flux prediction model.

References

[1] R.D. Vidic, S.L. Brantley, J.M. Vandenbossche, D. Yoxtheimer, J.D. Abad, Impact of shale gas development on regional water quality., Science. 340 (2013) 1235009. doi:10.1126/science.1235009.

[2] A. Vengosh, R.B. Jackson, N. Warner, T.H. Darrah, A. Kondash, A critical review of the risks to water resources from unconventional shale gas development and hydraulic fracturing in the United States, Environ. Sci. Technol. 48 (2014) 8334–8348. doi:10.1021/es405118y.

[3] J.M. Estrada, R. Bhamidimarri, A review of the issues and treatment options for wastewater from shale gas extraction by hydraulic fracturing, Fuel. 182 (2016) 292–303. doi:10.1016/j.fuel.2016.05.051.

[4] H. Thomas, Sampling and Analysis of Water Streams Associated with the Development of Marcellus Shale Gas, Final Rep. Marcellus Shale Coalit. (2009) 249 pp.

[5] A. Fakhru'l-Razi, A. Pendashteh, L.C. Abdullah, D.R.A. Biak, S.S. Madaeni, Z.Z. Abidin, Review of technologies for oil and gas produced water treatment, J. Hazard. Mater. 170 (2009) 530–551. doi:10.1016/j.jhazmat.2009.05.044.

[6] A.J. Kondash, E. Albright, A. Vengosh, Quantity of flowback and produced waters from unconventional oil and gas exploration, Sci. Total Environ. 574 (2017) 314–321. doi:10.1016/j.scitotenv.2016.09.069.

[7] R. Yang, E. Goktekin, K. K. Gleason, Zwitterionic Antifouling Coatings for the Purification of High-Salinity Shale Gas Produced Water, Langmuir. 31 (2015) 11895–11903. doi:10.1021/acs.langmuir.5b02795.

[8] D.M. Akob, A.C. Mumford, W. Orem, M.A. Engle, J.G. Klinges, D.B. Kent, I.M. Cozzarelli, Wastewater Disposal from Unconventional Oil and Gas Development Degrades Stream Quality at a West Virginia Injection Facility, Environ. Sci. Technol. 50 (2016) 5517–5525. doi:10.1021/acs.est.6b00428.

[9] K.B. Gregory, R.D. Vidic, D. a. Dzombak, Water Management Challenges Associated with the Production of Shale Gas by Hydraulic Fracturing, Elements. 7 (2011) 181–186. doi:10.2113/gselements.7.3.181.

[10] D.L. Shaffer, L.H. Arias Chavez, M. Ben-Sasson, S. Romero-Vargas Castrill??n, N.Y. Yip, M. Elimelech, Desalination and reuse of high-salinity shale gas produced water: Drivers, technologies, and future directions, Environ. Sci. Technol. 47 (2013) 9569–9583. doi:10.1021/es401966e.

[11] K.B. Gregory, R.D. Vidic, D.A. Dzombak, Water management challenges associated with

the production of shale gas by hydraulic fracturing, Elements. 7 (2011) 181–186. doi:10.2113/gselements.7.3.181.

[12] D.J. Miller, X. Huang, H. Li, S. Kasemset, A. Lee, D. Agnihotri, T. Hayes, D.R. Paul, B.D. Freeman, Fouling-resistant membranes for the treatment of flowback water from hydraulic shale fracturing: A pilot study, J. Memb. Sci. 437 (2013) 265–275. doi:10.1016/j.memsci.2013.03.019.

[13] B.D. Lutz, A.N. Lewis, M.W. Doyle, Generation, transport, and disposal of wastewater associated with Marcellus Shale gas development, Water Resour. Res. 49 (2013) 647–656. doi:10.1002/wrcr.20096.

[14] K. Sardari, P. Fyfe, D. Lincicome, S.R. Wickramasinghe, Aluminum electrocoagulation followed by forward osmosis for treating hydraulic fracturing produced waters, Desalination. 428 (2018) 172–181. doi:10.1016/j.desal.2017.11.030.

[15] Y. Zhang, K. Ghyselbrecht, R. Vanherpe, B. Meesschaert, L. Pinoy, B. Van der Bruggen, RO concentrate minimization by electrodialysis: Techno-economic analysis and environmental concerns, J. Environ. Manage. 107 (2012) 28–36. doi:10.1016/j.jenvman.2012.04.020.

[16] O.R. Lokare, S. Tavakkoli, S. Wadekar, V. Khanna, R.D. Vidic, Fouling in direct contact membrane distillation of produced water from unconventional gas extraction, J. Memb. Sci. 524 (2017) 493–501. doi:10.1016/j.memsci.2016.11.072.

[17] N.H. Aly, A.K. El-Fiqi, Mechanical vapor compression desalination systems - A case study, Desalination. 158 (2003) 143–150. doi:10.1016/S0011-9164(03)00444-2.

[18] L.M. Camacho, L. Dumée, J. Zhang, J. de Li, M. Duke, J. Gomez, S. Gray, Advances in membrane distillation for water desalination and purification applications, Water (Switzerland). 5 (2013) 94–196. doi:10.3390/w5010094.

[19] B.D. Coday, P. Xu, E.G. Beaudry, J. Herron, K. Lampi, N.T. Hancock, T.Y. Cath, The sweet spot of forward osmosis: Treatment of produced water, drilling wastewater, and other complex and difficult liquid streams, Desalination. 333 (2014) 23–35. doi:10.1016/j.desal.2013.11.014.

[20] A. Alkhudhiri, N. Darwish, N. Hilal, Produced water treatment: Application of Air Gap Membrane Distillation, Desalination. 309 (2013) 46–51. doi:10.1016/j.desal.2012.09.017.

[21] M.S. El-Bourawi, Z. Ding, R. Ma, M. Khayet, A framework for better understanding membrane distillation separation process, J. Memb. Sci. 285 (2006) 4–29. doi:10.1016/j.memsci.2006.08.002.

[22] E. Curcio, E. Drioli, Membrane Distillation and Related Operations—A Review, Sep. Purif. Rev. 34 (2005) 35–86. doi:10.1081/SPM-200054951.

[23] D. Singh, K.K. Sirkar, Desalination of brine and produced water by direct contact membrane distillation at high temperatures and pressures, J. Memb. Sci. 389 (2012) 380–388. doi:10.1016/j.memsci.2011.11.003.

[24] K.W. Lawson, D.R. Lloyd, Membrane distillation, J. Memb. Sci. 124 (1997) 1–25. doi:10.1016/S0376-7388(96)00236-0.

[25] F. He, J. Gilron, H. Lee, L. Song, K.K. Sirkar, Potential for scaling by sparingly soluble salts in crossflow DCMD, J. Memb. Sci. 311 (2008) 68–80. doi:10.1016/j.memsci.2007.11.056.

[26] S. Srisurichan, R. Jiraratananon, A.G.G. Fane, Humic acid fouling in the membrane distillation process, Desalination. 174 (2005) 63–72. doi:10.1016/j.desal.2004.09.003.

[27] L.D. Tijing, Y.C. Woo, J.-S. Choi, S. Lee, S.-H. Kim, H.K. Shon, Fouling and its control in membrane distillation ─ A review, J. Memb. Sci. 475 (2014) 215–244. doi:10.1016/j.memsci.2014.09.042.

[28] M. Gryta, Fouling in direct contact membrane distillation process, J. Memb. Sci. 325 (2008) 383–394. doi:10.1016/j.memsci.2008.08.001.

[29] M. Malmali, J. Askegaard, K. Sardari, S. Eswaranandam, A. Sengupta, S.R. Wickramasinghe, Evaluation of ultrafiltration membranes for treating poultry processing wastewater, J. Water Process Eng. 22 (2018). doi:10.1016/j.jwpe.2018.02.010.

[30] S. Karimi, K. Sardari, A.A. Khodadadi, M. Esmaili, Y. Mortazavi, Urea-functionalized silica on top of graded structured gamma-alumina membranes, in: Sep. Div. 2015 - Core Program. Area 2015 AIChE Annu. Meet., 2015.

[31] D.M. Warsinger, J. Swaminathan, E. Guillen-Burrieza, H.A. Arafat, J.H. Lienhard V, Scaling and fouling in membrane distillation for desalination applications: A review, Desalination. 356 (2015) 294–313. doi:10.1016/j.desal.2014.06.031.

[32] A.C.M. Franken, J.A.M. Nolten, M.H. V Mulder, D. Bargeman, C.A. Smolders, Wetting criteria for the applicability of membrane distillation, J. Memb. Sci. 33 (1987) 315–328. doi:10.1016/S0376-7388(00)80288-4.

[33] R.B. Saffarini, B. Mansoor, R. Thomas, H.A. Arafat, Effect of temperature-dependent microstructure evolution on pore wetting in PTFE membranes under membrane distillation conditions, J. Memb. Sci. 429 (2013) 282–294. doi:10.1016/j.memsci.2012.11.049.

[34] S. Lin, S. Nejati, C. Boo, Y. Hu, C.O. Osuji, M. Elimelech, Omniphobic Membrane for Robust Membrane Distillation, Environ. Sci. Technol. Lett. 1 (2014) 443–447. doi:10.1021/ez500267p.

[35] A. Deshmukh, C. Boo, V. Karanikola, S. Lin, A.P. Straub, T. Tong, D.M. Warsinger, M. Elimelech, Membrane distillation at the water-energy nexus: limits, opportunities, and challenges, Energy Environ. Sci. (2018). doi:10.1039/C8EE00291F.

[36] A.. Fallis, Membrane Handbook, 2013. doi:10.1017/CBO9781107415324.004.

[37] I. Sutzkover-Gutman, D. Hasson, Feed water pretreatment for desalination plants, Desalination. 264 (2010) 289–296. doi:10.1016/j.desal.2010.07.014.

[38] C.T. Tanneru, S. Chellam, Mechanisms of virus control during iron electrocoagulation - Microfiltration of surface water, Water Res. 46 (2012) 2111–2120. doi:10.1016/j.watres.2012.01.032.

[39] S. Chellam, M.A. Sari, Aluminum electrocoagulation as pretreatment during microfiltration of surface water containing NOM: A review of fouling, NOM, DBP, and virus control, J. Hazard. Mater. 304 (2016) 490–501. doi:10.1016/j.jhazmat.2015.10.054.

[40] S. Zhao, G. Huang, G. Cheng, Y. Wang, H. Fu, Hardness, COD and turbidity removals from produced water by electrocoagulation pretreatment prior to reverse osmosis membranes, Desalination. 344 (2014) 454–462. doi:10.1016/j.desal.2014.04.014.

[41] E. Anfruns-Estrada, C. Bruguera-Casamada, H. Salvadó, E. Brillas, I. Sirés, R.M. Araujo, Inactivation of microbiota from urban wastewater by single and sequential electrocoagulation and electro-Fenton treatments, Water Res. 126 (2017) 450–459. doi:10.1016/j.watres.2017.09.056.

[42] P.K. Holt, G.W. Barton, C.A. Mitchell, The future for electrocoagulation as a localized water treatment technology., Chemosphere. 59 (2005) 355–367. doi:10.1016/j.chemosphere.2004.10.023.

[43] D. Ghernaout, A.I. Al-Ghonamy, N. Ait Messaoudene, M. Aichouni, M.W. Naceur, F.Z. Benchelighem, A. Boucherit, Electrocoagulation of Direct Brown 2 (DB) and BF Cibacete Blue (CB) Using Aluminum Electrodes, Sep. Sci. Technol. 50 (2015) 1413–1420. doi:10.1080/01496395.2014.982763.

[44] N.P. Gamage, S. Chellam, Aluminum electrocoagulation pretreatment reduces fouling during surface water microfiltration, J. Memb. Sci. 379 (2011) 97–105. doi:10.1016/j.memsci.2011.05.051.

[45] A. Bagga, S. Chellam, D.A. Clifford, Evaluation of iron chemical coagulation and electrocoagulation pretreatment for surface water microfiltration, J. Memb. Sci. 309 (2008) 82–93. doi:10.1016/j.memsci.2007.10.009.

[46] M.Y. Mollah, R. Schennach, J.R. Parga, D.L. Cocke, Electrocoagulation (EC)--science and applications., J. Hazard. Mater. 84 (2001) 29–41. doi:10.1016/S0304-3894(01)00176-5.

[47] A comprehensive review of electrocoagulation for water treatment: Potentials and challenges, J. Environ. Manage. 186 (2017) 24–41. doi:10.1016/J.JENVMAN.2016.10.032.

[48] Y. Yun, R. Ma, W. Zhang, A.G. Fane, J. Li, Direct contact membrane distillation mechanism for high concentration NaCl solutions, Desalination. 188 (2006) 251–262. doi:10.1016/j.desal.2005.04.123.

[49] S. Al-Obaidani, E. Curcio, F. Macedonio, G. Di Profio, H. Al-Hinai, E. Drioli, Potential of membrane distillation in seawater desalination: Thermal efficiency, sensitivity study and cost estimation, J. Memb. Sci. 323 (2008) 85–98. doi:10.1016/j.memsci.2008.06.006.

[50] W.C.L. Lay, J. Zhang, C. Tang, R. Wang, Y. Liu, A.G. Fane, Factors affecting flux performance of forward osmosis systems, J. Memb. Sci. 394–395 (2012) 151–168. doi:10.1016/j.memsci.2011.12.035.

[51] T. Picard, G. Cathalifaud-Feuillade, M. Mazet, C. Vandensteendam, Cathodic dissolution in the electrocoagulation process using aluminium electrodes., J. Environ. Monit. 2 (2000) 77–80. doi:10.1039/a908248d.

[52] Electrocoagulation treatment of raw landfill leachate using iron-based electrodes: Effects of process parameters and optimization, J. Environ. Manage. 204 (2017) 75–81. doi:10.1016/J.JENVMAN.2017.08.028.

[53] M. Rebhun, M. Lurie, Control of organic matter by coagulation and floc separation, in: Water Sci. Technol., 1993: pp. 1–20.

[54] E. Metcalf, H. Eddy, Wastewater engineering: treatment and reuse, 2003. doi:10.1016/0309-1708(80)90067-6.

[55] M. Malmali, P. Fyfe, D. Lincicome, K. Sardari, S.R. Wickramasinghe, Selecting membranes for treating hydraulic fracturing produced waters by membrane distillation, Sep. Sci. Technol. 52 (2017) 266–275. doi:10.1080/01496395.2016.1244550.

[56] K. Smolders, A.C.M. Franken, Terminology for Membrane Distillation, Desalination. 72 (1989) 249–262. doi:10.1016/0011-9164(89)80010-4.

[57] D. Ghernaout, B. Ghernaout, A. Boucherit, M.W. Naceur, A. Khelifa, A. Kellil, Study on mechanism of electrocoagulation with iron electrodes in idealised conditions and electrocoagulation of humic acids solution in batch using aluminium electrodes, Desalin. Water Treat. 8 (2009) 91–99. doi:10.5004/dwt.2009.668.

[58] B.E. Poling, G.H. Thomson, D.G. Friend, R.L. Rowley, W.V. Wilding, Perry's Chemical Engineers' Handbook, 2007. doi:10.1036/0071511253.

[59] S. Karimi, D. Korelskiy, Y. Mortazavi, A.A. Khodadadi, K. Sardari, M. Esmaeili, O.N.

Antzutkin, F.U. Shah, J. Hedlund, High flux acetate functionalized silica membranes based on in-situ co-condensation for CO2/N2 separation, J. Memb. Sci. 520 (2016) 574–582. doi:10.1016/j.memsci.2016.08.017.

[60] L. Han, Y.Z. Tan, T. Netke, A.G. Fane, J.W. Chew, Understanding oily wastewater treatment via membrane distillation, J. Memb. Sci. 539 (2017) 284–294. doi:10.1016/j.memsci.2017.06.012.

[61] A.L. McGaughey, R.D. Gustafson, A.E. Childress, Effect of long-term operation on membrane surface characteristics and performance in membrane distillation, J. Memb. Sci. 543 (2017) 143–150. doi:10.1016/j.memsci.2017.08.040.

[62] E. Drioli, S. Santoro, S. Simone, G. Barbieri, A. Brunetti, F. Macedonio, A. Figoli, ECTFE membrane preparation for recovery of humidified gas streams using membrane condenser, React. Funct. Polym. 79 (2014) 1–7. doi:10.1016/j.reactfunctpolym.2014.03.003.

[63] M. Sillanpää, S. Metsämuuronen, M. Mänttäri, Natural Organic Matter in Water, 2015. doi:10.1016/B978-0-12-801503-2.00005-7.

[64] H. Susanto, Towards practical implementations of membrane distillation, Chem. Eng. Process. Process Intensif. 50 (2011) 139–150. doi:10.1016/j.cep.2010.12.008.

[65] K.A. Salls, D. Won, E.P. Kolodziej, A.E. Childress, S.R. Hiibel, Evaluation of semi-volatile contaminant transport in a novel, gas-tight direct contact membrane distillation system, Desalination. 427 (2018) 35–41. doi:10.1016/j.desal.2017.11.001.

[66] J. Phattaranawik, R. Jiraratananon, A.G. Fane, Heat transport and membrane distillation coefficients in direct contact membrane distillation, J. Memb. Sci. 212 (2003) 177–193. doi:10.1016/S0376-7388(02)00498-2.

[67] A.R. Da Costa, A.G. Fane, D.E. Wiley, Spacer characterization and pressure drop modelling in spacer-filled channels for ultrafiltration, J. Memb. Sci. 87 (1994) 79–98. doi:10.1016/0376-7388(93)E0076-P.

Chapter 4. Aluminum Electrocoagulation Followed by Forward Osmosis for Treating Hydraulic Fracturing Produced Waters

Abstract

Forward osmosis is an emerging membrane based separation technology that could find niche applications in the treatment of oil and gas produced water. Here, the feasibility of treating hydraulic fracturing produced waters using a combined electrocoagulation (EC) and forward osmosis (FO) process has been investigated. EC is shown to be effective in removing suspended solids and organic compounds which foul the membrane during FO. The amount of suspended solids and organic compounds that are removed depends on the EC reaction time. By accounting for internal and external concentration polarization as well as fouling due to deposition on the feed side barrier surface of the FO membrane, the expected flux may be determined. The effectiveness of removal of suspended solids and organic compounds may be modeled as changes in the permeability of the foulant layer that develops on the feed side of the membrane. The results obtained for real produced waters from Southwestern Energy operations in the Fayetteville Shale indicate that combined EC and FO could be an effective method for water recovery from hydraulic fracturing produced waters.

4.1. Introduction

Freshwater is a fundamental resource and integral to all ecological and societal activities. Improper wastewater discharge can adversely affect nearby communities and ecosystems [1]. Produced water is a by-product from oil and gas recovery operations. Often produced waters are highly impaired containing organic and inorganic contaminants. Development of cost-effective

treatment processes for produced waters is of tremendous societal importance due to significant possibility of surface and underground water and soil pollution. [2]. This is especially important for development of unconventional gas reservoirs, including coalbed methane, tight gas and shale gas [3]. Here we focus on hydraulic fracturing operations.

Economically viable gas production from shale reserves is achieved by horizontal drilling followed by hydraulic fracturing [4]. Hydraulic fracturing is a stimulation technique used to increase oil and gas production from shale and underground rock formations [5]. Hydraulic fracturing flowback water, a subset of produced water, is defined as the stream returning to the surface after the hydraulic fracturing process. This stream is often highly impaired containing hazardous organic and inorganic constituents. The concentration of total dissolved solids (TDS) in these streams can vary between about 13,000 to 400,000 mg/L [6,7]. Thus, treatment of these produced waters is critical for developing economically viable hydraulic fracturing operations.

Treatment of highly impaired produced waters is challenging given the very high TDS as well as the presence of dissolved organic contaminants. Membrane based separation technologies such as microfiltration, ultrafiltration and nanofiltration are routinely used for treatment of wastewater [8]. In addition, reverse osmosis (RO) is used for desalination of seawater to produce drinking water [9]. RO is a very effective and applicable desalination process for treatment of low TDS waters (TDS <47,000 mg L^{-1}) [10]. However, membrane fouling and scaling is a primary concern when operating RO systems [10,11]. The feed water requires rigorous pre-treatment to prevent fouling of the reverse osmosis membrane [11,12]. Many new processes involving osmotically and thermally driven membrane technologies are being investigated for desalination of highly impaired wastewaters [9-13]. Here we consider forward osmosis.

Osmosis is defined as the net movement of water across a selectively permeable membrane driven by a difference in osmotic pressure across the membrane [14]. In FO, a draw solution having a significantly higher osmotic pressure than the produced water flows on the permeate side of the membrane. Due to the osmotic pressure gradient water flows from the feed to the draw solution [15]. Using dense non-porous membranes with rejection properties similar to reverse osmosis membranes, the feed solution is concentrated and the draw solution diluted [14,15]. The advantages of FO include a high rate of water recovery, minimization of brine discharge, low fouling and low energy consumption [16]. However, the viability of FO depends on efficient regeneration of the draw solution. The availability of low-grade waste heat during oil and gas production provides the possibility of using a thermolytic salt such as NH_4HCO_3, as a draw solute, which can be easily regenerated by heating. Alternatively, nanofiltration or RO may be used to concentrate the draw solution. Ge *et al.* [16] highlighted the importance of optimizing the draw solute.

FO can be a very promising process for treating produced water streams especially as low-grade waste heat is often present to aid in regenerating the FO draw solution. Unlike RO, FO does not require the use of large hydraulic pressures [17]. FO can operate in harsh conditions (on-site) with minimal access to electric power and supplies [11]. Mazlan *et al.* [18] indicated that there is effectively no difference in specific energy consumption between FO combined with nanofiltration for draw solution recovery and RO treatment of produced waters.

Although there is no pressure driven convection of rejected species towards the membrane in FO, internal concentration polarization (CP) leads to reduced rates of water recovery. Internal CP combined with the presence of small, highly fouling organic species can lead to significant

flux decline due to fouling when treating produced waters [19]. Maltos *et al.* [20] reported major fouling of FO membranes while treating raw produced water. Thus, pretreatment of the produced water prior to FO is essential.

Numerous pretreatment processes have been considered prior to membrane filtration [21]. Biological pretreatment is impractical for treating hydraulic fracturing produced waters due to long retention times and the low biodegradability of most of the contaminants [22]. Coagulation, adsorption, preoxidation and prefiltration are among the most popular pretreatment methods prior to membrane filtration [23]. Chemical pretreatment such as coagulation is frequently used to remove colloidal and organic matter [23]. Here we focus on Electrocoagulation (EC) for removal of colloidal and dissolved organic compounds that could foul the FO membrane.

EC is an electrochemical method for treating polluted water whereby sacrificial anodes corrode to release active coagulant precursors into solution [24]. Compared to chemical coagulation (e.g., using alum), EC provides a number of advantages including simple equipment, easy operation, less maintenance, colorless and odorless effluent, low sludge production and efficient removal of colloidal particles. Flocs formed by EC are similar to chemical flocs, except that EC flocs tend to be much larger, contain less bound water, are acid-resistant and more stable, and therefore, can be separated faster [25,26]. Further, in EC there are no moving parts, thus requiring less maintenance compared to coagulation where efficient mixing is required. Use of electricity, which can be expensive in many places, and regular replacement of sacrificial electrodes are two major disadvantages of EC technology [25,27,28]. However, Kobya *et al.* [25] indicated that electrical energy consumption decreases dramatically when the wastewater has

higher conductivity due to the presence of dissolved salts. In case of hydraulic fracturing produced waters, the conductivity is high due to high TDS.

In this study, and for the first time, we investigate the impact of produced water pretreatment via EC prior to FO for fouling mitigation and water recovery. We design and develop an EC system as a pre-treatment operation prior to FO.

4.2. Theory

4.2.1. Mass Transfer in FO System

The FO water flux may be represented by [29]:

$$J_w = A\,(\Pi_{Db} - \Pi_{Fb}) \quad (1)$$

where J_w is water flux across the membrane, A is the pure water permeability coefficient, Π_{Db} and Π_{Fb} are the osmotic pressures of the bulk draw and feed solution respectively. The pure water permeability coefficient will depend on the resistance to water flow through the membrane. In reality, CP compromises performance. Fig. 1 shows the effect of CP on the osmotic pressure across the membrane.

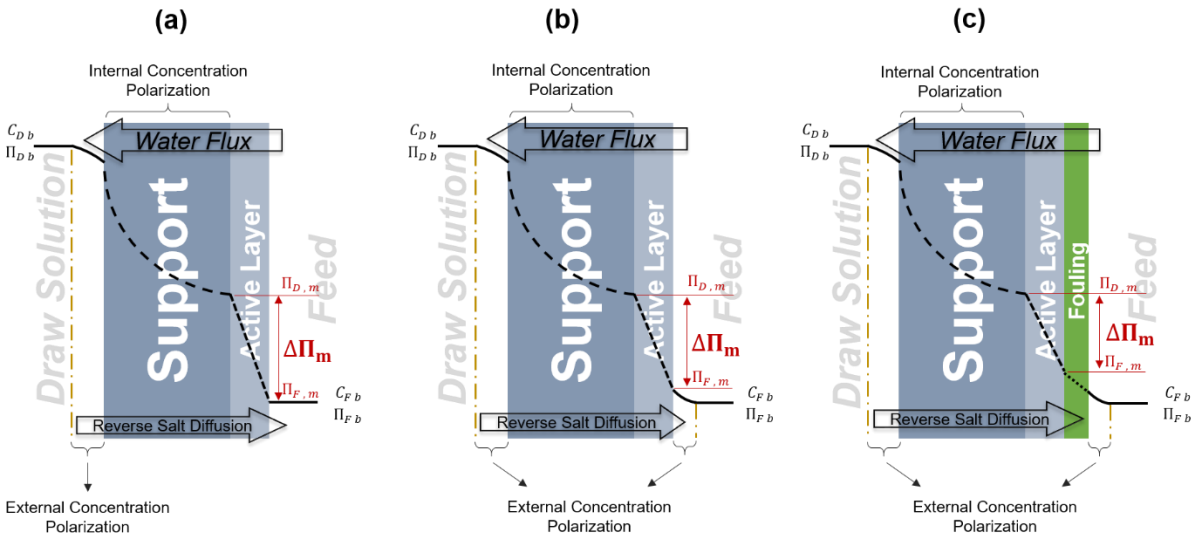

Fig. 1. Effects of internal and external CP. a) De-ionized (DI) water as feed, b) synthetic produced water as feed, c) raw produced water as feed.

In FO, the high ionic strength draw solution is pumped parallel to the membrane support structure. External CP, leading to boundary layer formation adjacent to the support structure, will dilute the draw solute relative to the bulk solution. Consequently, the value of Π_{Db} will be higher than the osmotic pressure at the external surface of the support structure. Further, internal CP will occur within the support structure which will lead to a further dilution of the draw solute. This will lead to a further decrease in the osmotic pressure of the draw solute at the internal surface of the membrane barrier layer relative to Π_{Db}. On the feed side of the membrane, an external CP boundary layer will form leading to an increase in the solute concentration of the feed at the membrane surface relative to the bulk feed. This will lead to an increase in the osmotic pressure of the feed relative to Π_{Fb} [30].

Fig. 1 (a) shows the variation of osmotic pressure across the membrane for a de-ionized (DI) water feed stream and a high concentration NaCl draw solution. A reverse salt flux from the draw to the feed side is included [30]. However, it is assumed that the reverse salt flux is low;

therefore, there is no external CP boundary layer on the feed side. Fig. 1 (b) shows the variation of osmotic pressure across the membrane when the feed consists of NaCl in DI water. This feed stream is referred to as synthetic produced water. Due to the presence of NaCl in the feed solution, an external CP boundary layer develops on the feed side of the membrane. As can be seen, the presence of internal and external CP will lead to a decrease in the osmotic pressure difference across the membrane which in turn will lead to a reduced flux.

In the case of real feed streams, fouling of the membrane by deposition of suspended solutes and dissolved organic compounds, will further compromise the permeate flux [31]. Fig. 1 (c) shows the variation of osmotic pressure for a raw produced water feed stream and a draw solution consisting of NaCl in DI water. The fouling of the feed side of the membrane due to deposition of suspend solids and dissolved organic compounds is shown.

Bui *et al.* [30] have derived the following expression for the water flux during FO:

$$J_w = A.\left[\frac{\Pi_{Db}\,.\,e^{\left(-J_w\left\{\frac{1}{k_D}+\frac{S}{D_D}\right\}\right)}-\Pi_{Fb}\,.\,e^{\left(\frac{J_w}{k_F}\right)}}{1+\frac{B}{J_w}\left\{e^{\left(\frac{J_w}{k_F}\right)}-e^{\left(-J_w\left\{\frac{1}{k_D}+\frac{S}{D_D}\right\}\right)}\right\}}\right] \quad (2)$$

This expression assumes that in the concentration boundary layer the osmotic pressure varies linearly with salt concentration. In Eq. (2) k_F and k_D are mass transfer coefficients describing the transport of water through the external CP boundary on the feed and draw solution side of the membrane. For laminar flow (as is the case here), these mass transfer coefficients may be estimated from the Sieder-Tate correlation for heat transfer in laminar flow [32]:

$$Sh = 1.86\left(\frac{d_h^2\,v}{DL}\right)^{0.33} \quad (3)$$

where *Sh* is the Sherwood number defined by

$$Sh = \frac{kd_h}{D} \quad (4).$$

In Eqs. (3) and (4), d_h is the hydraulic diameter defined as 4(cross sectional area)/wetted perimeter, *v* is the average velocity parallel to the membrane, *D* is the diffusion coefficient of the species transferring through the membrane and *L* is the length of the channel. For a rectangular channel:

$$d_h = \frac{4LW}{2(L+W)} \quad (5)$$

where *W* is the width of the channel. Finally, *k* is either the feed or draw side mass transfer coefficient, k_f or k_d, respectively.

S is the membrane structural parameter, defined as [30]:

$$S = t_s \, \tau/\epsilon \quad (6)$$

where t_s ε and τ are the thickness, porosity and tortuosity of the support layer. D_D is the diffusion coefficient of the draw solute while *A* and *B* are the water and solute (in this case NaCl) permeabilities, respectively. Lay *et al.* [31] have developed a resistance in series model to account for changes in membrane permeability due to fouling. Here, we assume that fouling only occurs on the barrier surface of the membrane that faces the feed solution. We further assume that no fouling occurs on the membrane support structure. It is assumed that fouling does not affect the feed side external CP boundary layer. Finally, we assume that as the reverse salt flux is low, fouling has a minimal effect on the salt permeability coefficient. Analogous to Lay *et al.* [31], we define:

$$\frac{1}{A} = \frac{1}{A_m} + \frac{1}{A_f} \quad (7)$$

where the overall water permeability depends on the membrane permeability (A_m) as well as the permeability of a fouling layer (A_f) on the feed side of the membrane (Fig. 1 (c)). We will use these equations to model our experimental results. Table 1 lists the values of the various parameters used here.

Table 1. Values of parameters and their source.

Parameter	Definition	Unit	Value/Range	Comments
A	Pure water permeability coefficient	m s^{-1} bar^{-1}	≈1.8 – 3.0 (X 10^{-7})	Calculated in this study
A_m	Membrane permeability coefficient	m s^{-1} bar^{-1}	≈1.75 – 3.0 (X 10^{-7})	From [30,33]
A_f	Fouling layer permeability coefficient	m s^{-1} bar^{-1}	≈0.5 – 7.0 (X 10^{-6})	Calculated in this study
B	Solute permeability coefficient	m s^{-1}	≈2.0 – 3.0 (X 10^{-7})	From [30,33]
C	Concentration	mol L^{-1}	0.0 – 5.0	Used in this study
D	Solute (NaCl) diffusion coefficient	m^2 s^{-1}	1.3 – 4.14	From [34]
d_h	Hydraulic diameter	m	0.0038	Calculated in this study
I	Current	A (Ampere)	0.5	Used in this study
J_w	Water flux	m s^{-1}	≈1.12 – 5.28 (X 10^{-6})	Calculated in this study
k	Convective mass transfer coefficient	m s^{-1}	≈2.5 – 3.15 (X 10^{-5})	Calculated in this study

Table 1. Values of parameters and their source (Cont.)

Parameter	Definition	Unit	Value/Range	Comments
L	Membrane module length	m	0.045	Used in this study
Q	Flow rate	L min^{-1}	0.8	Used in this study
Re	Reynolds number		≈479 - 646	Calculated in this study
S	Structural parameter	m	≈450 - 650	From [33]
Sh	Sherwood number		≈52 - 58	Calculated in this study
t_s	Membrane thickness	m	≈30 – 52 (X 10^{-6})	From [35]
v	Velocity	m s^{-1}	0.148	Used in this study
V	Voltage	V (volt)	≈7.5 – 18.2	Observed in this study
V_r	EC reactor volume	L (liter)	0.6	Used in this study
W	Membrane channel width	m	0.002	Used in this study
ε	Porosity		N/A	Indirectly used in S
τ	Tortuosity		N/A	Indirectly used in S
Π	Osmotic pressure	bar	0.0 – 123.8	Calculated in this study

4.2.2. EC

Chemical coagulation by adding aluminum sulfate salts (such as alum, $Al_2(SO_4)_3.18H_2O$) is frequently practiced [36–38]. Coagulation is a complicated process that is highly pH sensitive, and depends on the presence of other dissolved and suspended species. When alum is added, the following overall reaction describes what happens immediately after dissolution of the salt:

$$Al_2(SO_4)_3.18H_2O \rightarrow 2Al^{3+} + 3SO_4^{2-} + 18H_2O \quad (8)$$

$$2Al^{3+} + 3SO_4^{2-} + 18H_2O \rightarrow 2Al(OH)_3 + 6H^+ + 3SO_4^{2-} + 12H_2O \quad (9)$$

Besides $Al(OH)_3$, several other mononuclear complexes such as $AlOH^{2+}$, $Al(OH)_2^+$, $Al(OH)^-_4$, etc. also form depending on the pH and other dissolved species present. As indicated by Eqs. (8) and (9), hydrolysis of the coagulant leads to a decrease in pH. As the concentration of aluminum in solution increases and the solution 'ages', polynuclear aluminum complexes form and aluminum hydroxide precipitates as given by the following general scheme according to complex precipitation kinetics [25];

$$Al^{3+} + n\,OH^- \rightarrow Al(OH)_n^{3-n} \rightarrow Al_2(OH)_2^{4+} \rightarrow Al_n(complex) \rightarrow Al(OH)_{3(s)} \quad (10)$$

Formation of the various polymeric species is important in the coagulation process. Precipitation and adsorption of the aluminum species with colloidal matter have been proposed as the two main mechanisms of coagulation, both of which are highly pH dependent. In the case of EC, the following electrode reactions occur [39]:

Anode: $Al \rightarrow Al^{3+} + 3e^-$ (11)

Cathode: $3H_2O + 3e^- \rightarrow \frac{3}{2}H_2 + 3OH^-$ (12)

Other reactions are also possible depending on the other dissolved ions in solution [25,26]. Analogous to coagulation by alum addition, the Al^{3+} and OH^- ions from various monomeric species such as $Al(OH)^{2+}$, $Al(OH)_2^-$ and also polymeric species such as $Al_6(OH)_{15}^{3+}$ and $Al_7(OH)_{17}^{4+}$, again eventually transforming to $Al(OH)_3$ with a large surface area that can adsorb organic compounds and also trap suspended particles [25]. Finally, $Al(OH)_3$ flocs (with adsorbed organics and colloidal particles) will polymerize and deposit according to the following reaction [40]:

$$n\,Al(OH)_3 \rightarrow Al_n(OH)_{3n} \quad (13)$$

While the fundamental chemical reactions for alum based coagulation and EC are similar, there are a number of advantages to EC [41]. In EC, the coagulant is produced in situ as the anode is consumed; thus, no addition of liquid coagulant is needed. Hydrolysis of the coagulant does not lead to a decrease in pH (consumption of alkalinity). EC requires less coagulant and produces less sludge [42]. Addition of sulfate ions (or other counter ions) is not required.

4.3. Experimental

4.3.1. Produced Water

Produced water samples were collected from Southwestern Energy (Houston, TX) shale gas production facilities in Fayetteville, Arkansas and were characterized at the Arkansas Water Resources Center, University of Arkansas. In addition to the inorganic composition of the wastewater samples, TDS, total suspended solids (TSS), total organic carbon (TOC) and turbidity were measured. Cations and anions present were measured using Spectro Genesis ICP OES

(Kleve, Germany) and Dionex DX-120 ion chromatograph (Sunnyvale, CA), respectively. TDS and TSS were measured using EPA standard methods 160.1 and 160.2 [43], respectively. TOC was measured using a Skalar Formacs TOC analyzer (Breda, Netherlands) and turbidity was measured using a Turb 550 (WTW, Weilheim, Germany) turbidity-meter. Accuracy of the chemical analysis was checked by the principle of electroneutrality, using the percent difference between sum of anions and cations in equivalent weight per liter.

4.3.2. EC

The EC setup consisted of a polycarbonate vessel (600 mL), five electrodes with an active surface area of 180 cm^2 (6061 aluminum alloy, Sapa, Rosemont, IL) and a DC power source (Hewlett Packard, Palp Alto, CA). As shown in Fig. 2, the electrodes were placed vertically in the reactor with an 8 mm spacing between them. The first and last electrodes were connected to the DC power source and acted as the cathode and anode, while the other three were bipolar and not connected to the DC power source. All EC experiments were carried out in batch mode. The current was maintained at 0.5 A (equivalent to current density of 2.78 mA cm^{-2}) during each experiment. The voltage was recorded every 20 seconds. Different reaction times were investigated. After EC, wastewater samples were transferred to a separatory funnel for sedimentation. After 6 h of sedimentation, the deposited sludge was removed from separatory funnel and the pre-treated water was recovered.

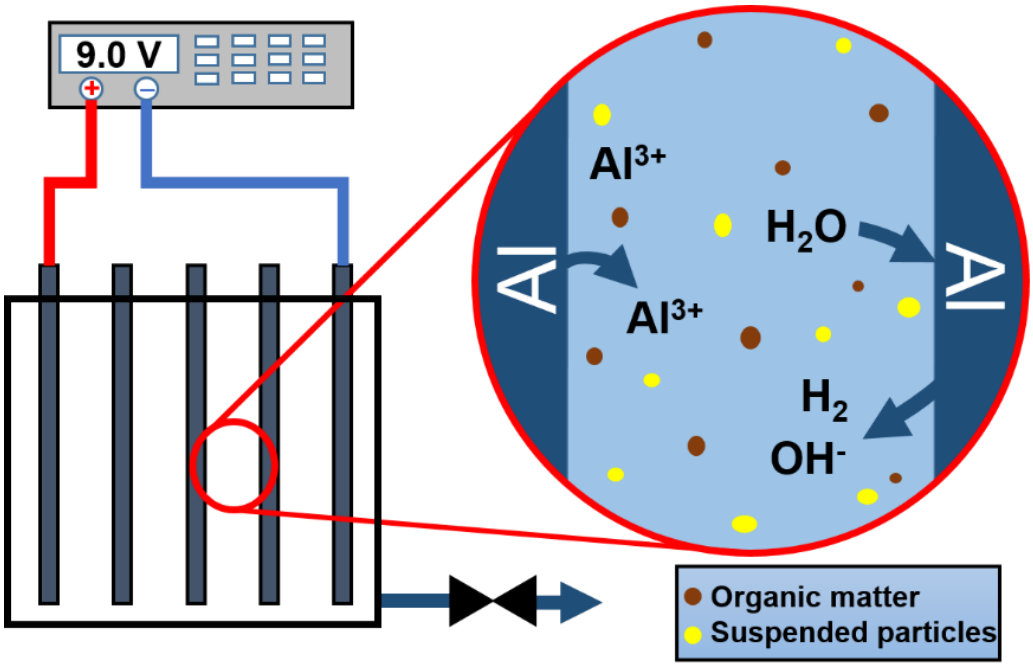

Fig. 2. EC setup.

4.3.3. Forward Osmosis Membrane

Cellulose triacetate (CTA) membranes with an embedded polyester screen support (HTI, Albany, OR) were used as the salt rejecting semi-permeable FO membrane [44–47]. Membranes were received in flat sheets containing glycerin in order to protect the membranes during shipping. CTA membranes were soaked in DI water for 2 h and rinsed with DI water several times before use.

4.3.4. Forward Osmosis Setup

Fig. 3 is a schematic representation of the FO apparatus. A polycarbonate tangential flow cell, with 33.75 cm^2 effective surface area and 2 mm channel depth, was used. In order to provide mechanical support to the membrane and also to mitigate fouling, a mesh spacer (XN4510) was

acquired from Industrial Netting (Minneapolis, MN) to fill the channels on both sides of the membrane cell. Feed was circulated on the active (shiny) surface of the membrane with a flow velocity of 14.8 cm s^{-1} (0.8 L min^{-1}) and draw solution circulated on the opposite side of the membrane (support layer) with the same flow velocity using two peristaltic pumps (Masterflex I/P, Cole Parmer, Vernon Hills, IL). The feed and draw solution were returned to their respective reservoirs. A computer-connected analytical balance (Mettler Toledo, Columbus, OH) recorded the reduction in weight of the feed, which was used to calculate the water flux. Feed and draw solution temperatures were monitored with digital thermometers employing k type thermocouples. In addition, a digital conductivity-meter (VWR, Radnor, PA) was placed in the feed tank to record the conductivity of the feed.

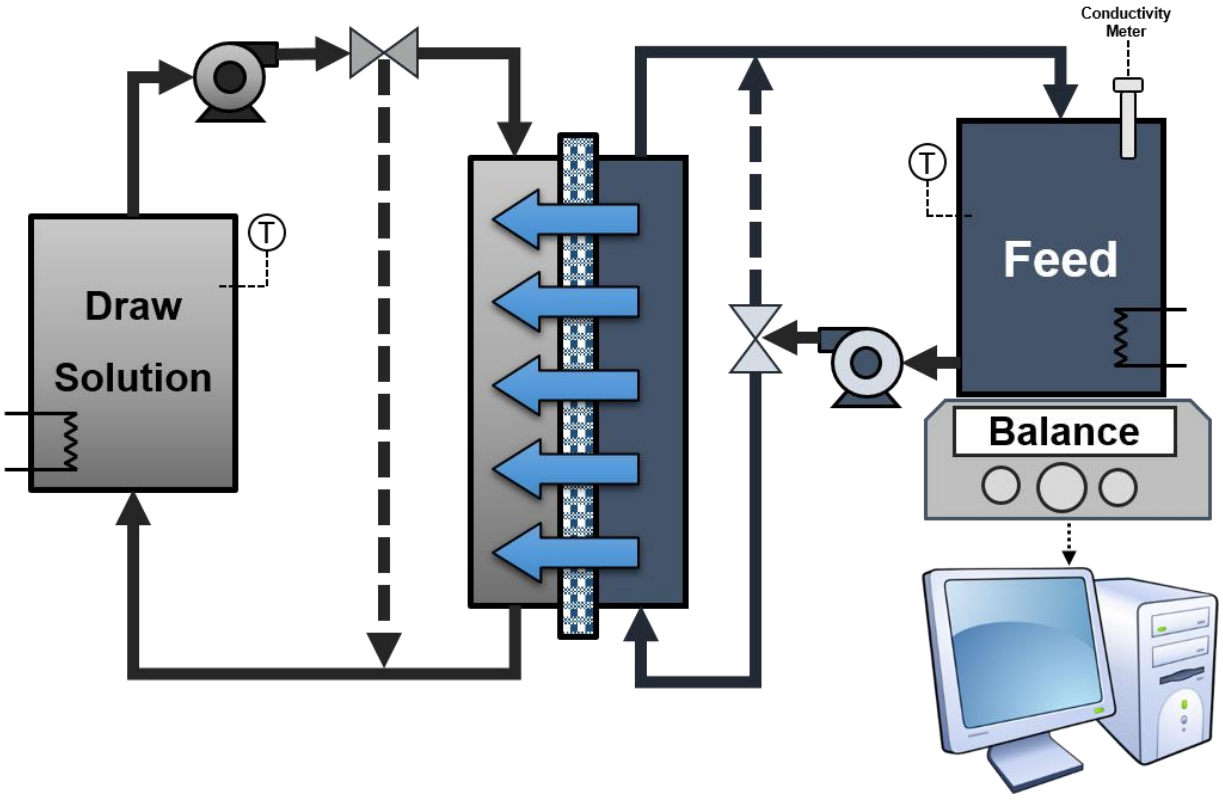

Fig. 3. Schematic diagram of FO setup

4.3.5. FO Experiments

For each FO experiment, a CTA membrane coupon was first placed inside the membrane cell. Feed and draw solution tanks were filled with 2 L of feed and 4 L of 4 M NaCl in DI water, respectively. The peristaltic pumps were started and both feed and draw solutions were recirculated back to their respective tanks while bypassing the membrane module (see Fig. 3), until the temperature was stabilized at 23±1 °C for both streams. Then feed and draw solution streams were allowed to flow on opposite surfaces of the CTA membrane inside the module at the same flow rate of 14.8 cm s^{-1} (0.8 L min^{-1}). Counter current flow continued until 600 mL of permeate was recovered.

Table 2 lists the feed streams tested. Using DI water as the feed stream the reverse salt flux was measured. Testing with a model produced water, containing the same TDS as raw produced water by addition of NaCl to DI water, was conducted in order to determine membrane performance in the absence of colloidal and dissolved organic species. Produced water as received as well as after EC was tested. Some experiments were run for 24 hours in order to determine membrane performance over longer periods. In addition, the effect of changing the NaCl concentration in the draw solution was investigated. Finally, a high recovery FO experiment was run with 1 L of pretreated produced water using 1 L of 2 M ammonium bicarbonate as draw solution.

Table 2. FO experiments conducted.

Experiments	Feed	Draw solution	Length of experiment
Reverse salt flux measurement	DI water	4 M	Until 600 mL permeate was collected
Control experiment	Synthetic produced water	4 M	Until 600 mL permeate was collected
Fouling study	Non-pretreated produced water	4 M	Until 600 mL permeate was collected
Fouling study	Pre-treated produced water	4 M	Until 600 mL permeate was collected
Effect of draw solution concentration	Pre-treated produced water	Range of 1 to 5 M	Until 600 mL permeate was collected
Recovery comparison	Non-pretreated and pretreated produced water	4 M	24 hours
Ammonium bicarbonate as draw solution	Non-pretreated and pretreated produced water	2 M ammonium bicarbonate	32 hours

4.3.6. Scanning Electron Microscopy (SEM)

SEM using a Nova Nanolab 200 Duo-Beam Workstation (FEI, Hillsboro, Oregon) was used to observe changes in the membrane surface before and after FO. SEM images were taken of both the active and support structure.

4.4. Results and Discussion

4.4.1. Produced Water Characterization

Characteristics of the produced water prior to EC (as received) and after EC for reaction times of 1, 2 and 3 min are shown in Table 3. As it can be seen, there are three main categories of contaminants; dissolved solids, suspended solids and organic matter. In this study, pretreatment was employed to remove organic matter and suspended solids.

Table 3. Characterization of raw produced water as well as pretreated produced water by EC. Characterization results are shown for 1, 2 and 3 min EC reaction times.

Parameter	Unit	Raw produced water	1:00 min EC Reaction Time	2:00 min EC Reaction Time	3:00 min EC Reaction Time
TDS	mg L^{-1}	23254.8	22833.2	21791.6	21514.7
TSS	mg L^{-1}	639.1	294.0	25.6	24.8
TOC	mg L^{-1}	154.7	89.7	27.8	27.5
Turbidity	NTU	117.1	12.8	3.51	2.34
pH	-	7.74	7.83	7.88	8.05
Chloride	mg L^{-1}	12717	12355	12101	11841
Nitrate	mg L^{-1}	1.90	2.23	1.19	1.94
Sulfate	mg L^{-1}	123.35	119.44	111.86	104.69
Aluminum	mg L^{-1}	0.00	0.27	0.65	0.71
Barium	mg L^{-1}	3.36	0.97	2.13	2.23
Boron	mg L^{-1}	14.80	11.29	13.15	8.65
Calcium	mg L^{-1}	169.12	171.31	120.08	137.48

Table 3. Characterization of raw produced water as well as pretreated produced water by EC. Characterization results are shown for 1, 2 and 3 min EC reaction times (Cont.).

Parameter	Unit	Raw produced water	1:00 min EC Reaction Time	2:00 min EC Reaction Time	3:00 min EC Reaction Time
Iron	mg L^{-1}	0.08	0.02	0.14	0.94
Lead	mg L^{-1}	0.03	0.01	0.01	0.01
Magnesium	mg L^{-1}	35.07	31.28	29.93	34.76
Potassium	mg L^{-1}	27.91	28.81	24.77	21.34
Selenium	mg L^{-1}	0.202	0.15	0.16	0.22
Sodium	mg L^{-1}	7602	7613	7568	7498
Electroneutrality Percent Difference	%	< 2.0	< 0.5	< 0.5	< 1.0

4.4.2. EC Performance

During EC pretreatment, Al^{3+} and OH^- ions produced by the electrodes (Al^{3+} at the anode and OH^- at the cathode) react to form a variety of aluminum species such as $Al(OH)_4^-$, $Al_6(OH)_{15}^{3+}$ and $Al_7(OH)_{17}^{4+}$. These monomeric and polymeric species eventually turn into amorphous $Al(OH)_{3(s)}$ with large surface area [48]. The $Al(OH)_{3(s)}$ remains in the aqueous phase in the form of a gelatinous suspension that can remove organics and suspended solids from the produced water by either complexation, electrostatic attraction, followed by coagulation and flotation or sedimentation [49]. The remainder of the positively charged aluminum species such as $Al(OH)^{2+}$ contribute to the destabilization of the organic macromolecules by charge neutralization, producing *X-Al* complexes (*X* representing negatively charged organic compounds). *X-Al*

complexes are then agglomerated as neutral colloidal entities and then carried up by hydrogen gas flotation or precipitated by sedimentation [50,51]. On the other hand, presence of negatively charged $Al(OH)_4^-$ restricts the adsorption and complexation by charge repulsion. However, in the pH range of 6 to 8 (here 7.73), conditions for rapid formation of $Al(OH)_{3(s)}$ solids prevail and removal most likely occurs by adsorption [51].

Fig. 4 shows the coagulation process from the moment that produced water is placed in separatory funnel. While the voltage is applied in the EC reactor, various Al species are produced at the anode. After transferring the water sample from the EC reactor to the separatory funnel, formed *Al* species will continue the coagulation process that was started in the EC reactor (Fig. 4a). Al species in solution agglomerate organic species as well as suspended solutes (Fig. 4b) which leads to the development of low-density flocs. The low-density flocs are driven to the liquid-air interface by the rising hydrogen bubbles produced at the cathode. As the flocs accumulate at the liquid-air interface they aggregate, densify and sink to the bottom (Fig. 4c). Thus, three different zones exist in the separatory funnel: the region next to the liquid-air interface contains low-density flocs; the middle region contains clear water while aggregated flocs collect at the bottom. The water from the middle region was removed after 6 hour sedimentation and used as the feed for FO experiments. Flocs collected from top and bottom of the separatory funnel were wasted.

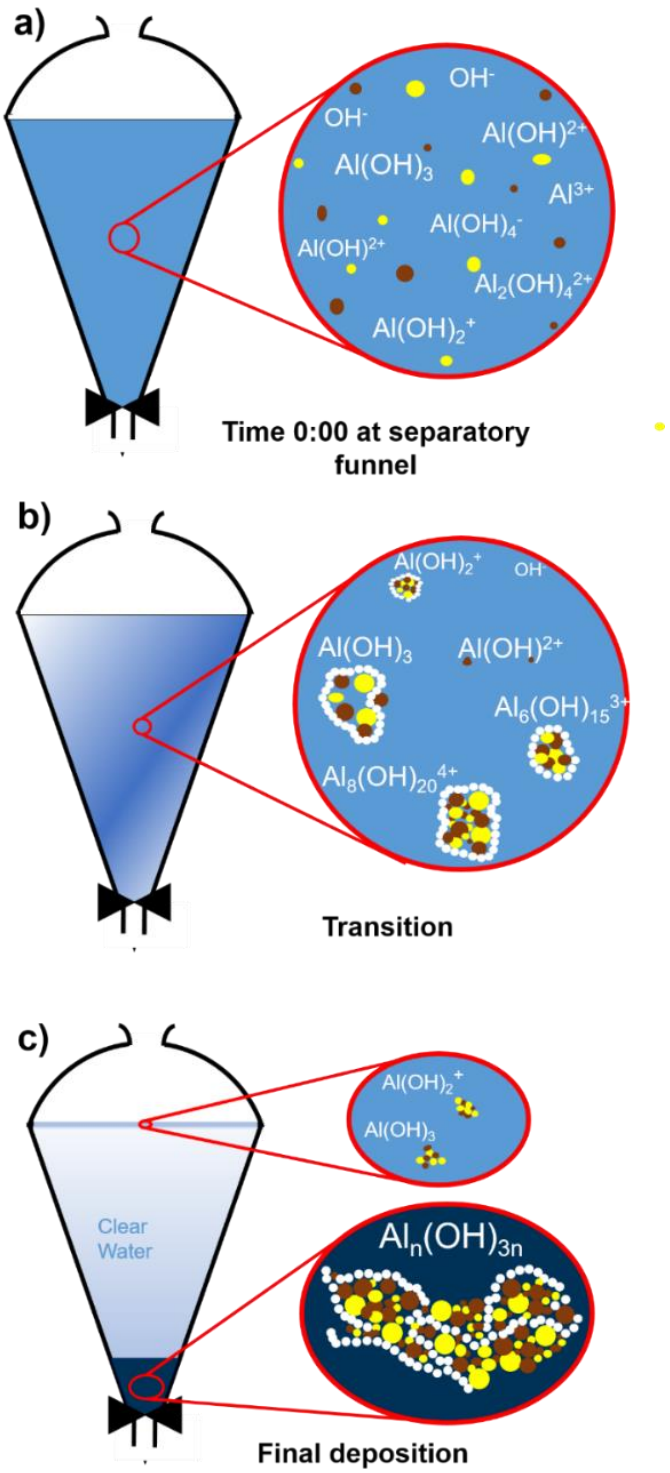

Fig. 4. Pretreated wastewater inside separatory funnel at: a) beginning of the coagulation process, b) transition stage and c) after sedimentation for 6 hours.

Different parameters can affect EC performance including current, voltage, reaction time, electrode material, etc. Here, we try to optimize the electrochemical reaction time by applying a fixed current 0.5 A for all experiments. Reaction times in the range of 1 to 3 min were tested. Water recovered after EC was characterized in terms of TSS, TOC and turbidity. Fig. 5 gives the removal of each of these parameters as a function of reaction time. The removal and energy consumption are both functions of reaction time. As expected, longer reaction times resulted in higher TSS, TOC and turbidity removal. Table 3 gives the characteristics of pretreated produced water for reaction times of 1, 2 and 3 min. As can be seen, the TDS did not change much after EC. Results in Fig. 5 show that the removal of TSS and TOC tend to plateau after a reaction time of 2 min.

The voltage was recorded every 20 seconds. Due to the generation of ionic species during EC, the voltage was decreased to ensure a constant current of 0.5 A. The electrical energy consumption per volume during EC was calculated using Eq. (14) [25]:

$$E = \frac{V X I X t}{Vr} \tag{14}$$

where V is average voltage, I is applied current, t is reaction time and V_r is volume of feed water. Increasing the EC reaction time from 1 to 3 min resulted in over 75 percent increase in turbidity and TOC removal as well as over 10 percent increase in TSS removal. Higher removal was achieved for longer reaction times which resulted in higher energy consumption. However, increase in reaction time over 2 min did not greatly increase the removal.

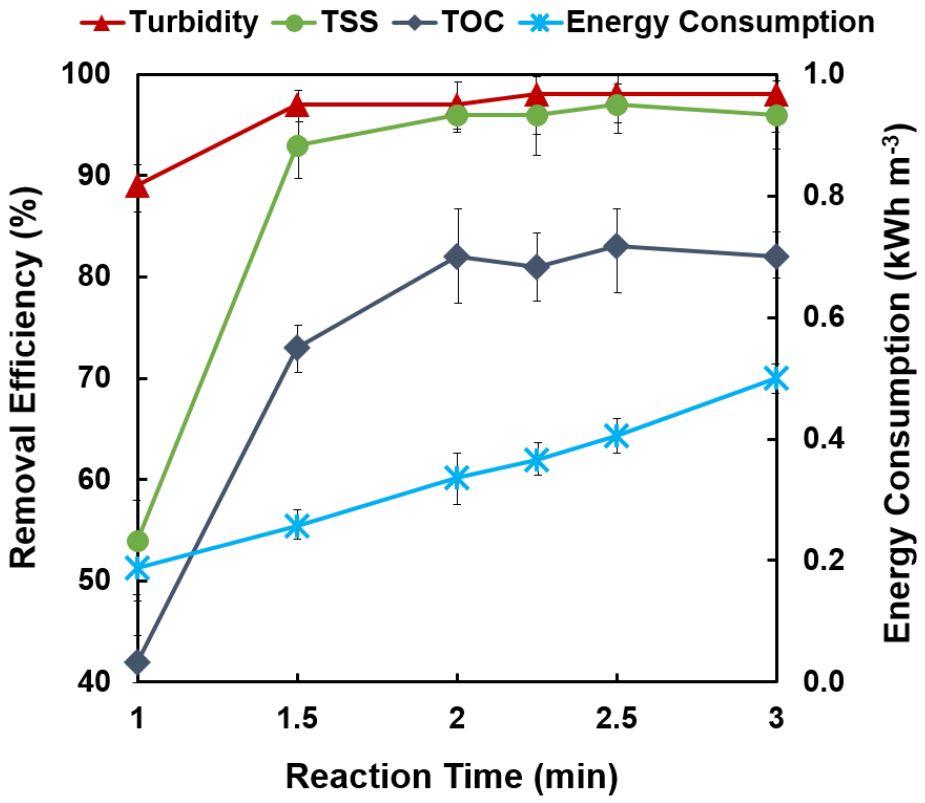

Fig. 5. Removal efficiency of turbidity, TSS and TOC as a function of EC reaction time. Energy consumption of EC process as a function of reaction time is shown on the secondary vertical axis.

4.4.3. FO Performance

4.4.3.1. DI Water Feed

FO experiments were carried out using DI water as the feed in order to determine the reverse salt flux. The results were also used to fit Eq. (1) and determine values for *A* and *B*. As it can be seen, the average Reynolds number is 561 (see Table 1). For flow in channels (rectangular duct), the critical Reynolds is 1500 [52] indicating laminar flow. The draw solution consisted of 4 M NaCl. The feed and draw solution were pumped countercurrent to the barrier and membrane

support layer, respectively. Though the critical Reynolds number is likely to be lower for spacer filled channels, the Reynold number in these experiments is much less than 1,500. Thus, we assume laminar flow.

Fig. 6 shows the variation of water flux and conductivity as functions of permeate volume. Values of $3X10^{-7}$ m s^{-1} bar^{-1} and $2X10^{-7}$ m s^{-1} where used for *A* and *B* respectively in Eq. (2) in order to model the water flux as a function of permeate volume (dashed line). As can be seen in Fig. 6, the flux decline occurs simultaneously with an increase in feed conductivity. The conductivity increases due to the reverse salt flux, i.e., salt passage, from the draw solution to feed (DI water).

The reverse salt flux was found to be 29.17 g m^{-2} h^{-1}. It was calculated by multiplying the rate of change of feed concentration with time by the volume of the feed solution and then dividing by the area of the membrane after 600 mL of feed solution had passed through the membrane [33]. Cath et. al. [33] reported that the reverse salt flux for CTA membranes to be less than 25 g m^{-2} h^{-1} when 1 M draw solution is used. Boo et. al. [19] reported the reverse salt flux for a CTA membrane to be ≈0.24 mol m^{-2} h^{-1} (≈14 g m^{-2} h^{-1}) with 0.5 M draw solution. Our results are in keeping with these earlier results as the concentration of our draw solution is 4 M. It is important to realize that the error in empirical mass transfer correlations is on the order of 10% [53]. Consequently, error sin *A* and *B* are likely to be of at least a similar order.

As can be seen from Fig. 6, the water flux declines slightly during the experiment. This is due to the increase in conductivity of the feed and decrease in conductivity of the draw solution due to dilution of the draw solution. The reverse salt flux is very low. For a membrane area of 33.75 cm^2 and a run time of 9 h and 8 min (time taken for 600 mL to transfer from feed to draw

solution) the total mass of NaCl transferred is 0.89 g. No noticeable deposition on the membrane support was observed.

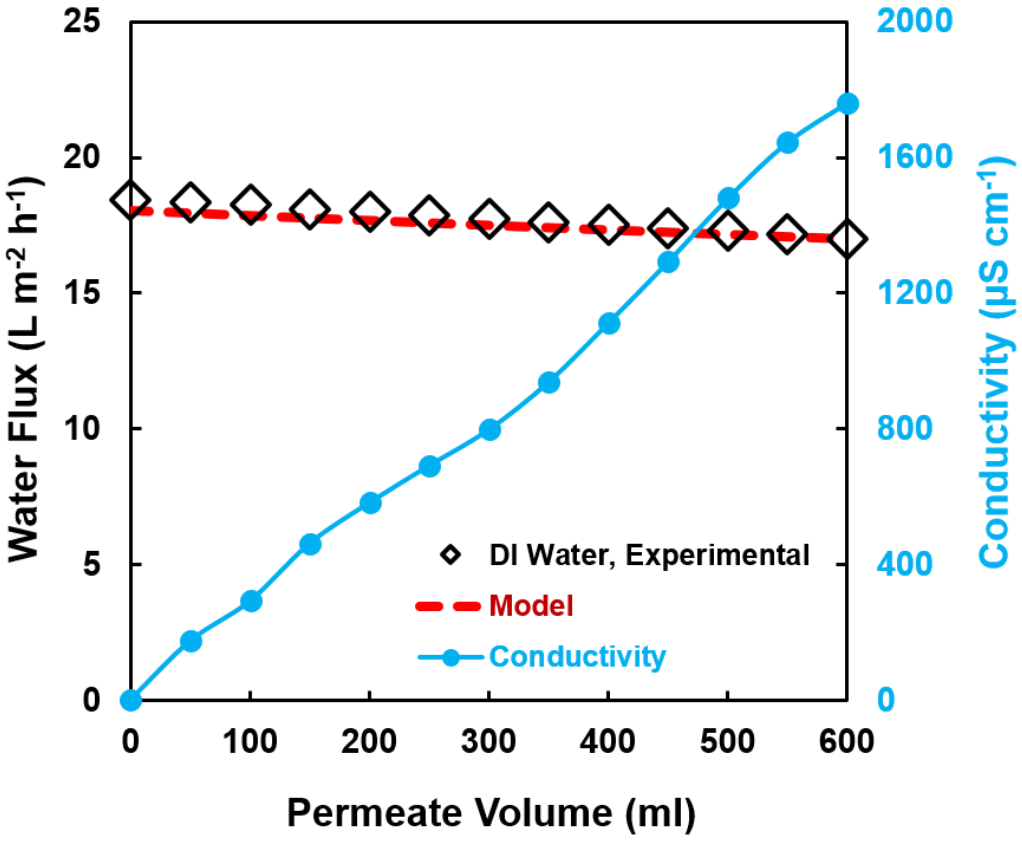

Fig. 6. Water flux and conductivity as functions of permeate volume for feed and draw solutions consisting of DI water and 4 M NaCl in DI water, respectively.

4.4.3.2. FO Experiments with Synthetic, Raw and Pretreated Produced Water

FO experiments were conducted using synthetic, raw and pretreated produced waters. The synthetic produced water consisted of 23,254 mg L^{-1} (0.4 M) NaCl in DI water. This represents the same TDS as the raw produced water (see Table 3). Fig. 7 shows the variation of water flux with the permeate volume. The water flux decreases for all feed streams as water is transferred

from the feed to the draw solution. The predicted water flux, dashed line, using the values of A and B that gave the best fit for a DI water feed ($3X10^{-7}$ m s^{-1} for *A* and $2X10^{-7}$ m s^{-1} for *B*, see Figure 6) is in excellent agreement with results obtained for the synthetic produced water flux. However, in the case of raw or pretreated produced water, membrane fouling leads to a lower water flux. Improved removal of TSS and TOC, by increasing the EC reaction time, leads to improved flux.

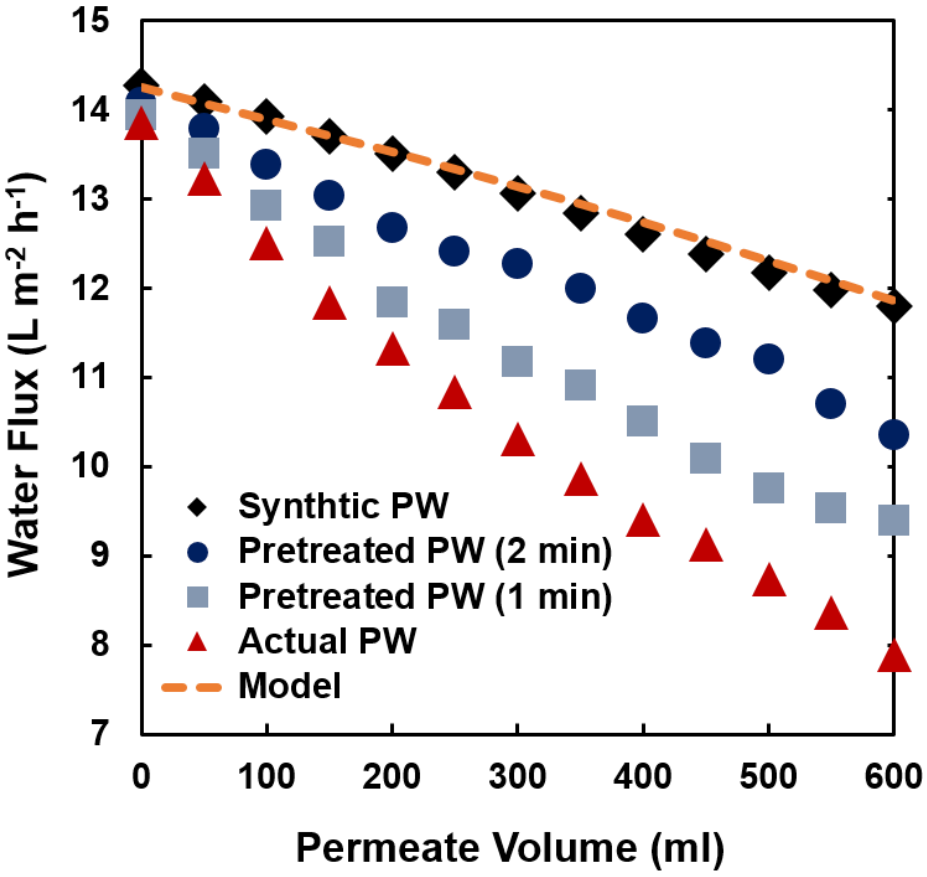

Fig. 7. Water flux as a function of permeate volume for synthetic, non-pretreated and pretreated (2 min and 1 min EC reaction times) produced water.

Fig. 8 gives the corresponding SEM images of the membrane barrier layer after FO using the 4 feed streams tested in Fig. 7. Comparing Fig. 7 and 8, the greater the degree of deposition the lower the flux after removal of the same permeate volume. Comparing Fig. 7 and Table 2, the

more effective the removal of TSS and TOC during pretreatment, the less deposition on the membrane surface and the greater the permeate flux.

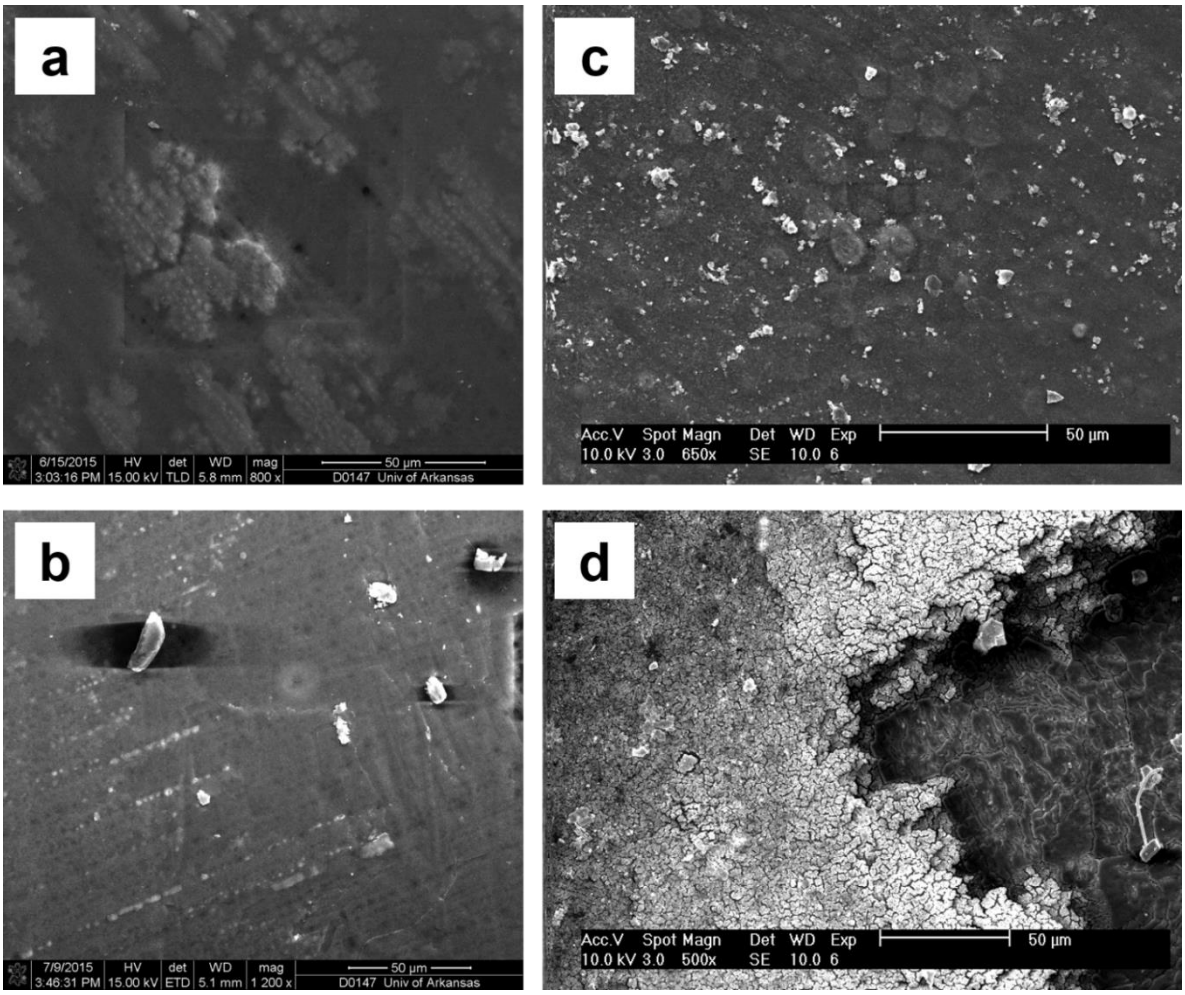

Fig. 8. SEM images of the membrane barrier layer after FO. (a) synthetic produced water, (b) produced water pretreated with 2.0 min EC reaction time; (c) produced water pretreated with 1.0 min EC reaction time, d) non-pretreated produced water

Figs. 7 and 8 indicate that the observed decrease in flux for real produced waters compared to synthetic produced water is due mainly to adsorption of rejected species, suspended solids and dissolved organic compounds, on the membrane active surface. Using Eq. (7), we have modeled this decrease in flux in terms of a change in the water permeability coefficient of the membrane. Fig. 9 gives the calculated water permeability coefficient of the fouling layer A_f for pretreated and

non-pretreated produced waters. As can be seen, the permeability of fouling layer decreases as the permeate volume increases.

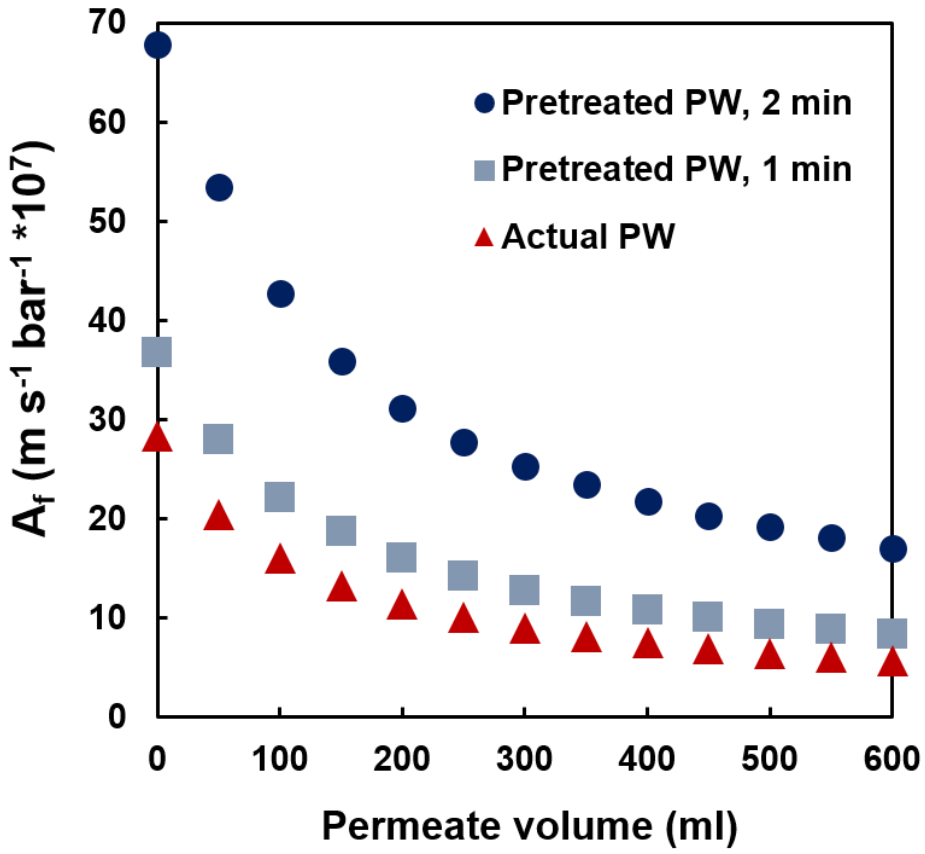

Fig. 9. Water permeability coefficient of fouling layer (A_f) as a function of permeate volume for pretreated (2 min and 1 min EC reaction time) and non-pretreated produced water.

4.4.4. Effect of Draw Solution Concentration on FO Performance

In order to verify the utility of Eqs. (2) and (7) at predicting the permeate flux during FO, additional experiments were conducted using produced water pretreated with 2.0 min EC reaction time. The NaCl concentration in the draw solution was varied from 1 to 4 M. Fig. 10 gives the water flux as a function of NaCl concentration in the draw solution after 600 mL of permeate has

been recovered. The dashed curve gives our model prediction. The value of A_f, the water permeability of the fouling layer, was taken from Fig. 9 for produced water pretreated with 2.0 min EC reaction time after recovery of 600 mL of permeate. Fig. 10 indicates that while an increase in activity of the draw solution will lead to an increase in permeate flux the increase is not linear. As can be seen, as the NaCl concentration deviates from 4.0 M, the difference between the predicted and experimentally determined fluxes increases. This is not unexpected.

At lower NaCl concentrations, the reverse salt flux will be less. The external and internal CP boundary layers on the draw solution side will be altered by changes in the NaCl concentration in the draw solution. Further, Boo *et al.* [19] indicate that a decrease in draw solution concentration results in a decrease in the level of fouling. Fouling will depend on the water flux as well as the concentration of foulants in the feed solution. Since the value of A_f used here was for a 4.0 M NaCl draw solution, it is not surprising that our predicted flux is less than the observed flux for lower NaCl concatenation draw solutions. Analogously, for draw solutions containing more than 4.0 M NaCl, our model over-predicts the permeate flux.

The results obtained here indicate the importance of considering the various mass transfer resistances that exist as water is transferred for the feed to the draw solution. Further for real produced waters, membrane fouling can be significant. Predicting changes in water permeability due to membrane fouling is complex as it depends on several factors including (e.g. draw solution concentration, flow rates etc.) as well as the concentration and type of foulants present in the feed.

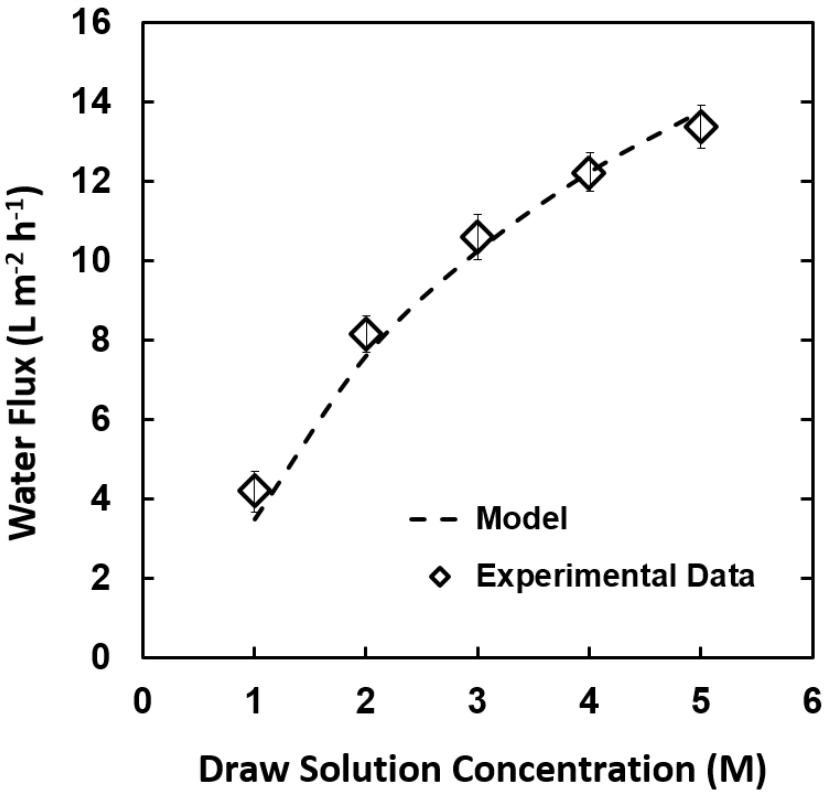

Fig. 10. Variation of water flux with draw solution concentration. All experiments continued until 600 mL permeate was recovered. Pretreated produced water, 2 min EC reaction time, was used as the feed.

4.4.5. Effect of EC Pretreatment on Water Recovery

The economic viability of FO will depend on the cost of the recovered water or the total volume of permeate. While EC leads to higher permeate fluxes, it is the increase in water recovery versus the additional cost of the EC step that will determine the economic viability of the process. In addition, membrane cleaning and regeneration costs will have to be considered. Fig. 11 gives the volume of recovered water as a function of time. For this specific set of experiments, which were run for 24 hours, water recovery increased by close to 21% with EC pretreatment.

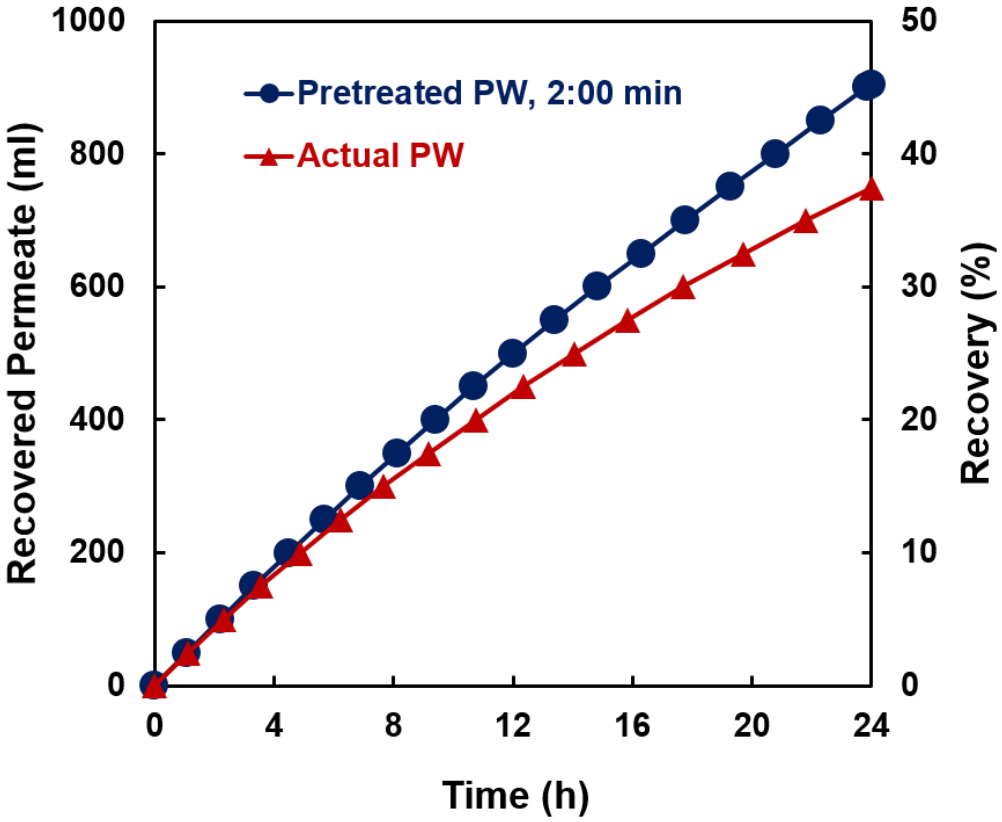

Fig. 11. Water recovery for raw and pretreated (2 min EC reaction time) produced water. Experiments were conducted in 24 hours.

Besides maximizing water recovery while minimizing cost, the feasibility of developing a combined EC-FO system for recovering produced water will depend on a number of other factors. Suitable FO membranes and adequate EC pretreatment of the feed to suppress fouling is essential. Development of efficient cleaning protocols for membrane regeneration will be necessary as well as the availability of a draw solution that has a high enough activity such that the activity difference between the feed and draw solution is sufficient to lead to practical permeate fluxes and water recovery.

Recovery and reuse of the draw solute is essential when considering FO[54]. McCutcheon *et al.* [55] introduced the mixture of two highly soluble gases, ammonia and carbon dioxide, as a

low-cost, effective and regenerable draw solution. This draw solution is made by dissolving ammonium bicarbonate in water. In addition to NaCl, we have investigated the effect of EC pretreatment on water recovery by FO using 2 M ammonium bicarbonate as draw solution. Figure 12 represents the volume of recovered water as well as water recovery as functions of time. As can be seen, 2 min EC pretreatment resulted in 19 percent water recovery increase over 32 hours of experiment. In a practical applications loss of the draw solute must be investigated as this will affect the viability of the process [56,57]. Finally, the cost of a combined EC FO process must be compared to current treatment options such as trucking to a centralized treatment facility as well as the benefit of recovering water for reuse on site.

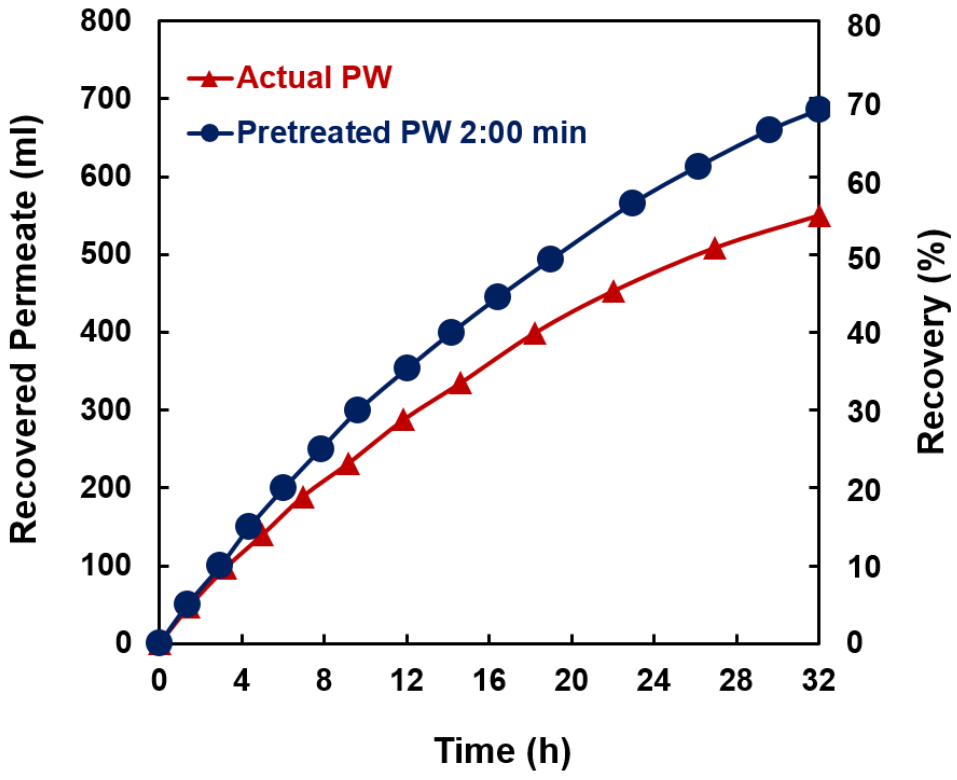

Fig. 12. Water recovery for raw and pretreated (2 min EC reaction time) produced water. 1 L raw/pretreated PW and 1 L of 2 M ammonium bicarbonate solutions were used as feed and draw solutions, respectively. Experiments were conducted in 32 hours.

4.5. Conclusion

Here we have focused on pretreatment of a produced water feed stream prior to FO. We show that significant fouling and consequently, a drop in flux will occur when treating hydraulic fracturing produced waters due to the presence of high values of TOC and TSS. We show that EC prior to FO significantly reduces membrane fouling. Though NaCl is used as the draw solute, development of an actual combined EC-FO process will require the use of a draw solute that can be economically recovered. Further, cross-over of the draw solute into feed will affect the viability of the process. We show that for an EC reaction time of two min as a pretreatment step, over 70% reduction of TSS, TOC and turbidity results. Over a 24 hour period, suppression in fouling due to this pretreatment, leads to close to 21% increase in water recovery.

Pretreatment of hydraulic fracturing flowback waters will be essential if membrane-based separation processes such as FO are to be used to treat these highly impaired waters. The permeate flux may be predicted by using a resistance in series model to account for internal and external CP as well as fouling of the membrane barrier layer by adsorbed species in the produced water. EC units with a small footprint could be integrated with a FO system. The economic feasibility of the process will depend on the cost of the recovered water, membrane lifetime and recovery and reuse of the draw solute.

Acknowledgements

Funding for this work was provided by Southwestern Energy through the National Science Foundation Industry/University Cooperative Research Center for Membrane Science, Engineering and Technology, the National Science Foundation (IIP 1361809) and the University of Arkansas.

References

[1] P.H. Gleick, L. Allen, M.J. Cohen, H. Cooley, J. Christian-Smith, M. Heberger, J. Morrison, M. Palaniappan, P. Schulte, The World's Water, Vol. 7, The Biennal Report on Freshwater Resources, 2012. doi:10.1007/978-1-59726-228-6.

[2] A. Fakhru'l-Razi, A. Pendashteh, L.C. Abdullah, D.R.A. Biak, S.S. Madaeni, Z.Z. Abidin, Review of technologies for oil and gas produced water treatment, J. Hazard. Mater. 170 (2009) 530–551. doi:10.1016/j.jhazmat.2009.05.044.

[3] C.R. Clarkson, Production data analysis of unconventional gas wells: Review of theory and best practices, Int. J. Coal Geol. 109–110 (2013) 101–146. doi:10.1016/j.coal.2013.01.002.

[4] K.B. Gregory, R.D. Vidic, D. A. Dzombak, Water Management Challenges Associated with the Production of Shale Gas by Hydraulic Fracturing, Elements. 7 (2011) 181–186. doi:10.2113/gselements.7.3.181.

[5] United States Environmental Protection Agency, Study of the Potential Impacts of Hydraulic Fracturing on Drinking Water Resources, EPA Prog. Rep. 601/R (2012) 1–7.

[6] N. Abualfaraj, P.L. Gurian, M.S. Olson, Characterization of Marcellus Shale Flowback Water, Environ. Eng. Sci. 31 (2014) 140716083132007. doi:10.1089/ees.2014.0001.

[7] R. Yang, E. Goktekin, K. K. Gleason, Zwitterionic Antifouling Coatings for the Purification of High-Salinity Shale Gas Produced Water, Langmuir 31 (2015) 11895–11903. doi:10.1021/acs.langmuir.5b02795.

[8] S. Munirasu, M.A. Haija, F. Banat, Use of membrane technology for oil field and refinery produced water treatment—A review, Process Saf. Environ. Prot. 100 (2016) 183–202. doi:10.1016/j.psep.2016.01.010.

[9] T.Y. Cath, Osmotically and thermally driven membrane processes for enhancement of water recovery in desalination processes, Desalin. Water Treat. 15 (2010) 279–286. doi:10.5004/dwt.2010.1760.

[10] J. Drewes, T. Cath, P. Xu, J. Graydon, An Integrated Framework for Treatment and Management of Produced Water, Tech. Assess. Prod. Water Treat. Technol. (2009) 8–128. http://www.rpsea.org/media/files/user/cath1.pdf.

[11] B.D. Coday, P. Xu, E.G. Beaudry, J. Herron, K. Lampi, N.T. Hancock, T.Y. Cath, The sweet spot of forward osmosis: Treatment of produced water, drilling wastewater, and other complex and difficult liquid streams, Desalination 333 (2014) 23–35. doi:10.1016/j.desal.2013.11.014.

[12] C. Fritzmann, J. Löwenberg, T. Wintgens, T. Melin, State-of-the-art of reverse osmosis desalination, Desalination 216 (2007) 1–76. doi:10.1016/j.desal.2006.12.009.

[13] F. Edwie, T.S. Chung, Development of hollow fiber membranes for water and salt recovery from highly concentrated brine via direct contact membrane distillation and crystallization, J. Memb. Sci. 421–422 (2012) 111–123. doi:10.1016/j.memsci.2012.07.001.

[14] T. Cath, A. Childress, M. Elimelech, Forward osmosis: Principles, applications, and recent developments, J. Memb. Sci. 281 (2006) 70–87. doi:10.1016/j.memsci.2006.05.048.

[15] J.R. McCutcheon, R.L. McGinnis, M. Elimelech, A novel ammonia-carbon dioxide forward (direct) osmosis desalination process, Desalination. 174 (2005) 1–11. doi:10.1016/j.desal.2004.11.002.

[16] Q. Ge, M. Ling, T.S. Chung, Draw solutions for forward osmosis processes: Developments, challenges, and prospects for the future, J. Memb. Sci. 442 (2013) 225–237. doi:10.1016/j.memsci.2013.03.046.

[17] D.L. Shaffer, L.H. Arias Chavez, M. Ben-Sasson, S. Romero-Vargas Castrilln, N.Y. Yip, M. Elimelech, Desalination and reuse of high-salinity shale gas produced water: Drivers, technologies, and future directions, Environ. Sci. Technol. 47 (2013) 9569–9583. doi:10.1021/es401966e.

[18] N.M. Mazlan, D. Peshev, A.G. Livingston, Energy consumption for desalination — A comparison of forward osmosis with reverse osmosis, and the potential for perfect membranes, Desalination 377 (2016) 138–151. doi:10.1016/j.desal.2015.08.011.

[19] C. Boo, M. Elimelech, S. Hong, Fouling control in a forward osmosis process integrating seawater desalination and wastewater reclamation, J. Memb. Sci. 444 (2013) 148–156. doi:10.1016/j.memsci.2013.05.004.

[20] R. Maltos, S. Fox, J. Regnery, B.D. Coday, T.Y. Cath, Onsite Treatment of Raw Produced Water through the Use of Forward and Reverse Osmosis, in: Am. Ist. Chem. Eng., 2016.

[21] K. Farahbakhsh, C. Svrcek, R.K. Guest, D.W. Smith, A review of the impact of chemical pretreatment on low-pressure water treatment membranes, J. Environ. Eng. Sci. 3 (2004) 237–253. doi:10.1139/s03-078.

[22] E. Metcalf, H. Eddy, Wastewater engineering: treatment and reuse, 2003. doi:10.1016/0309-1708(80)90067-6.

[23] H. Huang, K. Schwab, J.G. Jacangelo, Pretreatment for Low Pressure Membranes in Water Treatment: A Review, Environ. Sci. Technol. 43 (2009) 3011–3019. doi:10.1021/es802473r.

[24] P.K. Holt, G.W. Barton, C.A. Mitchell, The future for electrocoagulation as a localized water treatment technology., Chemosphere. 59 (2005) 355–367. doi:10.1016/j.chemosphere.2004.10.023.

[25] M. Kobya, O.T. Can, M. Bayramoglu, Treatment of textile wastewaters by electrocoagulation using iron and aluminum electrodes, J. Hazard. Mater. 100 (2003) 163–178. doi:10.1016/S0304-3894(03)00102-X.

[26] E. Butler, Y.-T. Hung, R.Y.-L. Yeh, M. Suleiman Al Ahmad, Electrocoagulation in Wastewater Treatment, Water. 3 (2011) 495–525. doi:10.3390/w3020495.

[27] M.Y. Mollah, R. Schennach, J.R. Parga, D.L. Cocke, Electrocoagulation (EC)--science and applications., J. Hazard. Mater. 84 (2001) 29–41. doi:10.1016/S0304-3894(01)00176-5.

[28] O. Sahu, B. Mazumdar, P.K. Chaudhari, Treatment of wastewater by electrocoagulation: A review, Environ. Sci. Pollut. Res. 21 (2014) 2397–2413. doi:10.1007/s11356-013-2208-6.

[29] J.R. McCutcheon, M. Elimelech, Influence of concentrative and dilutive internal concentration polarization on flux behavior in forward osmosis, J. Memb. Sci. 284 (2006) 237–247. doi:10.1016/j.memsci.2006.07.049.

[30] N.N. Bui, J.T. Arena, J.R. McCutcheon, Proper accounting of mass transfer resistances in forward osmosis: Improving the accuracy of model predictions of structural parameter, J. Memb. Sci. 492 (2015) 289–302. doi:10.1016/j.memsci.2015.02.001.

[31] W.C.L. Lay, J. Zhang, C. Tang, R. Wang, Y. Liu, A.G. Fane, Factors affecting flux performance of forward osmosis systems, J. Memb. Sci. 394–395 (2012) 151–168. doi:10.1016/j.memsci.2011.12.035.

[32] D. Jo, O.S. Al-Yahia, R.M. Altamimi, J. Park, H. Chae, Experimental Investigation of Convective Heat Transfer in a Narrow Rectangular Channel for Upward and Downward Flows, Nucl. Eng. Technol. 46 (2014) 195–206. doi:10.5516/NET.02.2013.057.

[33] T.Y. Cath, M. Elimelech, J.R. McCutcheon, R.L. McGinnis, A. Achilli, D. Anastasio, A.R. Brady, A.E. Childress, I. V. Farr, N.T. Hancock, J. Lampi, L.D. Nghiem, M. Xie, N.Y. Yip, Standard Methodology for Evaluating Membrane Performance in Osmotically Driven Membrane Processes, Desalination 312 (2013) 31–38. doi:10.1016/j.desal.2012.07.005.

[34] B.E. Poling, G.H. Thomson, D.G. Friend, R.L. Rowley, W.V. Wilding, Perry's Chemical Engineers' Handbook, 2007. doi:10.1036/0071511253.

[35] C.Y. Tang, Q. She, W.C.L. Lay, R. Wang, A.G. Fane, Coupled effects of internal concentration polarization and fouling on flux behavior of forward osmosis membranes

during humic acid filtration, J. Memb. Sci. 354 (2010) 123–133. doi:10.1016/j.memsci.2010.02.059.

[36] A. Amirtharajah, K.M. Mills, Rapid-Mix Design for Mechanisms of Alum Coagulation., J. Am. Water Work. Assoc. 74 (1982) 210–216. doi:10.2307/41271001.

[37] P.K. Holt, G.W. Barton, M. Wark, C.A. Mitchell, A quantitative comparison between chemical dosing and electrocoagulation, Colloids Surfaces A Physicochem. Eng. Asp. 211 (2002) 233–248. doi:10.1016/S0927-7757(02)00285-6.

[38] T. Harif, M. Khai, A. Adin, Electrocoagulation versus chemical coagulation: Coagulation/flocculation mechanisms and resulting floc characteristics, Water Res. 46 (2012) 3177–3188. doi:10.1016/j.watres.2012.03.034.

[39] T. Picard, G. Cathalifaud-Feuillade, M. Mazet, C. Vandensteendam, Cathodic dissolution in the electrocoagulation process using aluminium electrodes., J. Environ. Monit. 2 (2000) 77–80. doi:10.1039/a908248d.

[40] M. Rebhun, M. Lurie, Control of organic matter by coagulation and floc separation, Water Sci. Technol., 1993: pp. 1–20.

[41] B. Zhu, D.A. Clifford, S. Chellam, Comparison of electrocoagulation and chemical coagulation pretreatment for enhanced virus removal using microfiltration membranes, Water Res. 39 (2005) 3098–3108. doi:10.1016/j.watres.2005.05.020.

[42] D. Mills, New process for electrocoagulation, J. Am. Water Work. Assoc. 92 (2000) 34–43.

[43] E. Metcalf, H. Eddy, Wastewater engineering: treatment and reuse, 2003. doi:10.1016/0309-1708(80)90067-6.

[44] K.L. Hickenbottom, N.T. Hancock, N.R. Hutchings, E.W. Appleton, E.G. Beaudry, P. Xu, T.Y. Cath, Forward osmosis treatment of drilling mud and fracturing wastewater from oil and gas operations, Desalination 312 (2013) 60–66. doi:10.1016/j.desal.2012.05.037.

[45] Z.Y. Li, V. Yangali-Quintanilla, R. Valladares-Linares, Q. Li, T. Zhan, G. Amy, Flux patterns and membrane fouling propensity during desalination of seawater by forward osmosis, Water Res. 46 (2012) 195–204. doi:10.1016/j.watres.2011.10.051.

[46] S. Phuntsho, F. Lotfi, S. Hong, D.L. Shaffer, M. Elimelech, H.K. Shon, Membrane scaling and flux decline during fertiliser-drawn forward osmosis desalination of brackish groundwater, Water Res. 57 (2014) 172–182. doi:10.1016/j.watres.2014.03.034.

[47] M. Xie, W.E. Price, L.D. Nghiem, M. Elimelech, Effects of feed and draw solution temperature and transmembrane temperature difference on the rejection of trace organic contaminants by forward osmosis, J. Memb. Sci. 438 (2013) 57–64.

doi:10.1016/j.memsci.2013.03.031.

[48] D. Ghernaout, A.I. Al-Ghonamy, N. Ait Messaoudene, M. Aichouni, M.W. Naceur, F.Z. Benchelighem, A. Boucherit, Electrocoagulation of Direct Brown 2 (DB) and BF Cibacete Blue (CB) Using Aluminum Electrodes, Sep. Sci. Technol. 50 (2015) 1413–1420. doi:10.1080/01496395.2014.982763.

[49] D. Ghernaout, A. Al-Ghonamy, M.W. Naceur, N. Messaoudene, M. Aichouni, Influence of operating parameters on electrocoagulation of C.I. disperse yellow 3, J. Electrochem. Sci. Eng. 4 (2014) 271–283. doi:http://dx.doi.org/10.5599/jese.146.

[50] D. Ghernaout, B. Ghernaout, A. Saiba, A. Boucherit, A. Kellil, Removal of humic acids by continuous electromagnetic treatment followed by electrocoagulation in batch using aluminium electrodes, Desalination 238 (2009) 295–308. doi:10.1016/j.desal.2008.04.001.

[51] D. Ghernaout, B. Ghernaout, A. Boucherit, M.W. Naceur, A. Khelifa, A. Kellil, Study on mechanism of electrocoagulation with iron electrodes in idealised conditions and electrocoagulation of humic acids solution in batch using aluminium electrodes, Desalin. Water Treat. 8 (2009) 91–99. doi:10.5004/dwt.2009.668.

[52] E.M. Ephraim, M. Sparrow, J.P. John, P. Abraham, J.M. Gorman, Advances in Heat Transfer, San Diego, CA, Elsevier Science, 2016. http://www.sciencedirect.com/science/bookseries/00652717 (accessed March 26, 2017).

[53] E.L. Cussler, Diffusion: Mass Transfer in Fluid Systems, Engineering. Second Edition (1997) 580. doi:10.1017/CBO9780511805134.010.

[54] T.-S. Chung, S. Zhang, K.Y. Wang, J. Su, M.M. Ling, Forward osmosis processes: Yesterday, today and tomorrow, Desalination 287 (2012) 78–81. doi:10.1016/j.desal.2010.12.019.

[55] J.R. McCutcheon, R.L. McGinnis, M. Elimelech, Desalination by ammonia-carbon dioxide forward osmosis: Influence of draw and feed solution concentrations on process performance, J. Memb. Sci. 278 (2006) 114–123. doi:10.1016/j.memsci.2005.10.048.

[56] J.-J. Qin, G. Danasamy, W.C.L. Lay, K.A. Kekre, Challenges in Forward Osmosis of Seawater Using Ammonium Bicarbonate as Osmotic Agent, Am. J. Water Resour. 1 (2013) 51–55. doi:10.12691/ajwr-1-3-6.

[57] N.T. Hancock, T.Y. Cath, Solute coupled diffusion in osmotically driven membrane processes, Environ. Sci. Technol. 43 (2009) 6769–6775. doi:10.1021/es901132x.

Chapter 5. Integrated Electrocoagulation - Forward osmosis – Membrane Distillation System for Sustainable Water Recovery from Hydraulic Fracturing Produced Water

Abstract

Forward osmosis (FO) and membrane distillation (MD) are emerging technologies of interest for the treatment of high salinity brines. In this study, we aim to demonstrate the feasibility of an integrated FO-MD system for water recovery from actual high salinity produced waters obtained from shale gas extraction facilities. In the proposed hybrid system, FO draws water from high salinity feed, while MD regenerates the diluted FO draw solution. We show that this process integration can combine the advantages of both processes; low fouling tendency and high quality permeate. We further integrated the FO-MD system with an electrocoagulation (EC) system as pretreatment and showed a stable performance with minimal fouling. EC removed TOC and TSS by up to 78 and 96%, respectively. We studied the impact of experimental conditions (temperature, flow velocity and draw solution concentration) on performance of the integrated system in short-term experiments. In addition, we conducted long-term experiments using two different produced waters. We show that in order to achieve continuous high recoveries with maximized water flux, a combination of two MD membranes can provide a viable solution.

5.1. Introduction

The largest waste stream produced within the oil and gas industry is produced water (PW), with an annual estimated volume of 21 billion barrels in the United States (US) [1]. Discharging untreated PW, containing various organic and inorganic components, can pollute surface and underground water and soil. Major contaminants in PW (oil content and salinity) can be reduced

through various physical, chemical, and biological methods [2]. However, treating the vast amounts of PW in a cost-effective way, sometimes in remote locations, demands advanced solutions, often a combination of several separation processes, so the water can be safely discharged or re-used for other applications [3].

Hydraulic fracturing and horizontal drilling have enabled the oil and gas industry to rapidly develop a large number of unconventional oil and gas reserves over the past two decades [4]. The amount of dry natural gas produced directly from unconventional resources was increased from 0.3 trillion cubic feet (Tcf) in 2000 to 15.8 Tcf in 2016 [5,6]. The hydraulic fracturing process generates large volumes of PW, ranging from 1.7 to 14.3 million L per well in the first 5-10 years of production, requiring management [7]. The hydraulic fracturing PW mainly consists of injected fracturing fluid and naturally occurring formation brines and it usually represents high levels of total dissolved solids (TDS) (from 650 up to 400,000 mg L^{-1}) [7]. Deep-well injection has been the most common hydraulic fracturing PW management practice in the U.S. over the past two decades [8–10]. However, costs as well as environmental concerns associated with deep-well injection necessitate development of cost-effective and environmentally friendly technologies for treatment of these wastewater streams, with primary consideration of TDS reduction [10]. A number of treatment technologies are under investigation, such as forward osmosis (FO) [11], membrane distillation (MD) [12], electrodialysis [13] mechanical vapor compression [14], multi-effect distillation [15] and ion-exchange [16]. In this study, we focus an integrated FO-MD system.

FO has the potential to treat high TDS PW and generate high quality permeate. In FO, the osmotic pressure difference is the driving force for water transport from the feed to a high concentration draw solution (DS) across a semi-permeable membrane [17]. The FO process results

in concentration of the feed stream and dilution of the DS. The main advantages of using FO are operation at low or no hydraulic pressures, high rejection of a wide range of contaminants, simple equipment requirement and lower membrane fouling propensity than pressure-driven membrane processes such as reverse osmosis (RO) [18,19]. Research in the field of FO membrane technology has grown significantly over the last 10 years, but its real application in the scope of PW treatment has been much slower [20]. One of the main challenges associated with the widespread use of FO is the efficient regeneration of DS. In continuous FO operation, diluted DS must be repeatedly regenerated, using a thermodynamically favorable re-concentration system, in order to separate the original DS from the product water [17,20]. A range of processes have been investigated regarding DS recovery and reuse, including: conventional distillation, multi-stage flash, electrodialysis, RO, nanofiltration (NF), etc. [21–28]. The chosen recovery system depends on the type of application and solute, the recovery rate required and the energy consumption of the unit. For hydraulic fracturing PW treatment, high feed TDS leads to use of high DS concentration. RO and NF require elevated pressures when dealing with high TDS DS (e.g. 380 bar at 365,000 mg L^{-1} sodium chloride in de-ionized (DI) water) [29]. Here, we focus on MD regarding DS recovery.

MD is a thermally-driven separation technology whereby the water recovery from the hot feed takes place by the following steps: vaporization, transfer across a hydrophobic microporous membrane and condensation in the permeate side [12,30]. The vapor pressure difference across the membrane is the driving force for MD. Integrated FO-MD system has the potential for sustainable treatment of high TDS PW and production of clean product water. MD can offer complete rejection of nonvolatile substances in DS and its efficiency is relatively independent of DS concentration [31]. In the hybrid FO-MD system, FO draws water from the feed solution, while MD re-concentrates the diluted DS and produces clean product water. The integrated FO-

MD process combines the advantages of both processes, providing low fouling tendency and high permeate quality [32]. In addition, high operational temperature (e.g. 50-70 ^{o}C) in MD can result in higher recycled DS temperature and consequently, higher flux in FO as the FO driving force is a linear function of temperature [33]. Use of MD can be a favorable and cost-effective method for DS re-concentration, specifically when low-grade waste heat is abundant. So far, only a limited number of studies on hybrid FO-MD have been reported in the literature for wastewater treatment and feed solution concentration [21,31,33].

Although the fouling tendency of FO is thought to be lower than RO, NF and MD, the presence of small, highly fouling suspended and organic species combined with internal concentration polarization can lead to significant membrane fouling and flux deterioration when treating real PW streams with FO [19]. Maltos et al. [20] and Bell et al. [34] reported major fouling of FO membranes while treating raw PW In our previous work [11], we have demonstrated that a pretreatment step prior to FO can successfully suppress fouling during FO and increase water recovery. Here, we aim to further modify the hybrid FO-MD system by adding a pretreatment step. Electrocoagulation (EC) is our proposed pretreatment method.

EC is a physio-chemical method where the separation of suspended particles and dissolved macromolecular organic species from the feed water takes place by means of electrically forced dissolution of coagulant precursors into solution followed by flocculation, charge neutralization and consequently, phase separation (sedimentation or floatation) [11,35]. Although the chemical basis of EC is similar to conventional coagulation (e.g. alum and ferric chloride coagulation), it can provide the following advantages: lack of moving parts, ease of operation, reduced sludge production, minimal use of added chemicals and low operating costs [36–38]. In addition, EC

requires relatively low electrical energy input when treating wastewater streams with high conductivity, making it a favorable pretreatment for high TDS PW [39].

Here, we aim to demonstrate the feasibility and stability of the integrated EC-FO-MD process in water recovery from high salinity PW streams. We show that this process integration can be used to systematically enhance and reconcile various objectives, such as cost effectiveness, recovery and energy efficiency. Fig. 1 presents the concept of integrated EC-FO-MD process.

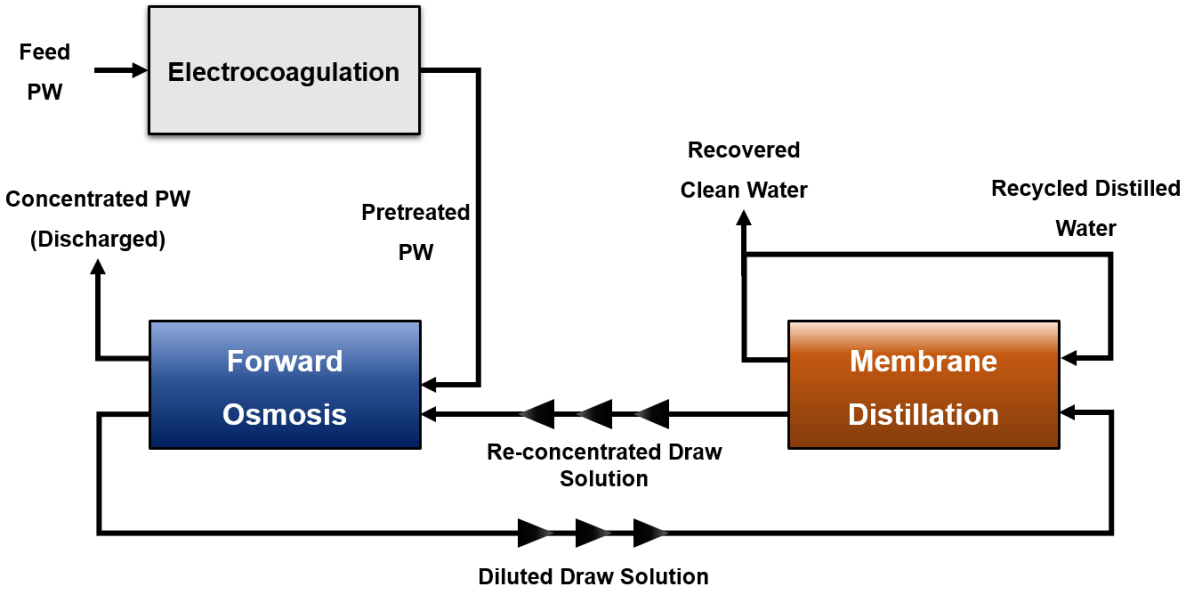

Fig. 1. Concept of integrated EC-FO-MD process. EC pretreats the feed PW, FO draws water from the pretreated PW and MD re-concentrates the diluted DS. Integrated process combines the strength of EC, FO and MD processes for high TDS PW treatment.

5.2. Summary of Theoretical Background

5.2.1. Electrocoagulation

The following reactions occur in the EC reactor when using aluminum electrodes [40]:

Anode: $Al_{(s)} \rightarrow Al^{3+}_{(aq)} + 3e^-$ (1)

Cathode: $2H_2O + 2e^- \rightarrow 2OH^- + H_2$ (2)

Analogous to chemical (alum) coagulation, the produced Al^{3+} and OH^- ions form variety of aluminum hydroxide species such as $Al(OH)^{2+}$, $Al(OH)_2^+$, $Al(OH)_4^-$ [11,41]. These species develop polynuclear complexes (coordination compounds containing two or more *Al* atoms) while the solution ages and transform to amorphous $Al(OH)_{3(s)}$ solids governed by complex-precipitation kinetics [39]:

As the solution ages: $Al_n(OH)_m^{(3n-m)+} \rightarrow n\, Al(OH)_{3(s)}$ (3)

With their large surface area, $Al(OH)_{3(s)}$ solids can adsorb organic compounds, polymerize and trap suspended particles and finally, deposit as settable flocs according to Eq. (4) [42]:

Deposition: $x\, Al(OH)_3 \rightarrow Al_x(OH)_{3x}$ (4)

Electrical energy consumption of the EC system can be calculated using the following equation:

$$E = \frac{I\ X\ V\ X\ t}{Vr} \quad (5)$$

where *I* is applied current, *V* is average voltage, t is EC reaction time and V_r is reactor volume.

5.2.2. Forward Osmosis

The FO water flux can be represented by Eq. (6):

$$J_{FO} = A\,(\pi_{DS} - \pi_F) \tag{6}$$

where J_{FO} is the transmembrane water flux, A is the pure water permeability coefficient and π_{DS} and π_F are the osmotic pressure of the bulk draw and feed solutions, respectively. The pure water permeability coefficient (A) depends on the resistance to water flow through the membrane, while the osmotic pressures are mainly a function of solution concentration and temperature [43]. In a real FO operation, permeability is compromised by internal and external concentration polarization [11,44]. The following expression may be used to model the water flux during FO, assuming the osmotic pressure varies linearly with salt concentration within the concentration boundary layer:

$$J_{FO} = A.\left[\frac{\Pi_{DS}.\,e^{\left(-J_{FO}\left\{\frac{1}{k_{DS}}+\frac{S}{D_{DS}}\right\}\right)} - \Pi_F.\,e^{\left(\frac{J_{FO}}{k_F}\right)}}{1+\frac{B}{J_{FO}}\left\{e^{\left(\frac{J_{FO}}{k_F}\right)} - e^{\left(-J_{FO}\left\{\frac{1}{k_{DS}}+\frac{S}{D_{DS}}\right\}\right)}\right\}}\right] \tag{7}$$

where k_F and k_{DS} are feed and DS convective mass transfer coefficients, S is membrane structural parameter, B is solute permeability coefficient and D_{DS} is solute diffusion coefficient [43]. In this study, the FO water flux is estimated using Eq. (7) along with the procedure described in our earlier work [11].

5.2.3. Membrane Distillation

Water Flux across a hydrophobic membrane in MD may be represented as:

$$J_{MD} = C\ (P_h - P_c) \tag{8}$$

where J_{MD} is transmembrane water flux, C is membrane permeability coefficient and P_h *and* P_c are partial pressure of water across the MD membrane in the hot and cold streams, respectively [30]. The membrane permeability coefficient is a function of different resistances in series for water transfer across the membrane including viscous, molecular and Knudsen diffusion and it strongly depends on the MD configuration. In direct contact MD (DCMD) (most commonly used and the focus in this study), the impact of viscous flow is negligible and vapor transfer is dominated by molecule-molecule and molecule-pore wall collisions [30]. The reduced Knudsen-molecular diffusion model (Eq. (9)) may be used to predict the water flux during DCMD when considering a membrane with approximately 0.2 μm average pore size [45,46]:

$$C = \frac{M_w}{R\delta T_m}\left(\frac{D_k D_m}{p_a D_k + D_m}\right) \tag{9}$$

where M_w is molecular weight of water, R is universal gas constant, δ is membrane thickness, T_m is average temperature of the hot and cold streams across the membrane and p_a is the partial pressure of the stagnant air within the membrane pores. D_k and D_m are Knudsen and molecular diffusion coefficients and are defined as follows:

$$D_k = \frac{2\varepsilon r}{3\tau}\left(\frac{8RT_m}{\pi M_w}\right)^{0.5} \tag{10}$$

$$D_m = 4.46 * 10^{-6}\left(\frac{\varepsilon}{\tau}\right) T_m^{2.334} \tag{11}$$

where $\mathcal{E}$ is the membrane porosity, r is the average pore radius and τ is membrane tortuosity. For membranes with very small pore sizes (e.g. 0.02 µm), the mean free path of water vapor molecules is much larger than the average pore size and the mass transfer is more likely controlled by Knudsen diffusion (molecule – pore wall collisions) [30,47]. Thus, membrane permeability coefficient can be estimated using only the Knudsen diffusion coefficient, as following:

$$C = \frac{D_k}{R\delta T_m} \tag{12}$$

Eqs. (9) to (12) along with the mathematical modeling procedure described by Yun *et al.* [45] are used to estimate the water flux across the MD membrane in DCMD configuration.

5.3. Experimental

5.3.1. Produced Water Samples

PW samples were received from Southwestern Energy (Houston, TX) shale gas production facilities in Pennsylvania (Marcellus shale) and Arkansas (Fayetteville shale). PW samples were passed through a 300 µm stainless steel mesh screen (Twp Inc. Berkley, CA) prior to storage at 4 ºC in order to remove larger particulate matter. All samples were analyzed at the Arkansas Water Resources Center, University of Arkansas. The following parameters were measured: TDS, total suspended solids (TSS), total organic carbon (TOC) and turbidity. TDS, TSS and TOC were measured using EPA standard methods 160.1, 160.2 and 415.1 [48], respectively. Turbidity was measured using a Turb 550 (WTW, Weilheim, Germany) turbidity-meter. In addition, the inorganic composition of PW samples were analyzed using EPA methods 200.7 (for cations) and 300.0 (for anions), respectively. Electroneutrality of each sample (percent difference between the

sum of anions and cations in equivalent weight per liter) was calculated to ensure the accuracy of the chemical analysis.

5.3.2. Electrocoagulation

Aluminum-based EC was employed as the primary pretreatment method. A schematic diagram of the EC setup is given in Fig. 2. As can be seen, 5 aluminum electrodes (6061 aluminum alloy) with total surface area of 0.18 m^2 were placed in a 0.6 L polycarbonate reactor. A DC power source (Hewlett Packard, Palp Alto, CA) was connected to the anode and cathode (first and last electrodes) and was used to provide the required electrical current for the EC experiments. The current density was maintained at 2.78 mA cm^2 by continuous adjustment of voltage using the DC power source. All experiments were run for 2 min, based on optimization results obtained in our previous publication [11]. After each EC run, electrocoagulated water was transferred to a 1 L glass separatory funnel for aging and phase separation. After 6 h aging time, deposited flocs (bottom) and floating skimmings (top) were wasted and the clear portion of water (middle section) was recovered as the pretreated water.

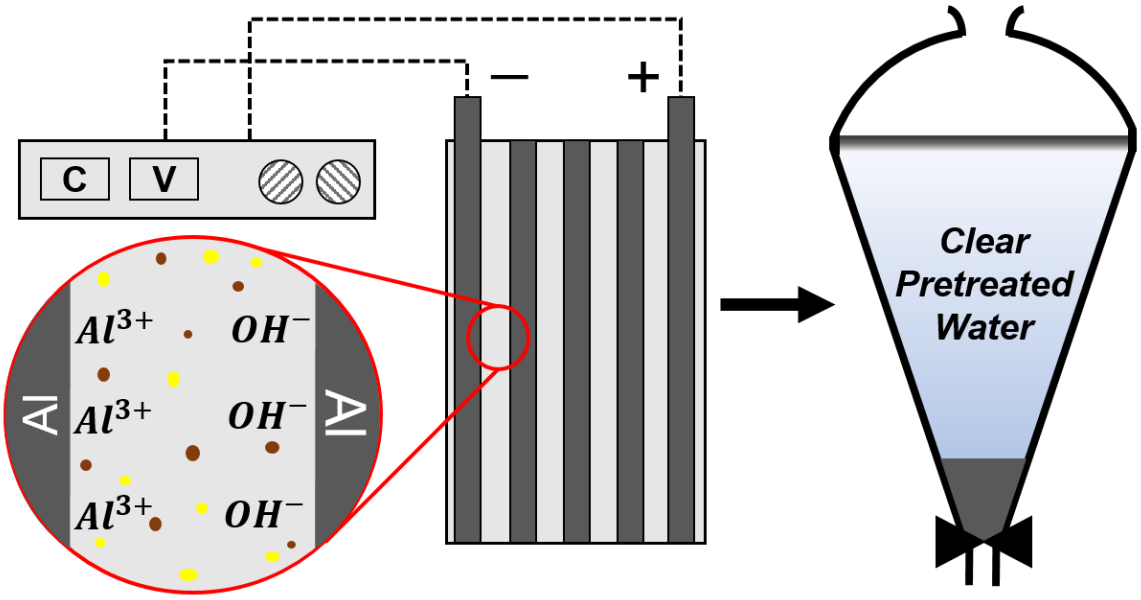

Fig. 2. Schematic diagram of the EC reactor and phase separation funnel. The anode and cathode are connected to the DC power source. Positively charged aluminum ions are released at anode and hydroxide ions are produced at the cathode following water hydrolysis. After 6 h sedimentation time, flocs are deposited at the bottom of the separatory funnel, with light flocs floating on the top.

5.3.3. Membranes

Flat sheet cellulose triacetate (CTA) membranes with an embedded polyester mesh support were acquired from HTI (Albany, OR) and used as the FO membrane. CTA membranes have been widely investigated by a number of researchers [11,49–52]. The CTA membranes were soaked in DI water for 2 h and rinsed with DI water several times before use in order to remove the glycerin in which they are shipped.

Following hydrophobic membranes were used in MD experiments: Ethylene chlorotrifluoroethylene (ECTFE) copolymer, provided by 3M (Maplewood, MN) and polytetrafluoroethylene (PTFE), provided by Pall Corporation (Port Washington, NY). Table 1

lists the characteristics of the studied MD membrane, including mean pore size, porosity, thickness, contact angle and liquid entry pressure (LEP). ECTFE membrane properties were extracted from our earlier publication [12]. PTFE membrane characteristics were measured using characterization procedures described in our previous work [12].

Table 1. Characteristics of MD hydrophobic membranes.

Membrane	Nominal pore size (μm)	Measured mean pore size (μm)	Porosity	Thickness (μm)	Contact angle (°)	LEP (kPa)
ECTFE	0.2	0.18	0.71	82±15	130±1	330
PTFE	0.02	0.03	0.76	54±5	153±4	540

5.3.4. Membrane Separation Setup

The membrane separation experimental setup (used in FO and MD experiments) was mainly composed of two 4 L reservoirs, two variable speed peristaltic pumps (Masterflex I/P, Cole Parmer, Vernon Hills, IL), two shell and tube titanium heat exchangers (Brazetek, Brooklyn, NY) and a computer-connected analytical balance (Mettler Toledo, Columbus, OH). Fig. 3 depicts the experimental apparatus employed in our study. Heat exchangers were used to adjust the solutions temperature. Heater and chiller oils were pumped through the tube side of the heat exchangers. The temperature of the heater and chiller oils were controlled using two circulating baths (PolyScience AD07R-40, Niles, IL). A digital thermometer employing two k type thermocouples was used to monitor both streams temperature. Two conductivity-meters (VWR, Radnor, PA)

were installed in both tanks. Weight change of the tank #1 was recorded by means of the computer-connected balance regarding water flux measurement.

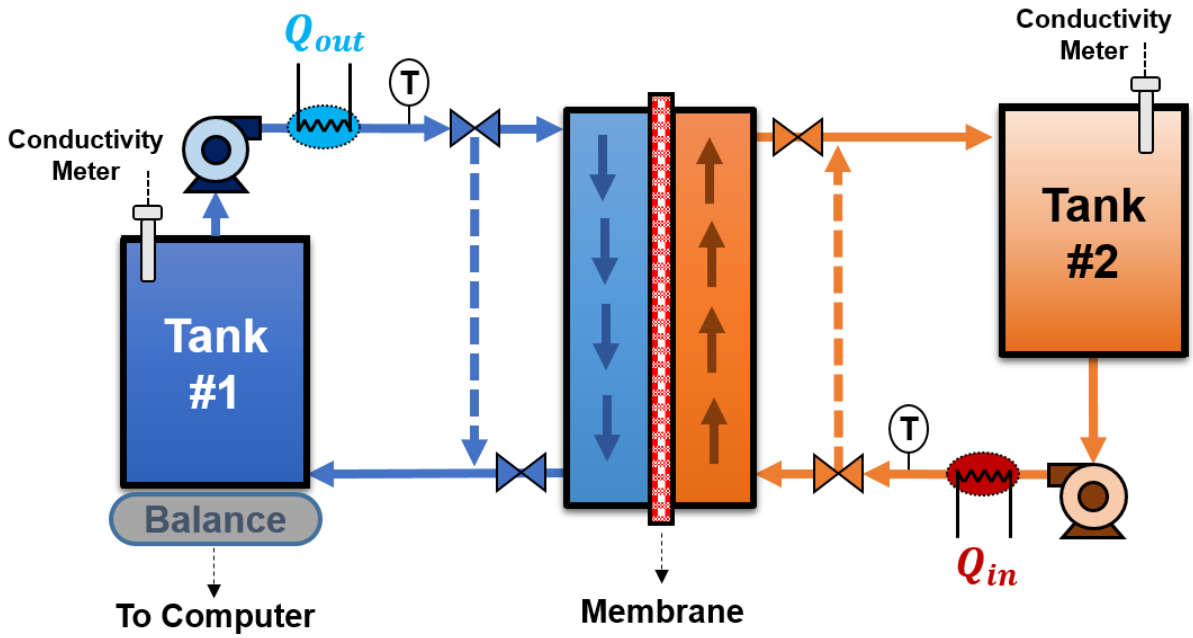

Fig. 3. Schematic diagram of the experimental apparatus for FO and MD experiments. In FO experiments, feed PW and DS were placed in tank#1 and tank#2, respectively. In MD experiments, tank#1 was filled with DI water and tank#2 was filled with diluted DS.

5.3.5. Forward Osmosis

A homemade polycarbonate tangential flow cell providing 33.75 cm^2 effective membrane area was used as FO membrane module. CTA membrane coupons were first soaked in DI water for 2 h and rinsed with DI water several times. Then they were installed in the polycarbonate membrane module. Mesh spacers (XN4510, Industrial Netting, Minneapolis, MN) filled the 2 mm deep channels on both sides of the membrane cell to improve support and flow turbulence. PW samples (raw or pretreated) were placed in the tank#1 and were recirculated on the active side of the FO membrane. DS was placed in the tank#2 and was recirculated on the support side of the

CTA membrane. Draw and feed solutions were recirculated counter-currently with equal flow velocities and were returned to their respective reservoirs. A range of flow velocities and DS temperatures were tested.

In each FO run, a CTA membrane was first installed in the membrane module. 2 L PPW feed and 2 L DS were placed in their respective reservoirs. Cross-flows of feed and DS were run until stable temperatures were attained, while bypassing the membrane module. After reaching the desired temperature, both streams were allowed to pass through both sides of the membrane module. FO experiments were carried out with various temperatures, a range of concentrations of sodium chloride in DI water as DS and two real hydraulic fracturing PW as feed solutions. Table A.1 (appendix A) represents the conditions of the FO experiments conducted in this work.

5.3.6. Membrane Distillation

Experimental apparatus showed in Fig. 3 was used for DCMD experiments. A custom-made PTFE membrane cell with 40 cm^2 effective membrane area and 2 mm deep channels was used as the MD module. PTFE spacers (ET 8700, Industrial Netting, Minneapolis, MN) were used within the module channels for mechanical support and flow mixing. Feed water (diluted FO DS) was placed in the tank#2 and was recirculated back to its reservoir, bypassing the membrane module, until the desired temperature was obtained. DI water was placed in the tank#1 and the same procedure as for the feed was followed, until temperature was stable at 20 ºC. After reaching the target temperatures, feed and DI water streams were allowed to flow over the opposite surfaces of the membrane at an equal flow rate of 0.9 L min^{-1} (equal to 16.7 cm s^{-1} flow velocity).

The water flux was calculated based on the rate of increase in the weight of tank#1. Experiments were continued until the target water recovery was attained. DI water conductivity was continuously monitored using the conductivity-meter installed in the tank#1 and was kept under 50 µS cm^{-1} to ensure the MD membrane was not wetted. Wetting (state were liquid water crossed the MD membrane) was assumed when the conductivity of the permeate was increased rapidly above 50 µS cm^{-1}. Experimental conditions of the MD experiments conducted here is shown in Table A.1.

5.3.7. Scanning Electron Microscopy (SEM) and Energy-dispersive X-ray Spectroscopy (EDX)

SEM using a Nova Nanolab 200 Duo-Beam (FEI, Hillsboro, Oregon) was used to visually analyze the membrane surface before and after FO and MD experiments. The same equipment was used to perform EDX elemental analysis on fouled membrane surface after experiments.

5.4. Results and Discussion

5.4.1. Wastewater Characterization

Table 3 gives the characteristics of raw (after screen filtration) and EC-pretreated hydraulic fracturing PW samples. The TDS, TSS, TOC, turbidity and inorganic species in the samples are shown. The TDS of the studied PW samples ranged from 11,341 to 57,523 mg L^{-1}. Hydraulic fracturing PW sample obtained from Marcellus shale (referred to as PW2) shows higher TDS and TOC content compared to the sample received from Fayetteville shale (PW1). PW1 shows higher

levels of TSS and turbidity than PW2. Sodium and chloride account for the majority of the dissolved ions in PW1. In addition to these two ions, calcium is also observed in PW2. PW1 and PW2 contain 111.86 and 6.19 mg L^{-1} sulfate. The presence of sulfate can lead to membrane scaling due to sulfate salts (e.g. calcium sulfate) precipitation.

Table 3. Characteristics of raw and EC-pretreated PW samples.

Parameter	Unit	PW1 Obtained from Fayetteville shale		PW2 Obtained from Marcellus shale	
		Raw	After EC	Raw	After EC
TDS	mg L^{-1}	11,341.60	11,212.70	57,523.10	57,193.50
TSS	mg L^{-1}	317.21	13.69	235.06	3.15
TOC	mg L^{-1}	87.27	24.13	139.10	29.57
Turbidity	Ntu	32.10	2.50	86.33	1.74
Chloride	mg L^{-1}	6,550.96	6,672.64	32,871.45	31,694.21
Sulfate	mg L^{-1}	111.86	113.40	6.19	6.12
Aluminum	mg L^{-1}	0.66	1.23	0.29	0.89
Calcium	mg L^{-1}	84.56	80.51	5,261.65	5,058.33
Iron	mg L^{-1}	0.00	0.36	0.85	0.71
Magnesium	mg L^{-1}	35.08	35.98	29.93	34.76
Potassium	mg L^{-1}	24.77	21.75	6.12	4.56
Sodium	mg L^{-1}	3,799.01	3,812.26	16,355.31	16,222.50

5.4.2. Electrocoagulation Performance

Here, EC using aluminum electrodes was used as the pretreatment step prior to FO. According to Eqs. (1) to (3) (see section 5.2.1), aluminum and hydroxide ions were released into the solution and reacted to form a variety of monomeric (e.g. $Al(OH)^{2+}$) and polynuclear (e.g. $Al_5(OH)_{12}^{3+}$) species. By transferring the electrocoagulated water into the separatory funnel and allowing the sample to age, these species were converted into amorphous $Al(OH)_{3(s)}$ particles [53]. Due to their large surface area, $Al(OH)_{3(s)}$ precipitates adsorbed organic compounds, trapped suspended particles, formed agglomerated flocs and were separated from the solution by 6 h sedimentation. The remainder of the positively charged aluminum hydroxide species (e.g. $Al(OH)_2^+$) contributed to charge neutralization of negatively charged suspended solids and destabilization of organic macromolecules and enhanced the contaminate removal [11]. However, negatively charged aluminum hydroxide compounds (e.g. $Al(OH)_4$-) restrict the adsorption and complexation by charge repulsion [54].

Performance of the EC process for removing different contaminates was evaluated using removal efficiency as following:

$$Removal\ Efficiency\ (\%) = \frac{x_{pw} - x_{rw}}{x_{pw}}\ X\ 100 \qquad (13)$$

where, x_{pw} and x_{rw} are the concentration in the raw PW and recovered water after EC, respectively. Removal efficiencies for both wastewaters tested are given in Fig. 4, while the characteristics of the pretreated samples are given in Table 3. As can be seen, TSS and turbidity were removed by greater than 90% for both PW samples. TOC was removed by 72 and 78% for PW1 and PW2, respectively. Minimal TDS removal was observed for both waters. This is not unexpected given

that EC removal mechanism cannot target dissolved inorganic compounds [55]. The removal of TSS, TOC and turbidity is higher for PW2 compared to PW1. The reason for this observation can be related to the nature of PW samples since all the EC experiments were conducted at similar conditions (2 min reaction at 2.78 mA cm^2 current density). As can be seen in Table 3, almost similar amount of aluminum is released into PW1 and PW2 during the EC reaction.

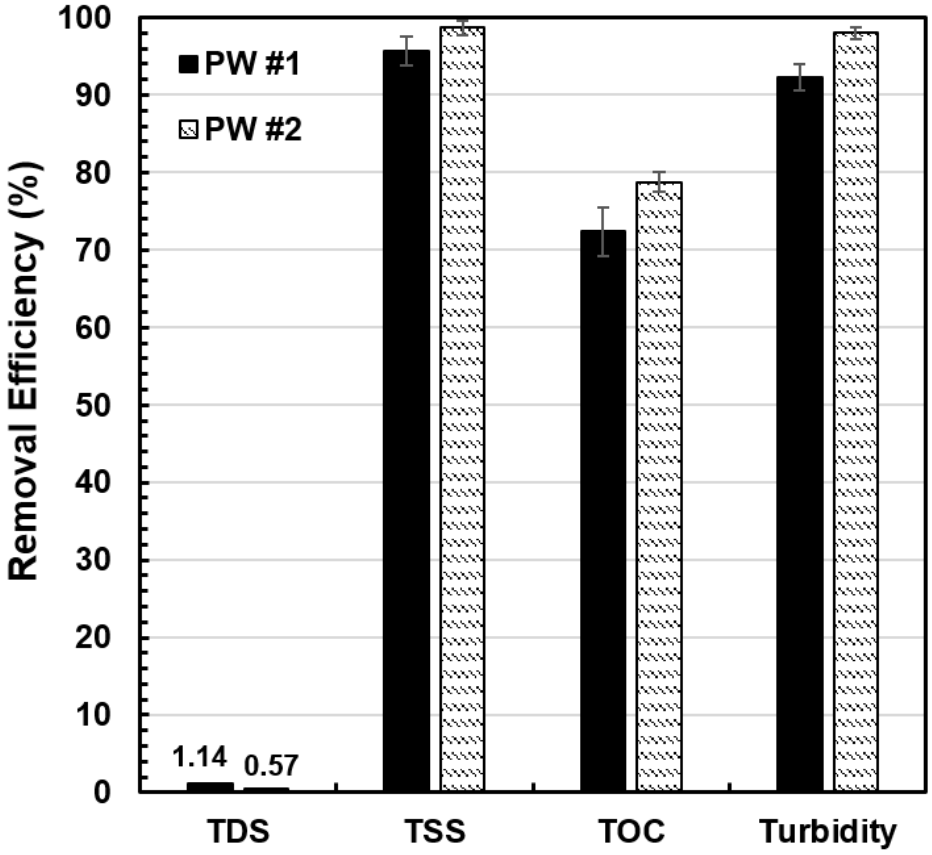

Fig. 4. Removal efficiency of EC for PW1 (Fayetteville shale) and PW2 (Marcellus shale). Minor TDS removal is observed. TSS and Turbidity are removed by over 90%. TOC is removed by 72 and 78% for PW1 and PW2, respectively.

5.4.3. Bassline Experiments

Baseline FO and MD experiments were carried out employing CTA membrane in FO and ECTFE membrane in MD system. Pretreated PW1 and PW2 were used as the FO feed stream and maintained at 20 °C in all experiments. The MD permeate stream was also maintained at 20 °C. A range of concentrations of sodium chloride in DI water were used as the FO DS as well as the MD feed stream. Figs. 5(a) to 5(c) present the permeate flow rate of the CTA and ECTFE membranes in FO and MD systems under a variety of experimental conditions. Dashed lines show the modeled results while the symbols give the experimental data.

Fig. 5(a) gives the variation of permeate flux variation for FO and MD membranes as a function of DS temperature. DS was used as the MD feed stream. In this set of experiments, all flow rates were maintained at 0.7 L min^{-1} and all experiments were run with an initial DS concentration of 4 M (234 g L^{-1} sodium chloride in DI water). As can be seen, the MD water flux increase exponentially as the feed water temperature increases. This is not unexpected since permeate transport trough the MD membrane is governed by the vapor pressure difference across the membrane (see Eq. (8)). The vapor pressure increases rapidly by increasing temperature, resulting in much higher permeate fluxes at higher temperatures [56]. In the case of FO experiments with PW1 and PW2 at different DS temperatures, permeate fluxes increased almost linearly with increasing temperature. This is not unexpected as the FO driving force (osmotic pressure) is a linear function of temperature. Zhao et al. [57] report a similar trend. Predicted permeate fluxes were in good agreement with the experimental results.

Fig. 5(b) gives the permeate flux of FO and MD membranes as a function of circulation rate. In this set of experiments, FO and MD feed temperatures were maintained at 25 and 60 °C,

respectively. In addition, all experiments were run with an initial DS concentration of 4 M. the MD permeate flux increased as the flow rate of feed and permeate increased. However, this increase was not linear. This observation is due to an increase in the heat transfer coefficient of the feed and permeate sides of the MD membrane by reducing the temperature and concentration polarization effects. As the heat transfer coefficient on both sides increases, the temperature at the membrane surface approaches the temperature in the bulk solution and higher permeate flux is observed due to higher water vapor pressure difference caused by the elevated temperature difference across the membrane [47].

On the contrary, increase in FO permeate flux in very minor compared to MD. As can be seen in Fig. 5(b), for both PW1 and PW2, FO water flux slightly increases by increasing the circulation rate. Increasing the circulation rate from 0.3 to 0.9 L min^{-1} (equal to 5.5 to 16.65 cm s^{-1} cross-flow velocity) resulted in 14% and 8% increase in FO permeate flux when operating PW1 and PW2, respectively. This flux enhancement is related to the reduced external concentration polarization as a result of the increased mass transfer coefficient at elevated cross-flow velocities [58].

Fig. 5(c) shows the variations in permeate flux for FO and MD membranes as a function of DS concentration. DS is used as the MD feed stream. FO and MD feed temperatures were maintained at 25 and 60 °C, respectively. All flow rates were maintained at 0.7 $L\ min^{-1}$. It is well known that MD can be used for treatment of highly concentrated brines without suffering the large drop in permeability observed in other membrane processes such as RO [47]. As can be seen in Fig. 5(c), MD permeate flux ranges from 48.9 $L\ m^{-2}\ h^{-1}$ to 36.5 $L\ m^{-2}\ h^{-1}$ when increasing the DS concentration from 115 to 295 g L^{-1}. The observed decreased is mainly due to the fact that the

increase in MD feed water salinity reduces the partial vapor pressure and consequently, reduces the driving force of the MD process [30,47].

In case of FO with PW1 and PW2, greater permeate flow rate was observed at higher DS concentration. This was due to the increased osmotic pressure difference across the CTA membrane when employing a higher DS concentration. This increase was less significant at higher DS concentrations (>200 g L^{-1}). During all bassline experiments (Figs. 5(a) to 5(c)), PW1 gave a higher FO permeate flux range compared to PW2. The reason for this observation was the presence of lower TDS in the PW1 which led to higher osmotic pressure difference across the CTA membrane and consequently, resulted in higher permeate flux. In all cases, the predicted permeate fluxes were in reasonable agreement with the experimental observation.

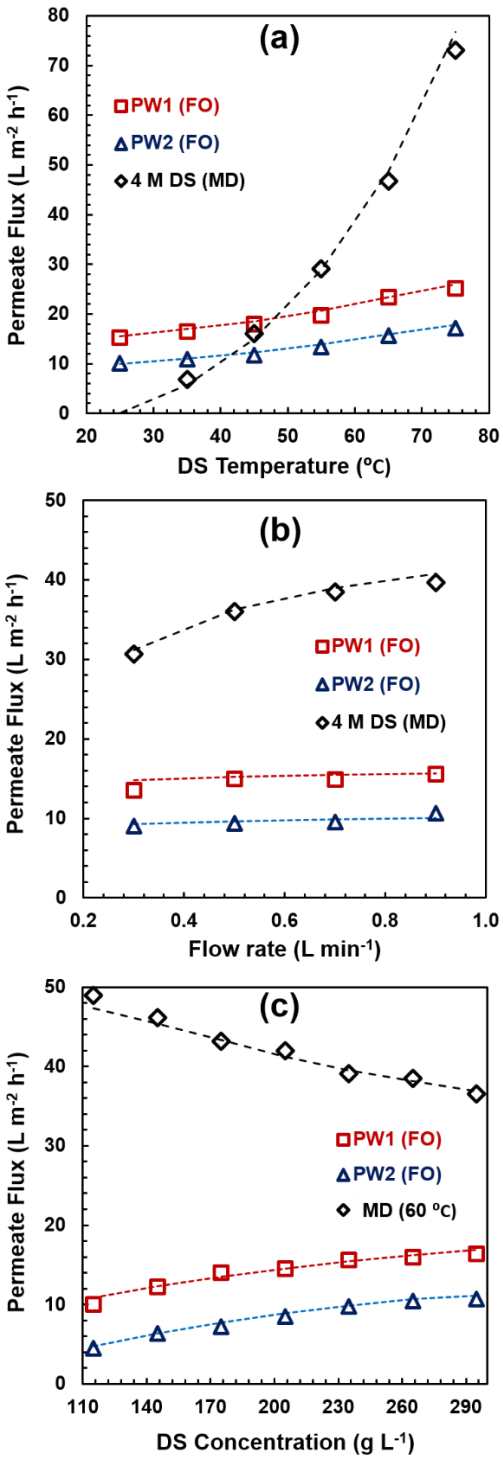

Fig. 5. FO and MD baseline results. DS was used as MD feed solution. **a)** water flux as a function of DS temperature. **b)** Water flux as a function of flow rate. **c)** Water flux as a function of DS concentration.

5.4.4. Actual Forward Osmosis-Membrane Distillation Runs

A second set of FO-MD experiments was carried out in concentration mode using EC-pretreated PW1 and PW2 as the FO feed water and a range of sodium chloride concentrations in DI water (2, 3.5 and 5 M) as the DS. Diluted DS during each FO experiment was then used as the MD feed water. All flow rates were adjusted at 0.7 L min^{-1}. FO and MD temperatures were adjusted at 25 and 60 ºC, respectively. Fig. 6(a) depicts the variations of model and experimental FO permeate flux as functions of recovered permeate volume for PW1 and PW2. Water recovery is shown in the secondary horizontal axis. 2.0 M DS concentration was used as the FO draw solution.

As can be seen in Fig. 6(a), permeate fluxes decreased as the collected permeate volume increased. PW1 and PW2 were continuously concentrated in the FO process, while the DS was continuously diluted by permeate cross-over from feed to DS. Thus, the observed decrease can be directly linked to a decrease in driving force (osmotic pressure). PW1 showed a higher permeate flux compared to PW2 due to the presence of less dissolved solids. PW1 was concentrated up to 80%, while PW2 only achieved 31% recovery and permeate flux dropped to zero upon collection of 620 ml permeate. This is not unexpected given the TDS content of PW2 and DS should be almost the same after over 30% permeate recovery, resulting in almost zero osmotic pressure difference across the membrane.

As can be seen, model and experimental FO permeate fluxes were in good agreement. SEM images taken from the CTA membrane surface before and after the FO experiment (see Fig. 6(a)) are shown in Fig. 7(a) and 7(b), respectively. As can be seen, minimal fouling was observed. Diluted DS during FO experiments with PW1 and PW2 were regenerated in the MD system. Fig.

6(b) shows the variation of MD permeate flux as a function of recovered permeate volume for diluted DS. Diluted DS were concentrated up to 2.0 M. As can be seen, both water fluxes decline during the collection of permeate due to concentration of MD feed. Final MD permeate fluxes for both samples were ~46.5 as both diluted DS were concentrated up to 2.0 M.

Figs. 6(c) and 6(e) give the FO water flux as a function of both permeate volume and recovery rate when treating PW1 and PW2 using 3.5 and 5.0 M sodium chloride in DI water as DS, respectively. Similar to the case of 2.0 M DS, PW1 gave a higher permeate flux range compared to PW2 due to the presence of less dissolved solids. As can be seen, the FO permeate flux increased with increasing sodium chloride concentration in the DS. PW2 was concentrated 54 and 67% using 3.5 and 5.0 M DS, while PW1 was concentrated up to ~85% in both cases. This results confirms the necessity of using high concentration DS (high osmotic pressure) for achieving higher recovery rates when treating PW containing high levels of dissolved solids (e.g. >57 g L^{-1}).

Figs. 6(d) and 6(f) show the MD water flux as a function of permeate volume for diluted 3.5 and 5.0 M DS. MD water fluxes decline during the collection of the permeate due to the increase in MD feed concentration. Diluted DS samples were concentrated back to their original concentrations. Comparing Figs. 6(b), 6(d) and 6(f), MD permeate fluxes in each figure achieve similar values. As can be seen in Figs. 6(a) to 6(f), the estimated permeate fluxes were in excellent agreement with the experimental data.

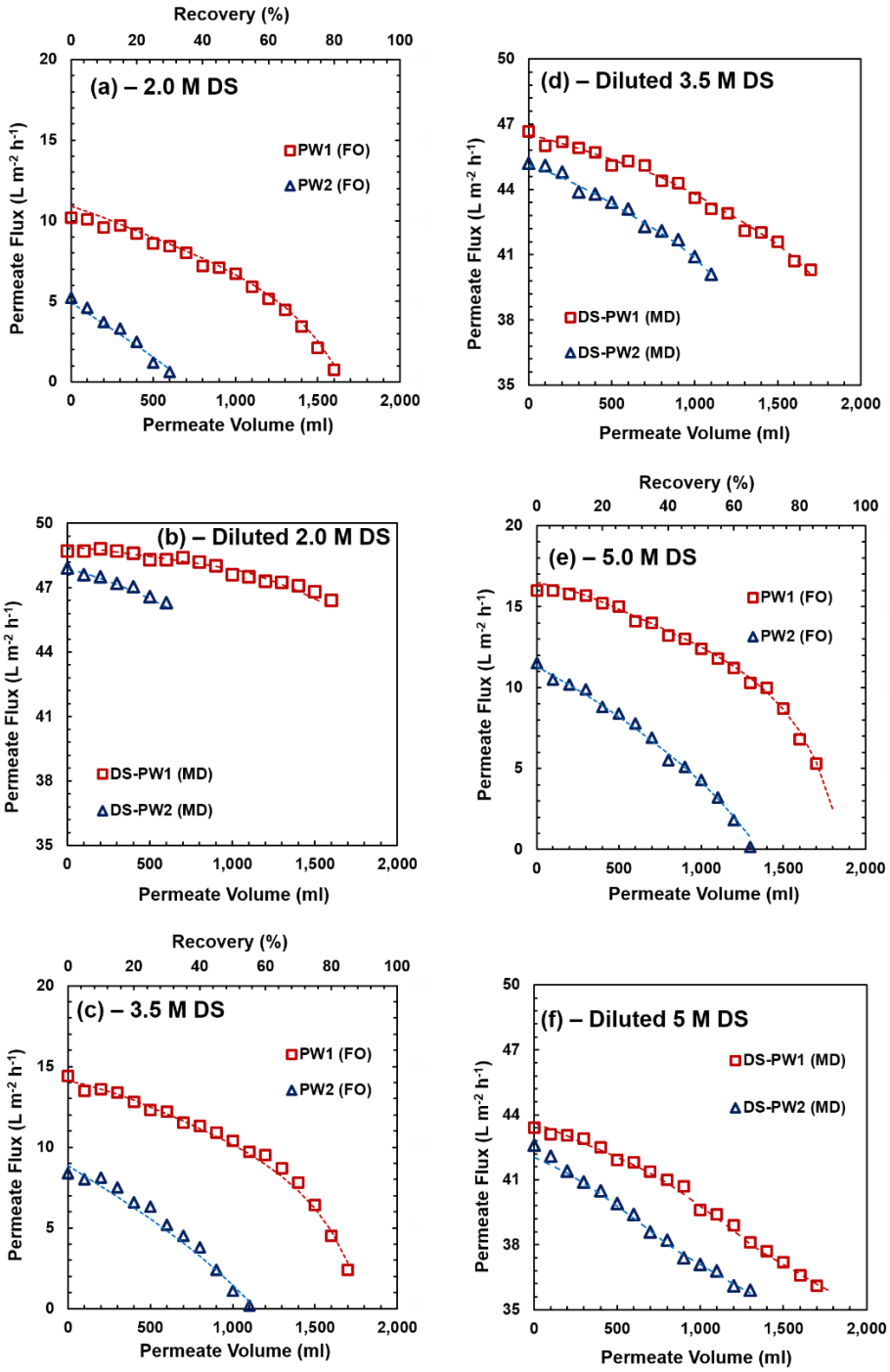

Fig. 6. FO-MD experiments for PW1 and PW2 using CTA (FO) and ECTFE (MD) membranes. Flow rates were adjusted at 0.7 L min^{-1}. FO and MD temperatures were adjusted to 25 and 60 °C, respectively. **a, c and e)** FO permeate flux as a function of permeate volume collected as well as the recovery rate for 2, 3.5 and 5 M NaCl in DI water as DS. **b, d and f)** MD permeate flux as a function of permeate volume using diluted DS in experiments shown in (a), (c) and (e) diagrams, respectively.

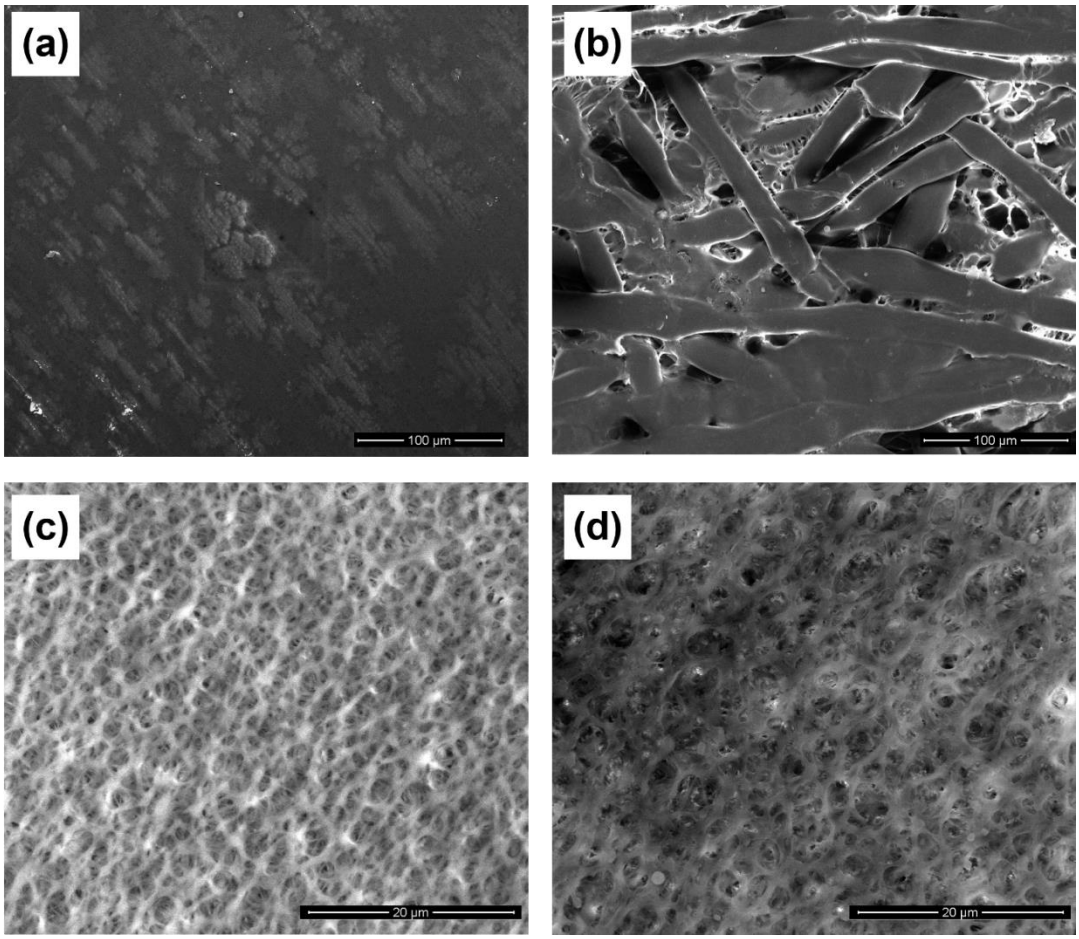

Fig. 7. SEM images taken from **a)** CTA membrane feed side (active side), **b)** CTA membrane DS side after FO experiment with PW2 using 2 M sodium chloride in DI water as DS, **c)** ECTFE membrane after DCMD experiment concentrating the diluted DS up to 2.0 M **and d)** ECTFE membrane after DCMD experiment concentrating the diluted DS up to 5.0 M.

5.4.5. Long-term EC-FO-MD

Long-term FO-MD experiments were carried using PW1 and PW2. Both samples were pretreated using the EC process described (see section 5.3.2) prior to FO-MD experiments. FO experiments for treating PW1 was performed employing 2.0 M sodium chloride in DI water as DS. All experiments were repeated for four times. After each FO run, the diluted DS was regenerated using the MD system using ECTFE membrane (experimental conditions shown in

Table A.1). Fig. 8(a) depicts the FO permeate flux as a function of collected permeate volume, while Fig. 8(b) shows the corresponding MD permeate flux. Modeled permeate fluxes are also shown. As can be seen, both FO and MD fluxes decrease as the collected permeate volume increases. MD permeate fluxes in the range of ~45 to 50 L m^{-2} h^{-1} are observed. Good agreement between experimental and modeled FO fluxes are observed. However, experimental MD fluxes deviate from the estimated data in the third and fourth runs. The reason for this observation could be membrane scaling, changes in membrane properties and adsorption of organics on membrane surface. However, SEM images taken of the surface of the tested ECTFE membrane showed minimal fouling/scaling. TOC content of the DS and MD permeate solutions were measured after the fourth run. Concentrated DS after fourth run contained 16.1 mg L^{-1}, while the MD permeate contained 4.6 mg L^{-1} TOC.

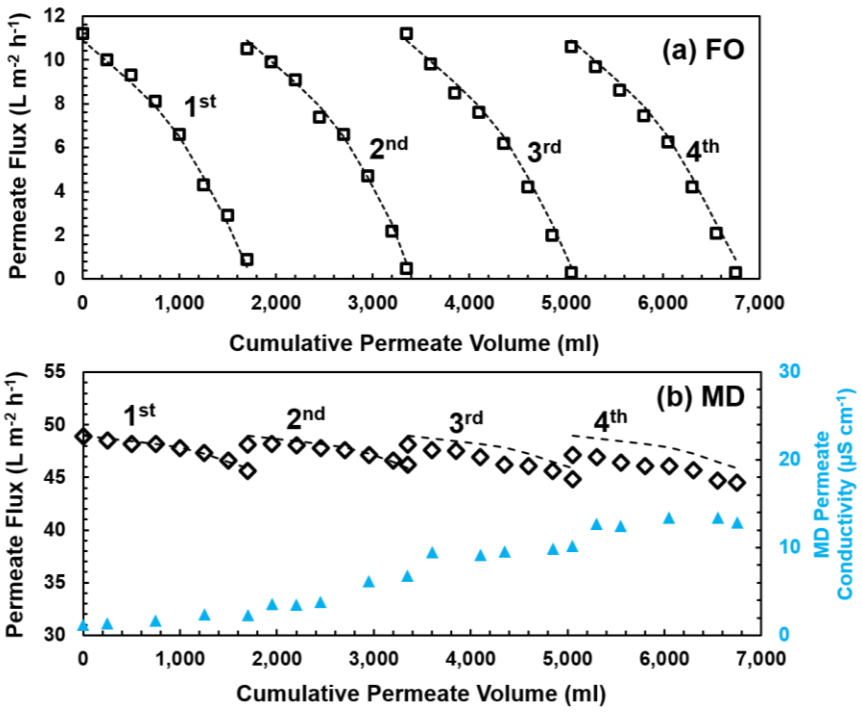

Fig. 8. Long-term FO-MD experiment with pretreated PW1 using 2.0 M sodium chloride in DI water as DS. **a)** FO permeate flux as a function of cumulative permeate volume, **b)** MD permeate flux as a function of cumulative permeate volume.

A second long-term EC-FO experiment was carried out using pretreated PW2 as feed and 5.0 M sodium chloride in DI water as DS. Experiment was repeated four times. After each FO experiment, diluted DS was re-concentrated using MD. Figs. 9(a) and 9(b) give the model and experimental permeate flux for FO and MD as a function of cumulative permeate volume, respectively. As can be seen, a similar FO permeate flux trend to the case of PW1 is observed. Model and experimental FO flux data are in good agreement. Minor localized fouling was observed on the CTA membrane surface. EDX analysis of the FO membrane surface is shown in Fig. 10. As can be seen, sodium chloride scale accounts for majority of fouling. Carbon and oxygen peaks, indicating the structure of CTA polymer were observed. These two peaks could also be attributed to the organic species adsorbed on the membrane surface.

Fig. 9(b) gives the MD permeate flux as a function of cumulative permeate volume. MD permeate fluxes deviated from the estimated curves in third and fourth runs. Membrane wetting was observed in the fourth MD run. As can be seen in Fig. 9(b), a concurrent rapid increase in MD permeate flux and MD permeate conductivity was observed in the fourth run, denoting membrane wetting. Membrane wetting may be due to crystal/scale growth within the membrane pores in high TDS concentration (up to 292 g L^{-1}). The MD experiment was repeated using 177 g L^{-1} sodium chloride in DI water as feed solution and was concentrated up to 293 g L^{-1} (~5.0 M) for four times. Similar wetting behavior was observed in the fourth run.

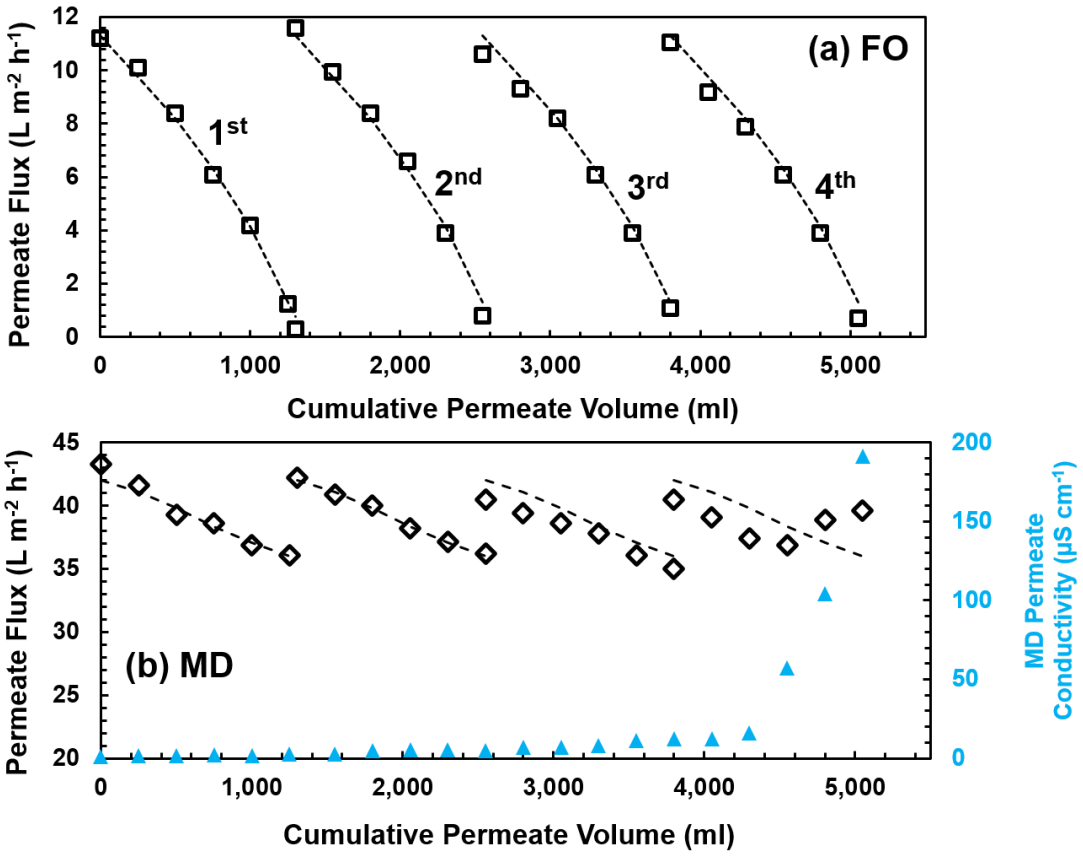

Fig. 9. Long-term FO-MD experiment with pretreated PW2 using 5.0 M sodium chloride in DI water as DS. **a)** FO permeate flux as a function of cumulative permeate volume, **b)** MD permeate flux as a function of cumulative permeate volume.

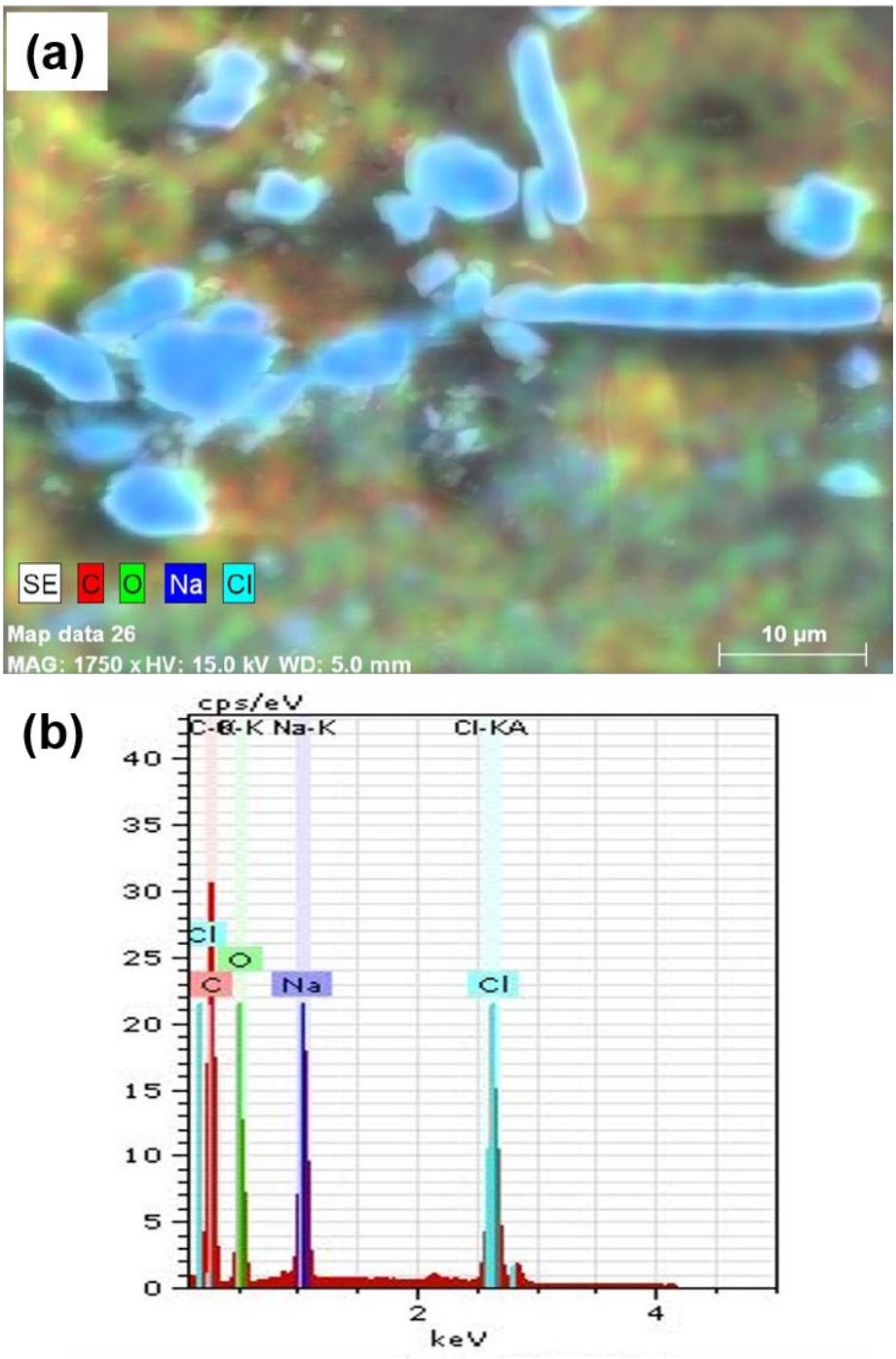

Fig. 10. EDX elemental analysis of the CTA membrane surface after four FO runs with PW2 as feed and 5.0 M sodium chloride in DI water as DS.

In order to mitigate membrane wetting during DS re-concentration in long-term experiments, a two membrane scenario was designed. In this set of experiments, two MD membranes were used for DS regeneration. ECTFE membrane was used for concentrating a simulated dilute DS, containing 177 g L^{-1} sodium chloride in DI water, up to 250 g L^{-1} and PTFE membrane (0.02 µm nominal pore size, see Table 1) was used to concentrate the DS from 250 to 293 g L^{-1} (~5.0 M). Experiments were repeated for six times. Permeate flux results as well as MD permeate conductivity throughout the experiment are shown in Fig. 11. As can be seen, wetting was successfully mitigated in this round of experiments.

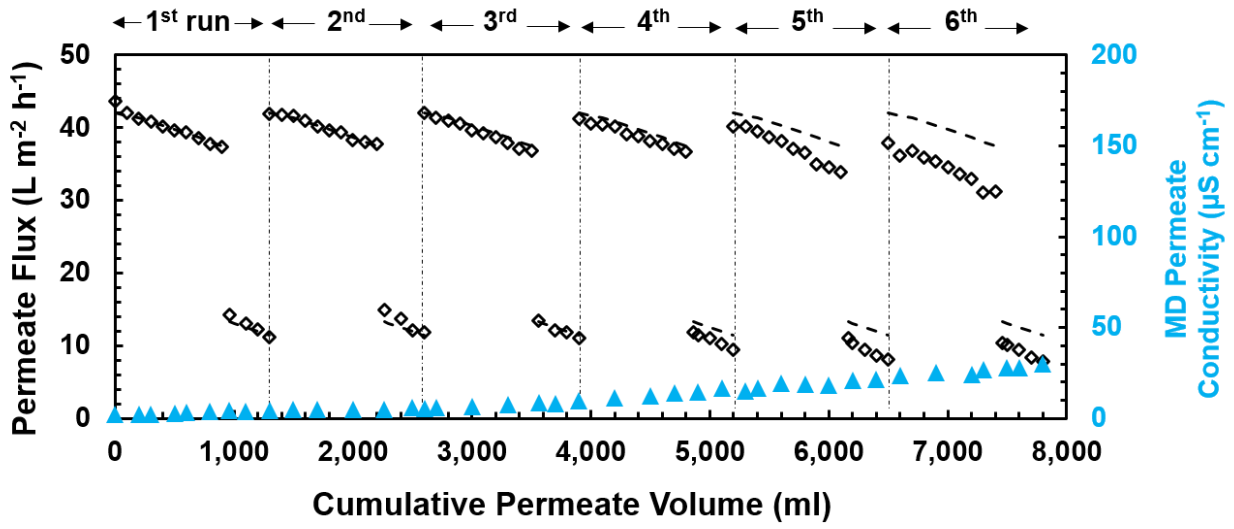

Fig. 11. Long-term FO-MD experiment with pretreated PW2 using 5.0 M sodium chloride in DI water as DS. MD permeate flux as well as permeate conductivity as functions of cumulative permeate volume. ECTFE membrane was used to concentrated the simulated DS up to 4.3 M. PTFE membrane was utilized to further concentrate the DS up to 5.0 M.

5.5. Conclusion

The results reported in this work indicate the potential of FO-MD integration for sustainable water recovery from high TDS produced waters. If appropriately chosen, a pretreatment system (e.g. EC) can significantly aid in fouling mitigation and achieving stable performance. Here, we showed that EC pretreatment led to TOC, TSS and turbidity removal of up to 78, 96 and 95%, respectively. Among different experimental conditions, temperature presented the most significant impact on increasing FO and MD water flux in short-term experiments.

Selection of DS concentration depends on a number of factors including feed water salinity content and target water recovery. Use of 2.0 M sodium chloride in DI water as DS resulted in 76% water recovery from PW1 (TDS=11.2 g L^{-1}) and 30% water recovery from PW2 (TDS=57.2 g L^{-1}). Increasing the DS concentration to 5.0 M significantly increased the water recovery for PW2, while this increase for PW1 was less than 10%. Long-term FO-MD experiments with PW1 using 2.0 M DS concentration, CTA membrane in FO module and ECTFE membrane in MD module was performed over 4 cycles. Long-term experiment with PW2 using 5.0 M DS concentration failed at the 4^{th} cycle due to MD membrane wetting. This problem was overcome using 2 separate membranes in the MD regeneration steps. ECTFE membrane was used to provide high flux and concentrate the diluted DS up to 4.2 M, while the PTFE was used to further concentrate the DS to 5.0 M.

Appendix A

Table. A.1. FO–MD experiments conducted.

Experiments		Feed	Permeate	Temperature (°C)	Flow rate (L min^{-1})	Length of experiment
Bassline 1.1	FO	PW1 & PW2	4.0 M DS	25 - 75	0.7	30 min after stabilization
	MD	4.0 M DS	DI Water	25 - 75	0.7	30 min after stabilization
Bassline 1.2	FO	PW1 & PW2	4.0 M DS	25	0.3 -0.9	30 min after stabilization
	MD	4.0 M DS	DI Water	60	0.3 -0.9	30 min after stabilization
Bassline 1.3	FO	PW1 & PW2	2.0-5.0 M DS	25	0.7	30 min after stabilization
	MD	2.0-5.0 M DS	DI Water	60	0.7	30 min after stabilization
Short-term 1.1	FO	PW1 & PW2	2.0 M DS	25	0.7	Up to maximum FO recovery
	MD	Diluted 2.0 M DS	DI Water	60	0.7	Concentrating diluted DS up to 2.0 M
Short-term 1.2	FO	PW1 & PW2	3.5 M DS	25	0.7	Up to maximum FO recovery

Table. A.1. FO–MD experiments conducted (cont.)

Experiments		Feed	Permeate	Temperature (°C)	Flow rate (L min^{-1})	Length of experiment
Short-term 1.2	MD	Diluted 3.5 M DS	DI Water	60	0.7	Concentrating diluted DS up to 3.5 M
Short-term 1.3	FO	PW1 & PW2	5.0 M DS	25	0.7	Up to maximum FO recovery
	MD	Diluted 5.0 M DS	DI Water	60	0.7	Concentrating diluted DS up to 5.0 M
Long-term 1.1	FO	PW1	2.0 M DS	25	0.7	4 runs, each up to maximum recovery
	MD	Diluted 2.0 M DS	DI Water	60	0.7	4 runs, concentrating diluted DS up to 2.0 M
Long-term 1.2	FO	PW2	5.0 M DS	25	0.7	4 runs, each up to maximum recovery
	MD	Diluted 5.0 M DS	DI Water	60	0.7	4 runs concentrating diluted DS up to 5.0 M, 4^{th} experiment failed due to wetting
Long-term 1.3	MD	Diluted 5.0 M DS	DI Water	60	0.7	6 successful runs, concentrating diluted DS up to 5.0 M

References

[1] J.A. Veil, Produced Water Management Options and Technologies, in: Prod. Water, 2011: pp. 537–571. doi:10.1007/978-1-4614-0046-2_29.

[2] A. Fakhru'l-Razi, A. Pendashteh, L.C. Abdullah, D.R.A. Biak, S.S. Madaeni, Z.Z. Abidin, Review of technologies for oil and gas produced water treatment, J. Hazard. Mater. 170 (2009) 530–551. doi:10.1016/j.jhazmat.2009.05.044.

[3] J.M. Dickhout, J. Moreno, P.M. Biesheuvel, L. Boels, R.G.H. Lammertink, W.M. de Vos, Produced water treatment by membranes: A review from a colloidal perspective, J. Colloid Interface Sci. 487 (2017) 523–534. doi:10.1016/J.JCIS.2016.10.013.

[4] D.S. Alessi, A. Zolfaghari, S. Kletke, J. Gehman, D.M. Allen, G.G. Goss, Comparative analysis of hydraulic fracturing wastewater practices in unconventional shale development: Water sourcing, treatment and disposal practices, Can. Water Resour. J. 42 (2017) 105–121. doi:10.1080/07011784.2016.1238782.

[5] U.S.E.I. Administration, Technically Recoverable Shale Oil and Shale Gas Resources : An Assessment of 137 Shale Formations in 41 Countries Outside the United States, U.S. Energy Inf. Adm. 2013 (2013) 76 pp. doi:www.eia.gov/analysis/studies/worldshalegas/.

[6] U.S. Energy Information Administration (EIA), (n.d.). https://www.eia.gov/tools/faqs/faq.php?id=907&t=8 (accessed January 17, 2018).

[7] A.J. Kondash, E. Albright, A. Vengosh, Quantity of flowback and produced waters from unconventional oil and gas exploration, Sci. Total Environ. 574 (2017) 314–321. doi:10.1016/j.scitotenv.2016.09.069.

[8] D.M. Akob, A.C. Mumford, W. Orem, M.A. Engle, J.G. Klinges, D.B. Kent, I.M. Cozzarelli, Wastewater Disposal from Unconventional Oil and Gas Development Degrades Stream Quality at a West Virginia Injection Facility, Environ. Sci. Technol. 50 (2016) 5517–5525. doi:10.1021/acs.est.6b00428.

[9] K.B. Gregory, R.D. Vidic, D. a. Dzombak, Water Management Challenges Associated with the Production of Shale Gas by Hydraulic Fracturing, Elements. 7 (2011) 181–186. doi:10.2113/gselements.7.3.181.

[10] D.L. Shaffer, L.H. Arias Chavez, M. Ben-Sasson, S. Romero-Vargas Castrill??n, N.Y. Yip, M. Elimelech, Desalination and reuse of high-salinity shale gas produced water: Drivers, technologies, and future directions, Environ. Sci. Technol. 47 (2013) 9569–9583. doi:10.1021/es401966e.

[11] K. Sardari, P. Fyfe, D. Lincicome, S.R. Wickramasinghe, Aluminum electrocoagulation followed by forward osmosis for treating hydraulic fracturing produced waters,

Desalination. 428 (2018) 172–181. doi:10.1016/j.desal.2017.11.030.

[12] M. Malmali, P. Fyfe, D. Lincicome, K. Sardari, S.R. Wickramasinghe, Selecting membranes for treating hydraulic fracturing produced waters by membrane distillation, Sep. Sci. Technol. 52 (2017) 266–275. doi:10.1080/01496395.2016.1244550.

[13] M. Çakmakce, N. Kayaalp, I. Koyuncu, Desalination of produced water from oil production fields by membrane processes, Desalination. 222 (2008) 176–186. doi:10.1016/j.desal.2007.01.147.

[14] A. Koren, N. Nadav, Mechanical vapour compression to treat oil field produced water, Desalination. 98 (1994) 41–48. doi:10.1016/0011-9164(94)00130-8.

[15] I.S. Al-Mutaz, Features of multi-effect evaporation desalination plants, Desalin. Water Treat. 54 (2015) 3227–3235. doi:10.1080/19443994.2014.910842.

[16] Q. Jiang, J. Rentschler, R. Perrone, K. Liu, Application of ceramic membrane and ion-exchange for the treatment of the flowback water from Marcellus shale gas production, J. Memb. Sci. 431 (2013) 55–61. doi:10.1016/j.memsci.2012.12.030.

[17] T. CATH, A. CHILDRESS, M. ELIMELECH, Forward osmosis: Principles, applications, and recent developments, J. Memb. Sci. 281 (2006) 70–87. doi:10.1016/j.memsci.2006.05.048.

[18] T.-S. Chung, S. Zhang, K.Y. Wang, J. Su, M.M. Ling, Forward osmosis processes: Yesterday, today and tomorrow, Desalination. 287 (2012) 78–81. doi:10.1016/j.desal.2010.12.019.

[19] B.D. Coday, P. Xu, E.G. Beaudry, J. Herron, K. Lampi, N.T. Hancock, T.Y. Cath, The sweet spot of forward osmosis: Treatment of produced water, drilling wastewater, and other complex and difficult liquid streams, Desalination. 333 (2014) 23–35. doi:10.1016/j.desal.2013.11.014.

[20] K. Lutchmiah, A.R.D. Verliefde, K. Roest, L.C. Rietveld, E.R. Cornelissen, Forward osmosis for application in wastewater treatment: A review, Water Res. 58 (2014) 179–197. doi:10.1016/J.WATRES.2014.03.045.

[21] L. Chekli, S. Phuntsho, J.E. Kim, J. Kim, J.Y. Choi, J.S. Choi, S. Kim, J.H. Kim, S. Hong, J. Sohn, H.K. Shon, A comprehensive review of hybrid forward osmosis systems: Performance, applications and future prospects, J. Memb. Sci. 497 (2016) 430–449. doi:10.1016/j.memsci.2015.09.041.

[22] J.R. McCutcheon, R.L. McGinnis, M. Elimelech, Desalination by ammonia–carbon dioxide forward osmosis: Influence of draw and feed solution concentrations on process performance, J. Memb. Sci. 278 (2006) 114–123. doi:10.1016/j.memsci.2005.10.048.

[23] T.S. Chung, X. Li, R.C. Ong, Q. Ge, H. Wang, G. Han, Emerging forward osmosis (FO) technologies and challenges ahead for clean water and clean energy applications, Curr. Opin. Chem. Eng. 1 (2012) 246–257. doi:10.1016/j.coche.2012.07.004.

[24] R.L. McGinnis, M. Elimelech, Energy requirements of ammonia-carbon dioxide forward osmosis desalination, Desalination. 207 (2007) 370–382. doi:10.1016/j.desal.2006.08.012.

[25] A. Altaee, G. Zaragoza, A conceptual design of low fouling and high recovery FO-MSF desalination plant, Desalination. 343 (2014) 2–7. doi:10.1016/j.desal.2013.09.025.

[26] C.H. Tan, H.Y. Ng, A novel hybrid forward osmosis - nanofiltration (FO-NF) process for seawater desalination: Draw solution selection and system configuration, Desalin. Water Treat. 13 (2010) 356–361. doi:10.5004/dwt.2010.1733.

[27] S. Zhao, L. Zou, D. Mulcahy, Brackish water desalination by a hybrid forward osmosis-nanofiltration system using divalent draw solute, Desalination. 284 (2012) 175–181. doi:10.1016/j.desal.2011.08.053.

[28] G. Blandin, A.R.D. Verliefde, C.Y. Tang, P. Le-Clech, Opportunities to reach economic sustainability in forward osmosis-reverse osmosis hybrids for seawater desalination, Desalination. 363 (2015) 26–36. doi:10.1016/j.desal.2014.12.011.

[29] G.P. Thiel, E.W. Tow, L.D. Banchik, H.W. Chung, J.H. Lienhard V, Energy consumption in desalinating produced water from shale oil and gas extraction, Desalination. 366 (2015) 94–112. doi:10.1016/j.desal.2014.12.038.

[30] K.W. Lawson, D.R. Lloyd, Membrane distillation, J. Memb. Sci. 124 (1997) 1–25. doi:10.1016/S0376-7388(96)00236-0.

[31] T.Y. Cath, D. Adams, A.E. Childress, Membrane contactor processes for wastewater reclamation in space: II. Combined direct osmosis, osmotic distillation, and membrane distillation for treatment of metabolic wastewater, J. Memb. Sci. 257 (2005) 111–119. doi:10.1016/j.memsci.2004.07.039.

[32] Q. Liu, C. Liu, L. Zhao, W. Ma, H. Liu, J. Ma, Integrated forward osmosis-membrane distillation process for human urine treatment, Water Res. 91 (2016) 45–54. doi:10.1016/j.watres.2015.12.045.

[33] K.Y. Wang, M.M. Teoh, A. Nugroho, T.S. Chung, Integrated forward osmosis-membrane distillation (FO-MD) hybrid system for the concentration of protein solutions, Chem. Eng. Sci. 66 (2011) 2421–2430. doi:10.1016/j.ces.2011.03.001.

[34] E.A. Bell, T.E. Poynor, K.B. Newhart, J. Regnery, B.D. Coday, T.Y. Cath, Produced water treatment using forward osmosis membranes: Evaluation of extended-time performance and fouling, J. Memb. Sci. 525 (2017) 77–88. doi:10.1016/j.memsci.2016.10.032.

[35] T. Harif, M. Khai, A. Adin, Electrocoagulation versus chemical coagulation: Coagulation/flocculation mechanisms and resulting floc characteristics, Water Res. 46 (2012) 3177–3188. doi:10.1016/j.watres.2012.03.034.

[36] Electrocoagulation for the treatment of textile industry effluent – A review, J. Environ. Manage. 128 (2013) 949–963. doi:10.1016/J.JENVMAN.2013.06.043.

[37] B. Zhu, D.A. Clifford, S. Chellam, Comparison of electrocoagulation and chemical coagulation pretreatment for enhanced virus removal using microfiltration membranes, Water Res. 39 (2005) 3098–3108. doi:10.1016/j.watres.2005.05.020.

[38] Electrocoagulation treatment of raw landfill leachate using iron-based electrodes: Effects of process parameters and optimization, J. Environ. Manage. 204 (2017) 75–81. doi:10.1016/J.JENVMAN.2017.08.028.

[39] M. Kobya, O.T. Can, M. Bayramoglu, Treatment of textile wastewaters by electrocoagulation using iron and aluminum electrodes, J. Hazard. Mater. 100 (2003) 163–178. doi:10.1016/S0304-3894(03)00102-X.

[40] T. Picard, G. Cathalifaud-Feuillade, M. Mazet, C. Vandensteendam, Cathodic dissolution in the electrocoagulation process using aluminium electrodes., J. Environ. Monit. 2 (2000) 77–80. doi:10.1039/a908248d.

[41] Electrocoagulation treatment of raw landfill leachate using iron-based electrodes: Effects of process parameters and optimization, J. Environ. Manage. 204 (2017) 75–81. doi:10.1016/J.JENVMAN.2017.08.028.

[42] D. Ghernaout, B. Ghernaout, A. Saiba, A. Boucherit, A. Kellil, Removal of humic acids by continuous electromagnetic treatment followed by electrocoagulation in batch using aluminium electrodes, Desalination. 238 (2009) 295–308. doi:10.1016/j.desal.2008.04.001.

[43] N.N. Bui, J.T. Arena, J.R. McCutcheon, Proper accounting of mass transfer resistances in forward osmosis: Improving the accuracy of model predictions of structural parameter, J. Memb. Sci. 492 (2015) 289–302. doi:10.1016/j.memsci.2015.02.001.

[44] J.R. McCutcheon, M. Elimelech, Influence of concentrative and dilutive internal concentration polarization on flux behavior in forward osmosis, J. Memb. Sci. 284 (2006) 237–247. doi:10.1016/j.memsci.2006.07.049.

[45] Y. Yun, R. Ma, W. Zhang, A.G. Fane, J. Li, Direct contact membrane distillation mechanism for high concentration NaCl solutions, Desalination. 188 (2006) 251–262. doi:10.1016/j.desal.2005.04.123.

[46] S. Al-Obaidani, E. Curcio, F. Macedonio, G. Di Profio, H. Al-Hinai, E. Drioli, Potential of membrane distillation in seawater desalination: Thermal efficiency, sensitivity study and

cost estimation, J. Memb. Sci. 323 (2008) 85–98. doi:10.1016/j.memsci.2008.06.006.

[47] M.S. El-Bourawi, Z. Ding, R. Ma, M. Khayet, A framework for better understanding membrane distillation separation process, J. Memb. Sci. 285 (2006) 4–29. doi:10.1016/j.memsci.2006.08.002.

[48] E. Metcalf, H. Eddy, Wastewater engineering: treatment and reuse, 2003. doi:10.1016/0309-1708(80)90067-6.

[49] K.L. Hickenbottom, N.T. Hancock, N.R. Hutchings, E.W. Appleton, E.G. Beaudry, P. Xu, T.Y. Cath, Forward osmosis treatment of drilling mud and fracturing wastewater from oil and gas operations, Desalination. 312 (2013) 60–66. doi:10.1016/j.desal.2012.05.037.

[50] Z.Y. Li, V. Yangali-Quintanilla, R. Valladares-Linares, Q. Li, T. Zhan, G. Amy, Flux patterns and membrane fouling propensity during desalination of seawater by forward osmosis, Water Res. 46 (2012) 195–204. doi:10.1016/j.watres.2011.10.051.

[51] S. Phuntsho, F. Lotfi, S. Hong, D.L. Shaffer, M. Elimelech, H.K. Shon, Membrane scaling and flux decline during fertiliser-drawn forward osmosis desalination of brackish groundwater, Water Res. 57 (2014) 172–182. doi:10.1016/j.watres.2014.03.034.

[52] M. Xie, W.E. Price, L.D. Nghiem, M. Elimelech, Effects of feed and draw solution temperature and transmembrane temperature difference on the rejection of trace organic contaminants by forward osmosis, J. Memb. Sci. 438 (2013) 57–64. doi:10.1016/j.memsci.2013.03.031.

[53] D. Ghernaout, A. Al-Ghonamy, M.W. Naceur, N. Messaoudene, M. Aichouni, Influence of operating parameters on electrocoagulation of C.I. disperse yellow 3, J. Electrochem. Sci. Eng. 4 (2014) 271–283. doi:http://dx.doi.org/10.5599/jese.146.

[54] D. Ghernaout, B. Ghernaout, A. Boucherit, M.W. Naceur, A. Khelifa, A. Kellil, Study on mechanism of electrocoagulation with iron electrodes in idealised conditions and electrocoagulation of humic acids solution in batch using aluminium electrodes, Desalin. Water Treat. 8 (2009) 91–99. doi:10.5004/dwt.2009.668.

[55] A comprehensive review of electrocoagulation for water treatment: Potentials and challenges, J. Environ. Manage. 186 (2017) 24–41. doi:10.1016/J.JENVMAN.2016.10.032.

[56] B.E. Poling, G.H. Thomson, D.G. Friend, R.L. Rowley, W.V. Wilding, Perry's Chemical Engineers' Handbook, 2007. doi:10.1036/0071511253.

[57] S. Zhao, L. Zou, Effects of working temperature on separation performance, membrane scaling and cleaning in forward osmosis desalination, Desalination. 278 (2011) 157–164. doi:10.1016/j.desal.2011.05.018.

[58] P. Bacchin, D. Si-Hassen, V. Starov, M.J. Clifton, P. Aimar, A unifying model for concentration polarization, gel-layer formation and particle deposition in cross-flow membrane filtration of colloidal suspensions, Chem. Eng. Sci. 57 (2002) 77–91. doi:10.1016/S0009-2509(01)00316-5.

Chapter 6: Conclusions and Future Directions

6.1. Conclusions

Treatment of high salinity produced waters often involves maximizing water recovery in order to minimize the volume of concentrated brine that has to be transported to a centralized treatment or disposal facility. The concentrated brine can also be sent to a crystallization unit for zero liquid discharge scenarios. Membrane distillation can be used to concentrate the wastewater to close to the solubility limit of the dissolved salts in the water. However, it is likely that an optimized process will be a multistep process. As the total dissolved solids (TDS) of the feed increases, lower flux membranes with larger thickness and smaller pore sizes will be required in order to prevent breakthrough the of the feed solution.

For real feed streams containing surfactant and other dissolved organic compounds, either pre-treatment or optimized membrane surface properties will be required in order minimize flux decline due to membrane fouling as well as early breakthrough of the feed due do adsorption of surfactant molecules onto the membrane surface. The results obtained here indicate the utility of defining an appropriate bulk membrane structural parameter that can provide insights into expected membrane performance when tested with low fouling model feed streams. Under these conditions, bulk membrane properties such as pore size, tortuosity and thickness will have a greater effect on membranes performance compared to surface properties such as hydrophobicity and roughness.

The results reported in this dissertation indicate the importance of pretreatment prior to membrane distillation when treating high salinity produced waters. Actual produced water streams

can lead to severe membrane fouling and consequent drop in water recovery due to containing hydrophobic suspended and dissolved organics. If appropriately designed, pretreatment could successfully mitigate fouling and wetting during treatment of real produced waters. We show that electrocoagulation could effectively remove most contaminations, except for TDS, from produced water samples obtained from natural gas extraction facilities in Marcellus Shale. Maintaining a 3 A current in the electrocoagulation reactor for 30 seconds, turbidity, total suspended solids (TSS) and total organic carbon (TOC) were removed by 96, 91 and 61%, respectively. Higher removal of contaminates such as TSS and TOC resulted in lower membrane fouling as well as lower water flux decline in membrane distillation.

Using resistance in series modeling for membrane permeability, considering a fouling layer permeability coefficient, water flux of membrane distillation system for pretreated high TDS produced water was accurately estimated. Pretreated produced water was concentrated up to 265 g L^{-1} in a continuous direct contact membrane distillation process for over 434 h reporting stable water flux. However, we indicate that even small levels of organic content could result in membrane fouling in longer experimental runs.

The application of forward osmosis for concentration of synthetic and actual high salinity produced waters was investigated. We show that significant fouling and consequently, a drop in flux will occur when treating actual hydraulic fracturing produced waters due to the presence of high values of TOC and TSS. It is shown that the feed water pretreatment will be essential if membrane-based separation processes such as forward osmosis are to be used to treat these highly impaired waters. We show that electrocoagulation prior to forward osmosis significantly reduces membrane fouling. Though sodium chloride is used in this research as the draw solute,

development of an actual combined electrocoagulation-forward osmosis process will require the use of a draw solute that can be economically recovered. Further, crossover of the draw solute into feed will affect the viability of the process. We show that for a reaction time of two min as a pretreatment step, over 70% reduction of TSS, TOC and turbidity results in electrocoagulation. Over a 24 hour period, suppression in fouling due to this pretreatment, leads to close to 21% increase in water recovery. In addition, the forward osmosis permeate flux may be predicted by using a resistance in series model to account for internal and external concentration polarization as well as fouling of the membrane barrier layer by adsorbed species in the produced water. The economic feasibility of the process will depend on the cost of the recovered water, membrane lifetime and recovery and reuse of the draw solute.

The feasibility of an integrated forward osmosis-membrane distillation system for water recovery from actual high salinity produced waters obtained from hydrocarbon extraction facilities at Marcellus and Fayetteville Shales has been demonstrated. In the proposed hybrid system, forward osmosis draws water from a high salinity feed, while membrane distillation regenerates the diluted draw solution and re-concentrates it back to its original concentration. We show that this process integration can combine the advantages of both processes; low fouling tendency membrane facing the majority of foulants and production of high quality permeate.

Selection of draw solution concentration depends on a number of factors including feed water salinity content and targeted water recovery. Utilization of 2.0 M sodium chloride in DI water as forward osmosis draw solution resulted in 76% water recovery from an actual produced water sample containing 11.2 g L^{-1} TDS and 30% water recovery from a second produced water sample with TDS content of 57.2 g L^{-1}. Increasing the draw solution concentration to 5.0 M

significantly increased the water recovery for the higher concentration feed water, while this increase for produced water containing 11.2 g L^{-1} TDS was less than 10%. Long-term integrated experiments with lower concentration produced water sample using 2.0 M draw solution, CTA membrane in FO module and ECTFE membrane in MD module, was successfully performed over 4 cycles. However, we showed that for higher concentration feed waters, a combination of two membranes with different tolerance for TDS are required in order to complete long-term cyclic experiments without breakthrough during membrane distillation.

6.2. Future Directions

Future work could be focused on development of anti-fouling hydrophobic membranes for membrane distillation. This research indicated the necessity of rigorous pretreatment prior to membrane distillation regarding fouling mitigation. Development of fouling resistant membranes can lead to significant capital and operational cost savings by pretreatment minimization. In addition, extended research on membrane distillation module design is required in order to integrate and maximize the use of low-grade waste heat as energy source. Moreover, the possibility of hydrophobic membrane regeneration after loss of anti-wetting characteristics (decrease in contact angle and liquid entry pressure) in membrane distillation operation can be investigated.

The application of hybrid forward osmosis-membrane distillation system can be extended to a variety of areas such as food and dairy industry. In addition, this integration can be investigated for production of ultra-pure water. Moreover, the possibility of using novel draw solutions such as thermolytic salts in this hybrid process can be studied.